THE UNIVERSITY OF
WARWICK

University of Warwick institutional repository: http://go.warwick.ac.uk/wrap

A Thesis Submitted for the Degree of PhD at the University of Warwick

http://go.warwick.ac.uk/wrap/4007

This thesis is made available online and is protected by original copyright.

Please scroll down to view the document itself.

Please refer to the repository record for this item for information to help you to cite it. Our policy information is available from the repository home page.

ON THE ELECTRICAL AND STRUCTURAL PROPERTIES OF BORON DELTA LAYERS IN SILICON

Nevil Lee Mattey

Thesis submitted for the degree

of Doctor of Philosophy.

University of Warwick,

Department of Physics.

September 1991.

CONTENTS

1. Introduction 1.

2. Previous Work 4.

2.1 δ Doping in III-V Semiconductors 4.

2.2 δ Doping in Silicon 6.

2.3 Transport in δ Layers 9.

3. The Growth and Structural Characterisation of Boron δ Layers 14.

3.1 Growth by MBE 14.

3.2 Structural and compositional characterisation 17.

a) Secondary ion mass spectrometry 17.

b) Cross-sectional transmission electron microscopy 19.

b) X-ray diffraction 19.

4. Electrical Measurements 21.

4.1 C-V profiling 21.

a) Sample preparation 21.

b) C-V measurement 21.

c) Automation of C-V profiling 24.

4.2 Transport Measurements 25.

a) Sample preparation 25.

b) Cryogenics 30.

c) Thermometry 30.

d) Transport measurement 33.

e) Computer control 36.

5. Theory 37.

5.1 The δ layer as a 2D system 37.

5.2 Capacitance-voltage profiling 41.

5.3 Transport in 2D systems 44.

a) Strong localisation and the metal-insulator transition 44.

b) Scaling theory and weak localisation 47.

c) Electron-electron interactions 54.

d) Corrections due to weak localisation and electron-electron interactions 55.

6. Results and Discussion 57.

6.1 Structural characterisation 57.

a) SIMS analysis 58.

b) XTEM 61.

c) XRD 63.

6.2 Electrical properties 65.

a) C-V measurements 65.

b) Transport measurements 71.

7. Conclusions and Further work 99.

References 102.

Figures and Tables

2.1 Schematic diagram of the δFET	13.
2.2 Band diagram of the sawtooth doping superlattice	13.
4.2 Equivalent circuit for C-V measurement	22.
4.3 SIMS profiles of as grown and annealled B δ layers	29.
4.4 Circuit used to measure resistivity, Hall effect and magnetoresistance	34.
5.1 "V" shaped quantum well due to δ layer	40.
5.2 Scaling behaviour of the conductivity	53.
5.3 Electron diffusing round a closed path of elastic scattering centres	53.
6.1 Densitometer plot from bevel and stain of a B δ layer	57.
6.2 SIMS profile of B δ layer and reconstucted profile	59.
6.3 Extrapolation of up and down slopes and FWHM	60.
6.4 Extrapolation of apparent depth and peak conc.	60.
6.5 XTEM micrograph of a B δ layer	62.
6.6 XRD rocking curve	64.
6.7 Structure used for C-V measurements	67.
6.8 Typical I-V characteristic for Al Schottky barrier	67.
6.9 C-V for Al Schottky barrier	68.
6.10 N-d for Al Scottky barrier	68.
6.11 C-V for Ti barrier	69.
6.12 N-d for T i barrier	69.
6.13 SIMS profile of C-V structure	70.

6.14 Resistance and Hall coefficient between 0.3K and
30K for a sample of sheet density $7.6x10^{13}cm^{-2}$ 76.
6.15 As above for a sample of sheet density $2.2x10^{13}cm^{-2}$ 77.
6.16 As above for a sample of sheet density $1.8x10^{13}cm^{-2}$ 78.
6.17 Calculated subband structure for Si:B δ layers 79.
6.18 Magnetoresistance of sample 3 in a magnetic field 83.
6.19 Change in resistance versus B/T for sample 3. 84.
6.20 Plot of LnR versus $B^{1/2}$ for sample 3 89.
6.21 Plot of Ln R versus $T^{1/2}$ for sample 3 with B=12 Tesla 90.
6.22 Plot of Ln R versus $B^{1/2}$ for sample 2 91.
6.23 Plot of Ln R versus $B^{1/2}$ for sample 1 92.
6.24 Log-log plot of resistance versus sheet density 97.
6.25 Temperature dependence of the conductivity of a B δ
layer of sheet density $9x10^{12}cm^{-2}$ 98.

Table I 75.
Table II 82.
Table III 88.
Table IV 94.

Acknowledgements

I should like to acknowldge the contributions of the following without whom this work would not have been possible:

Richard Kubiak and Richard Houghton for growing the layers, Mark Dowsett and Bob Barlow for SIMS analysis, Peter Augustus for TEM and Adrian Powell for the X-ray diffraction.

Thanks also to the remainder of the ASR group for their input, especially Robin Biswas, Pete Phillips and Dave Smith.

Finally I wish to acknowledge the contributions of Mike Kearney and my supervisor, Terry Whall, for their help with the theory of the transport results.

DECLARATION

The work described in this thesis was carried out either by or at the instigation of the author. It is presented according to the guidelines laid down in the regulations of the University of Warwick as prescribed by Phys/PG3(1988).

Some of the work described herein has been, or is in the process of being, published:

Mattey N L, Hopkinson M, Houghton R F, Dowsett M G, McPhail D S, Whall T E, Parker E H C, Booker G R, Whitehurst J, 1990, Thin Solid Films, 184, 15.

Mattey N L, Dowsett M G, Parker E H C, Whall T E, Taylor S, Zhang J F, 1990, Appl. Phys. Lett. 57 (16), 1648.

Powell A R, Mattey N L, Kubiak R A A, Parker E H C, Whall T E, Bowen D K, 1991, Semicond. Sci Technol. 6, 227.

Mattey N L, Whall, T E, Kubiak R A A, Kearney M, to be submitted to Semicond. Sci. Technol.

Mattey N L, Whall T E, Biswas R G, Kubiak R A A, Kearney M, to be submitted to Phil. Mag.

SUMMARY

This thesis describes the first successful growth of boron δ layers using silicon MBE. SIMS has been used to demonstrate that the layer widths are ~2nm as has been confirmed by TEM. This is probably an overestimate, an average value of (0.3 ± 0.5)nm being obtained from XRD, suggesting that these are the thinnest δ layers produced to date.

Hall and XRD measurements indicate that the boron dopant is fully activated up to sheet coverages of ½ monolayer, i.e. ~$3.5\text{x}10^{14}\text{cm}^{-2}$.

The CV profile obtained for a B δ layer of sheet density $2.5\text{x}10^{12}\text{cm}^{-2}$ has FWHM ~3nm, a result which is shown to be consisitent with δ doping in the light of recent theoretical work.

Resistivity, magnetoresistance and the Hall effect have been measured at temperatures down to 0.3K using magnetic fields of up to 12T on samples of sheet density in the range $4\text{x}10^{12}\text{cm}^{-2}$ to $8\text{x}10^{13}\text{cm}^{-2}$. 2D weak localisation and associated electron-electron interaction effects have been observed in samples of sheet density above $1.8\text{x}10^{13}\text{cm}^{-2}$ with evidence of spin-orbit scattering. These samples are shown to undergo a "metal-insulator" transition in high magnetic fields with variable range hopping at 12 T. Samples of sheet density $\leq 1\text{x}10^{13}\text{cm}^{-2}$, show activated transport from which it is concluded that the critical acceptor separation for the metal-insulator transition in this system is significantly less than the value found in bulk, uniformly doped, Si:B. It is suggested that this may be due to the splitting of the valence band degeneracy due to quantum confinement.

Chapter 1.

INTRODUCTION

The semiconductor industry is constantly striving towards producing integrated circuits of greater functional complexity and increased speed of operation with an associated demand for reduced power consumption. This has led to a continuous scaling down of device geometry.

This study is concerned with the properties of the so called "δ" doped system which represents the ultimate scale down of the dimensions in one direction - ideally to one atomic plane. Following the development of growth techniques such as molecular beam epitaxy (MBE) where the growth mechanism is essentially two-dimensional, the realisation of such structures becomes practicable.

Classical descriptions of the transport properties of such systems are invalid, quantum mechanical effects become the limiting factors and may also provide means of producing novel device actions. A complete understanding of the behaviour of these systems is thus essential, not only from a scientific viewpoint, but also a technological one.

This thesis describes the first study of the properties of the boron δ doping layer in silicon. A review of related work in the III-V semiconductor systems and antimony, arsenic and gallium δ layers in silicon is given in Chapter two.

Chapter three describes the growth procedure used to produce the first successful boron delta layers in silicon along with the techniques used to characterise the structural and compositional properties of the as grown layers.

The techniques developed for the electrical assessment of the layers are discussed in Chapter four along with details of the modified MOS process developed to fabricate test structures and devices.

Chapter five gives the theoretical background to the results presented and discussed in Chapter six. Analysis of data from secondary ion mass spectrometry (SIMS) carried out using a range of impact energies suggests that the as grown FWHM of the δ layers is $\sim$2nm, as is supported by transmission electron microscopy (TEM). More recent work on the interpretation of rocking curves from X ray diffraction suggests a width of $<$1nm (Powell et al, 1991a),b)), implying that these layers are the thinnest produced to date. Results obtained from capacitance-voltage profiling give a FWHM of $\sim$3nm for a sheet density of $2x10^{12}cm^{-2}$ which is shown to be consistent a quantum mechanical description.

The subband structure of the p-type δ layer in silicon has been calculated using a simple algorithm developed from the model of Schubert et al (1985) which takes into account the effect of free carriers.

The results from measurements of the transport properties of δ layers of sheet density in the range $4x10^{12}cm^{-2}$ to $4x10^{14}cm^{-2}$ at temperatures down to 0.3K are discussed in terms of 2D weak localisation and associated electron-electron interaction effects for sheet densities $\geq 1.8x10^{13}cm^{-2}$. A transition to strong localisation is shown to occur at a sheet density of $\sim 1x10^{13}cm^{-2}$ suggesting that the critical impurity separation for the metal-insulator transition is significantly

lower in the δ doped system than for bulk Si:B. It is suggested that this may be due to the splitting of the valence band degeneracy by the quantum confinement.

Magnetoresistance measurements on the weakly localised samples using fields of up to 12T are interpreted in terms of a magnetic field induced metal-insulator transition due to the shrinkage of the wavefunction.

It is concluded that measurements at low fields are required to further separate the weak localisation and interaction terms and that the present description of the magnetoresistance results requires a more detailed comparison with alternative theories of hopping transport.

CHAPTER 2.

PREVIOUS WORK.

2.1 δ Doping in III-V Semiconductors.

The concept of introducing dopants in one atomic plane was origonally proposed to improve the doping profile control of Ge in GaAs grown by MBE (Wood et al,1980). Previously Bass (1979) had reported sharp dopant spikes resulting from the absorption of Si onto a growth interrupted GaAs surface. Zrenner et al (1985) reported the observation of the 2D subband structure due to the V shaped quantum well and coined the term "δ" layer since the donor distribution was described by the Dirac δ function. The confinement of the Si donors to one atomic plane was inferred from the agreement between calculated and measured subband energies. The first direct demonstration of the donor distribution was provided by Schubert et al (1988) who showed that the width of the layers was comparable to the lattice constant for growth temperatures $\leq 550^{\circ}C$.

The work on Si δ layers in GaAs has been applied to produce P type layers using Be, to a number of other III-V semiconductor systems as discussed in the review by Schubert (1990a) and to other growth techniques such as CVD.

The development of δ doping techniques has advanced the understanding of fundamental processes such as surface segregation, especially the effect of Fermi level pinning (Schubert, 1990a). Also the diffusion coefficients of Si and

Be in GaAs and $Al_xGa_{1-x}As$ and C in GaAs have been determined for the first time using rapid thermal annealing of δ doped samples followed by C-V profiling (Schubert 1990a).

δ doping has also found a number of device applications in GaAs, including the δFET where a δ layer is used as channel in a MESFET structure as shown in figure 2.1. Provided the channel is at the optimum depth of $\sim$30nm, the δFET has been shown to have advantages over depletion mode MESFETs and HEMTs, at least for short gate lengths (Schubert et al, 1986, Schubert and Ploog, 1985). These include higher transconductance due to the proximity of the channel to the surface and the increased carrier density, higher breakdown voltage due to the lower electric field between the gate and channel and good high frequency linearity due to the linear dependence of the gate-source capacitance on the gate voltage. Non-alloyed ohmic source and drain contacts have been produced using δ layers near the surface (Ploog et al, 1987). δ layers have also been used as a source of carriers in modulation doped heterostructures as discussed in the reviews of Ploog et al (1987) and Schubert (1990a).

Sawtooth doping superlattices, consisting of a series of alternating N and P type δ layers in an undoped background with a period in the range 10-200nm, show a number of features common to doping superlattices. As shown in figure 2.2, these include spatial separation of electrons and holes resulting in an enhanced recombination lifetime and a reduced energy gap between electron and hole ground states compared to the host semiconductor. A third important property is the tunability of this gap by the injection of carriers which accumulate in the potential wells thus compensating the ionized impurity charge

and increasing the effective energy gap. This leads to a number of interesting optical properties (Schubert, 1990a) and has important applications in the area of semiconductor lasers, offering the prospect of operation at shorter wavelengths combined with frequency modulation. Both current injection and optically pumped superlattice lasers using δ doped GaAs have been demonstrated.

2.2 δ Doping in Silicon

Historically, developments in Si MBE have followed those in the III-V systems. The first reported growth of δ layers in Si was by Zeindl et al (1987) who achieved δ doping using Sb, the favoured N type dopant for Si MBE. The dopant profile was deduced from a combination of SIMS and TEM which suggested a layer width of $\sim$2nm. The existance of the V shaped quantum well was demonstrated by tunneling spectroscopy where structure in the differential current-voltage characteristic of a Schottky barrier was attributed to the subband structure of the δ layer. To enable accurate determination of the surface coverage of Sb during the growth interrupt it was necessary to reduce the substrate temperature to about room temperature, where the sticking coefficient of Sb is unity. In order to overcome the well-known surface segregation of Sb the Sb layer was buried by a thin amorphous Si cap of thickness $\sim$3nm deposited at room temperature which was subsequently recrystallized at 700°C using "solid phase epitaxy". An alternative method of overcoming these difficulties is to use a low energy (ie. a few hundred eV) ion beam as a dopant source, this technique has been used to produce Sb (Li et al, 1989) and As (Denhoff et al, 1989) δ layers in Si.

Eisele (1989) reported the growth of Sb δ layers in Si with a range of sheet densities from $\sim 10^{12}cm^{-2}$ to $>5x10^{14}cm^{-2}$ and, from TEM analysis, noted precipitates at doping levels $\sim 5x10^{14}cm^{-2}$. The degree of activation was investigated using Hall measurements carried out at 4.2K to freeze out parallel conduction paths. A maximum sheet density $>10^{14}cm^{-2}$ was obtained. The Hall mobility for the degenerate samples was almost independent of sheet density with a maximum value of $\sim 100cm^2V^{-1}s^{-1}$. A more thorough investigation into Sb δ layers was carried out by Van Gorkum et al (1989) where more accurate surface coverages were obtained by saturation coverage of Sb followed by partial desorption at a substrate temperature of 750°C. Hall measurements were used to determine a saturation sheet density of $8x10^{13}cm^{-2}$. Rutherford back-scattering was used to confirm that a large fraction of the Sb was not on lattice sites for a saturated Sb layer. The carrier distribution was investigated using C-V profiling which yielded extremely sharp carrier profiles which were modelled classically (Van Gorkum and Yamaguchi, 1990) in contrast to the quantum mechanical model developed for profiles obtained in GaAs (Schubert et al, 1987, 1990b). The range of applicability of these models is discussed in Chapter 5.

The growth of the first reported P type δ layers in Si (Mattey et al,1988) is fully described in Chapter 3. Other attempts at producing B δ layers using a compound B source (HBO_2) were hampered by surface segregation effects resulting from the necessity to use substrate temperatures >700°C to prevent oxygen incorporation (Tatsumi et al, 1988). The use of Ga in combination with the technique developed for Sb δ layers has also been reported (Zeindl et al, 1990), however Ga has the disadvantage of being a relatively deep acceptor and

is incompletely activated even at room temperature, although the degree of activation increases at high doping levels ($>10^{19}cm^{-3}$) due to the formation of an impurity band.

Device applications for δ layers in Si have also centred around FET structures. Zeindl et al (1989) reported the fabrication of a MESFET with a degenerate conducting channel, similar to that shown in figure 1.1. However, this prototype device was produced by crude in-house processing techniques resulting in gate dimensions of 2mm x 5mm and had to be operated at low temperature (in practice 4K) to freeze out parallel conduction paths. The high doping level meant that the channel could not be fully depleted before breakdown of the Schottky gate and thus the device could not be turned off. More satisfactory structures were produced following computer simulations (Yamaguchi and Shiraki, 1988) which also suggested that a δ layer of opposite type incorporated below the δ layer channel would act as a punch-through stopper in short gate applications. Depletion mode MOSFETs with gate length 2μm have been produced using these designs (Yamaguchi et al, 1988) and have shown complete pinch-off of the drain current as compared to conventional MOSFETs (also depletion mode) of the same geometry which could not be pinched off.

The possibility of optoelectronic applications for δ layers in Si arises from the intersubband spacing allowing direct transitions in the infra-red (IR). Park et al (1990) have reported the observation of hole intersubband absorption using Fourier transform infra-red spectroscopy with a structure consisting of ten B quasi-δ layers separated by 30nm of nominally undoped Si. The degree of absorption was found to be about a factor of four larger than that reported for

$GaAs/Al_xGa_{1-x}As$ quantum wells, although the resonance peaks were somewhat broader which was attributed to the non-parabolicity of the hole bands. The wavelength of the absorption peaks was also shown to be tunable by varying the doping sheet density. Tempel et al (1990) reported an IR detector based on a tunnel structure consisting an Sb δ layer 20nm below a Schottky contact. The structure was fashioned into a waveguide with the ends polished at an angle of 45° so that the IR beam made multiple passes through the δ layer. The device was cooled to 4.2K and illuminated with IR where it was found that the tunnel current was modulated by the IR signal.

2.3. Transport in δ Layers

Dohler (1978) pointed out the advantages of a 2D system consisting of a thin doping spike buried in an opposite type background as compared to the Si MOSFET inversion layer which has had a major role in the invesigation of transport in 2D, as discussed in the review by Pepper (1985). These advantages centre around the the location of the 2D carrier gas in a relatively homogeneous background rather than at the Si/SiO_2 interface where there are problems associated with interface charge, the interface structure is likely to deviate from ideal and where the differing dielectric constants on each side of the interface lead to image potentials. The doping spike also represents a well defined random impurity distribution which makes this system suitable for the study of metal-insulator transitions in 2D.

In contrast to the $GaAs/Al_xGa_{1-x}As$ modulation doped heterojunction which has been extensively used in the study of the integer and fractional quantum Hall

effect along with 1D, 0D and ballistic transport (see for example, Harris et al, 1989), the δ doping system is highly disordered, having carrier mobilities of below 100 $cm^2V^{-1}s^{-1}$ as compared to 10^5-$10^6 cm^2V^{-1}s^{-1}$ in the heterojunction.

Another area of interest in 2D systems arises from the work of Abrahams et al (1979) which suggested that there was an abscence of extended states in 2D - ie. all states are localised and there is no such thing as a truly metallic 2D system. This "weak localisation" appears as a logarithmic correction to the Boltzmann conductivity. It was subsequently found that a logarithmic correction also arises from electron-electron interactions in a disordered system (Alshuler et al, 1980, 1981, Fukuyama, 1980). The logarithmic correction was first observed in thin metal films (Dolan and Osheroff, 1979) and in Si inversion layers (Bishop et al,1980). Uren et al (1980) were able to separate the weak localisation and interaction effects in a Si inversion layer using a magnetic field. These effects have also been observed in GaAs/$Al_xGa_{1-x}As$ heterostructures (Poole et al, 1981) where the increased electron screening length, as compared to Si, gives rise to interaction effects at zero magnetic field. Weak localisation and electron-electron interaction effects are discussed more fully in Chapter 5.

Despite the potential for the study of transport in 2D using δ layers, little work has been reported in this area:

In the III-V systems Schubnikov de Haas oscillations have been used to study the subband energies and occupations (Gillmann et al, 1988, Cheng et al, 1989), the quantum Hall effect has been observed (Gillmann et al, 1988) along with the magnetic field induced metal-insulator transition (Zrenner et al, 1988). Strong localisation effects have been investigated by Ye et al (1989, 1990) using

a system of 20 Si δ layers in GaAs where variable range hopping with a value of 1/3 for the exponent in Mott's law (ie. $\sigma \approx \exp (T/T_0)^{1/3}$) was reported, however this value is open to question (Koch, 1990). The anisotropy of the magnetoresistance was taken as evidence for the 2D nature of the system with the expected shrinkage of the donor Bohr radius with increasing magnetic field giving rise to a positive high field magnetoresistance which was larger for perpendicular than for parallel fields. At low fields, $<1T$, a negative magnetoresistance was observed which was attributed to quantum interference between different hopping paths between initial and final states.

For δ layers in Si the work carried out by Zeindl et al. (1988) and Van Gorkum et al (1989) identified a metal-insulator transition at a sheet density of $\sim 1x10^{13}cm^{-2}$ for Sb layers, a similar value being obtained for As (Denhoff et al, 1989) and for B (Mattey et al, 1991) δ layers in Si. These values of critical sheet density are significantly in excess of what would be expected based on the average impurity separation for the transition observed in 3D (Mattey et al, 1990). Hui-Min et al (1989) observed strong freeze-out for Sb δ layers of sheet density $\leq 2.6x10^{12}cm^{-2}$ and note that even this sheet density is greater than would be expected for bulk Sb doped Si, their data suggests a critical sheet density of $\sim 5x10^{12}cm^{-2}$, although a limited number of low temperature measurements were undertaken.

Van Gorkum et al (1989) analysed the behaviour of the resistivity and Hall coefficient of a non-metallic sample in terms of activated transport with hopping conduction being dominant at low temperatures, however no comment was made on the elevated critical sheet density for the metal-insulator transition. Denhoff

et al (1989) asserted, from unpublished magnetoresistance data, that the metal-insulator transition in As δ layers is driven by the opening of the Coulomb gap caused by the 2D electron-electron interaction.

The angular dependence of the magnetoresistance of an Sb δ layer in Si has been used to confirm the 2D nature of the system (Van Gorkum et al, 1989), whereby a cosine dependance was found between the magnetoresistance and the angle of the magnetic field with respect to the δ layer in a plane perpendicular to the current flow. Thus the magnetoresistance depended only upon the component of magnetic field normal to the plane of the δ layer which suggested that the conduction is limited to a layer much thinner than the cyclotron radius ($\sim$30nm at 1T). The maximum value of the magnetoresistance amounted to $\sim$3% with a field of 1T at a temperature of 4K, the observation of a negative magnetoresistance was noted as "interesting" but could not be explained. It is possible that the negative magnetoresistance arises from the supression of weak localisation by the magnetic field (see Chapter 5.). Denhoff et al (1989) report that magnetoresistance measurements on an As δ layer revealed weak localisation and electron-electron interaction effects, however, to the best of the author's knowledge, these results remain unpublished.

This thesis describes the first major study of the transport properties of B δ layers.

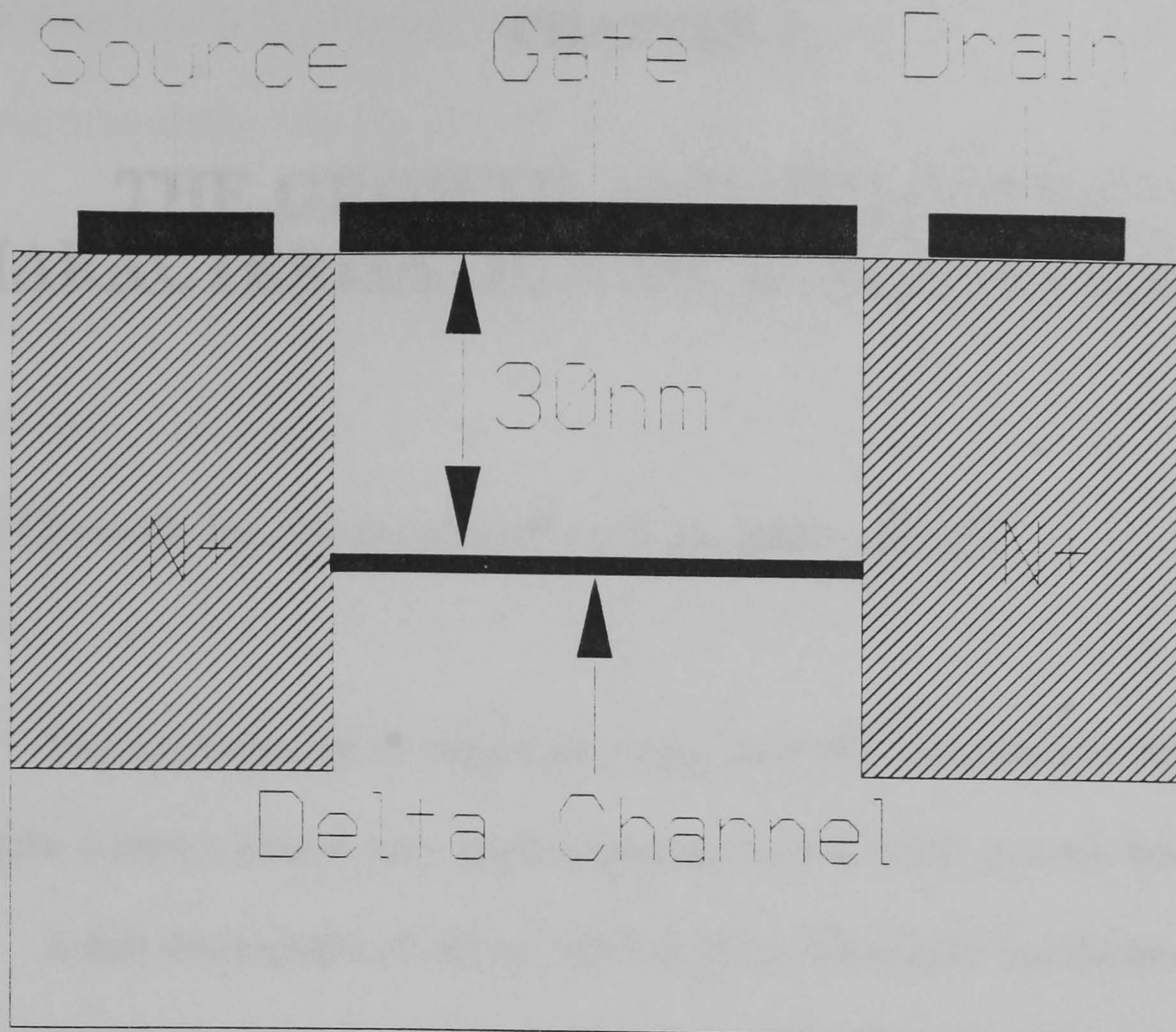

Figure 2.1

Schematic diagram of the δMESFET.

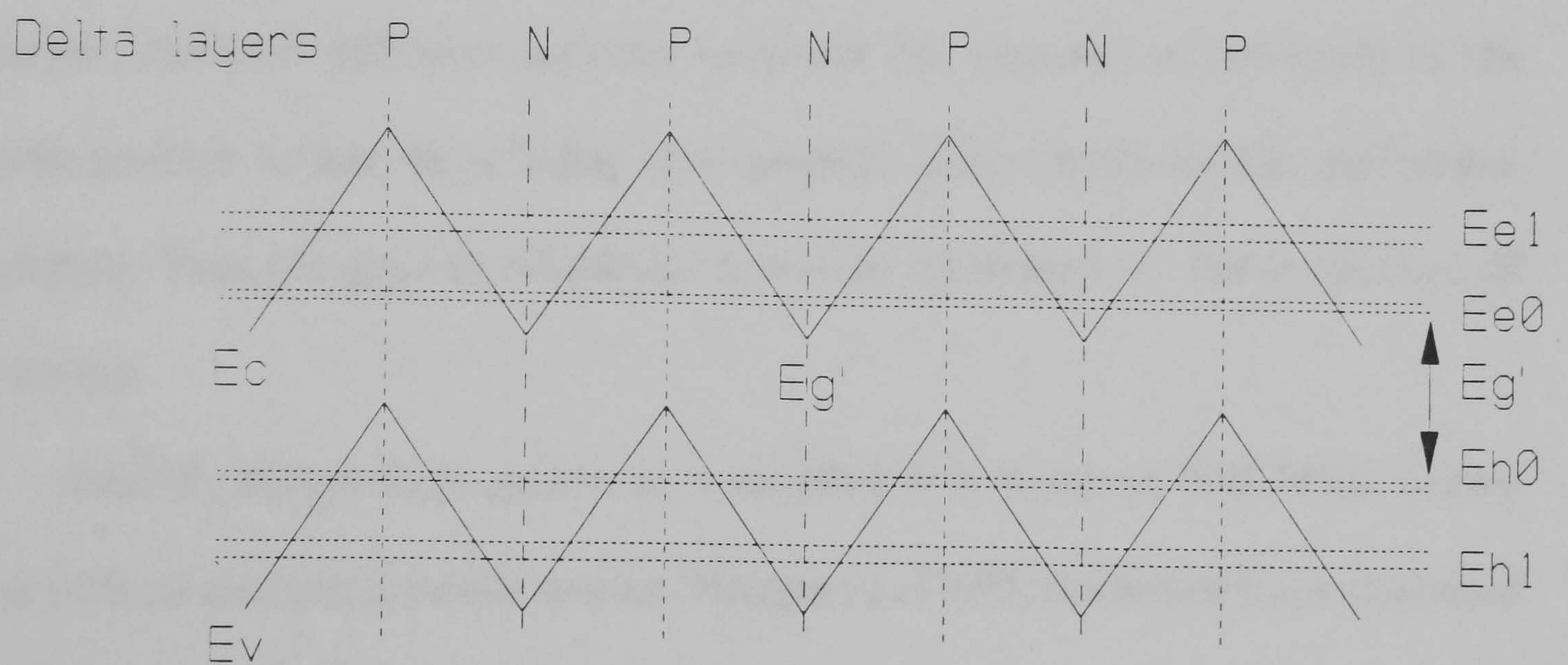

Figure 2.2

Band diagram of the sawtooth doping superlattice showing the effective bandgap E_g'.

CHAPTER 3.

THE GROWTH AND STRUCTURAL CHARACTERISATION OF BORON δ LAYERS.

3.1 Growth by Molecular Beam Epitaxy (MBE).

The confinement of impurity atoms to a few monolayers (ideally one) to produce δ layers places very high demands on the MBE growth technique.

A full description of silicon MBE is given elsewhere (eg Parker, 1985). The process involves epitaxial (single crystal) growth of Si on a heated Si substrate. An electron beam evaporator is used as a source of Si and dopant fluxes are provided by shuttered thermal effusion cells. To ensure high purity the process is carried out in an ultra-high vacuum environment. Growth occurs two-dimensionally offering the prospect of monolayer resolution of doping profile. However, thermal diffusion and the tendency for dopants to segregate at the growth surface rather than being incorporated place limits on the achievable resolution. Thus the growth conditions had to be optimised for the production of B δ layers.

Initially layers were grown in a modifed VG Semicon V80 MBE system fitted with an elemental boron source (Houghton, 1990). Standard back-damaged (100) substrates were used. Following a flux clean to desorb the native oxide, the substrate temperature, T_s, was lowered to 700°C and the interface buried by 0.3μm Si doped at $1x10^{16}cm^{-3}$ with boron grown at a rate of 0.5 nms^{-1} followed

by 0.4μm of Sb doping at $1x10^{16}cm^{-3}$. T_s was lowered to 400°C and growth interrupted whilst the layer was exposed to a B flux of $5x10^{11}cm^{-2}s^{-1}$ for between 40s and 240s to give surface coverages in the range $2x10^{12}cm^{-2}$ to $1x10^{13}cm^{-2}$, since B has a unity sticking coefficient. The reduction in T_s serves to limit diffusion of the B layer, any further reduction being undesirable due to the incorporation of hydrocarbons at temperatures below about 350°C. Finally T_s was returned to 700°C and a 100nm cap grown at a rate of $0.65nms^{-1}$. This stage being intended to provide complete activation of the δ layer along with good crystallinity in the capping layer.

This was the first reported successful growth of B δ layers (Mattey et al, 1988), a previous attempt having produced smeared profiles and only 70% activation (Tatsumi, 1988) due to the necessity of using growth tempertures above 700°C to prevent incorporation of O from the HBO_2 source along with possible clustering effects also common to compound sources.

The majority of layers used in this study were grown in a new generation VG Semicon V90S MBE system which is optimised for low growth rates and extremely high uniformity, as required for the growth of SiGe structures. Wafer diameters can be up to 150mm, although 75mm diameter wafers have to be used where processing at the Edinburgh Microfabrication Facility is required.

The growth method used in the V80 system had to be modified since the heater response time in the V90S system precludes rapid changes of temperature due to its physical size.

Also the understanding of B doping at low temperatures had advanced. A number of authors (Jorke and Kibble, 1990, Parry et al, 1991a) have identified

transitions from equilibrium to kinetically limited incorporation enabling doping above the bulk solid solubility limits at low temperatures, the transition temperature being dependent on growth rate. Any B flux above the incorporation limit under given conditions accumulates on the surface and will smear the profile as it incorporates after termination of the B flux. It has also been established that the Si(100) surface can accomodate a maximum of ~ 0.5 monolayers (one monolayer is equivalent to a sheet density of $6.8x10^{14}cm^{-2}$) of B and remain 100% electrically active (Headrick et al, 1990). In this case the surface undergoes a (2x1) reconstruction and an ordered layer may be preserved by low temperature epitaxial overgrowth (at 300°C). This effect is not observed without a growth interrupt, a saturation coverage of ~ 0.25 monolayers has been reported for continuous growth (Parry et al, 1991b).

The general conclusion is that for high B doping levels and high resolution a low growth temperature and a high growth rate are required given the constraint of achieving good material quality (Kubiak and Parry, 1991).

With regard to these factors the δ layers were grown as follows:

After a flux clean at 850°C the Si buffer layer was grown, doped as required, at a rate of $0.1nms^{-1}$ whilst T_s was reduced to ~ 480°C. The Si source was shuttered and the layer exposed to a B flux of between $10^9cm^{-2}s^{-1}$ and $10^{12}cm^{-2}s^{-1}$ for up to 10 minutes to achieve surface coverages in the range $10^{12}cm^{-2}$ to $3x10^{14}cm^{-2}$. The exposure time being a compromise between being long enough to ensure that accurate coverages are obtained and not so long as to lead to excessive unintentional impurity incorporation. Finally, the Si shutter was opened and the cap grown with T_s remaining at 480°C, since it was found that this

produced complete activation up to $3.5x10^{14}cm^{-2}$, the maximum level attainable (see Chapter 6).

3.2. Structural and Compostional Characterisation.

Having grown the layers it is necessary to confirm that they are δ doped, ie no excessive broadening has occurred during growth, and that the sheet density is as intended. Initially a quick check was provided using the well-known bevel and stain technique. A sample containing a B δ layer in an N-type background was bevelled at an angle of $\sim 0.1^{\circ}$ using a proprietry solution (Syton). A commercial stain which delineates P-N junctions was applied and the sample illuminated.

Three main, more quantitative, techniques have been used during the course of this study:

3.2(a). Secondary Ion Mass Spectroscopy (SIMS).

SIMS can provide information on the depth distribution of an impurity species within a sample. A full description of SIMS is given in a number of reviews (eg Clegg, 1990). The basic process involves directing a beam of primary ions, in this case O_2^+, at the sample which results in material being sputtered from the surface. The resulting secondary ions are directed to a mass spectrometer tuned to the species of interest. Thus a plot of counts versus time

is obtained which may be converted to concentration using a suitable calibration (generally an ion implanted standard) and to depth by measuring the final depth of the crater and assuming a constant erosion rate.

However the interaction of the ion beam with the sample leads to recoil implantation and atomic mixing effects which result in the SIMS profile differing from the true impurity distribution, although the integrated profile will give the total impurity dose. These effects are dependent upon the primary ion energy, generally decreasing the primary ion energy improves the depth resolution. However it is necessary to maintain a sufficient count rate which in turn depends on the beam current which decreases with energy. In practice a primary ion energy of 450 eV/O^+ was the minimum attainable using EVA2000 (a quadrupole instrument using O_2^+ ions at normal incidence). A further complication arises from the assumption of constant erosion rate. At the start of a profile there is a finite time before equilibrium is established. During this time, which increases with primary ion energy, an "altered layer" (in this case SiO_2) is established at the surface (Dowsett et al, 1988). The net effect is the "differential shift" - the apparent depth of a given feature decreases with increasing primary ion energy (Wittmaack and Wach, 1981).

In order to assess the impact of these effects on the SIMS profiles of δ layers a range of profiles were taken through a B δ layer of nominal sheet density $1x10^{13}cm^{-2}$. These results are presented in Chapter 6.1.

3.2(b). Cross-sectional Transmission Electron Microscopy (XTEM).

To provide confirmation of the results of the SIMS analysis XTEM was also undertaken. The technique has been developed for strained systems (Baxter, 1988). Mass contrast has been successfully used to image Sb δ layers in Si (Zeindl et al, 1987), the δ layer being seen as a dark line of width $\sim$2nm in a bright field image of a (110) oriented cross-section. This contrast mechanism cannot be applied to the lighter B atoms. However the B δ layer should lead to a degree of lattice strain which it should be possible to image.

Samples of sheet density $1\text{x}10^{13}\text{cm}^{-2}$ and $3.5\text{x}10^{14}\text{cm}^{-2}$ (the maximum attainable) were examined, the results are discussed in Chapter 6.1.

3.2(c). X-Ray Diffraction (XRD).

X-ray diffraction techniques, having the advantages of ease of sample preparation and being non-destructive, have been applied extensively to strained epitaxial layers (Dineen and Sherwood, 1989). The differences in lattice parameter between the components of a mismatched system lead to changes in the Bragg angle for a given reflection. Due to the small degree of lattice mismatch generally encountered double crystal XRD techniques are almost invariably necessary, single crystal techniques being hampered by the angular

width of the reflection due to the beam divergance. Since a highly B doped δ layer should produce an appreciable degree of lattice strain, it was though likely that XRD would have a role in characterising these layers.

Double crystal XRD was undertaken using a Bede 150 diffractometer with a monolithic four bounce channel-cut (004) beam conditioner used to enhance the fringe contrast in the region close to the Si (004) substrate reflection (Powell, Mattey, Whall, Parker and Bowen, 1991). Both (004) and (113) glancing incidence reflections were used since it was found necessary to consider two reflections to obtain unambiguously the degree of strain present.

In order to achieve maximum strain a sample of the maximum sheet density attainable ($3.5 \times 10^{14} cm^{-2}$) was used. To determine the structure of the B layer the rocking curves were simulated, using dynamical diffraction theory, for various strain profiles (Powell et al, 1991a,b). The results are presented in Chapter 6.1.

Chapter 4.

ELECTRICAL MEASUREMENTS

4.1 Capacitance-voltage profiling

4.1a) Sample preparation

For C-V measurements an ohmic contact to the substrate and a Schottky contact, of well defined area, to the epilayer surface are required.

Samples about 1cm square were taken from a wafer. The ohmic contact to the heavily doped substrate was made by sputtering aluminium in an Iontec Microvac 350 sputter coating system with a base pressure of 5×10^{-8} torr and an operating pressure of about 3 militorr of high purity argon.

The Schottky barrier proved much more problematic, as discussed in Chapter 6.

4.1b) C-V Measurement

Prior to C-V profiling the sample was mounted on a Wentworth Laboratories MP1000W probe station and the I-V characteristic determined using a Hewlett Packard 4145B parameter analyser. Providing the I-V characteristic was saisfactory, the diode was connected to a Hewlett Packard 4192A LF impedance analyser.

To measure the depletion capacitance of the diode as a function of applied bias, a small AC voltage, v_c is added to a steady state bias, V_b and a phase-sensitive detector used to measure the component of current, I_o 90° in advance of v_c. This gives the required capacitance as a function of V_b provided v_c is small compared to the steps in V_b. This assumes, however, that the diode can be adequetely modelled as a simple parallel RC network as shown in figure 4.1a). If there is a significant series resistance, R_s as shown in figure 4.1b), the measured capacitance, C_m will differ from the "true" capacitance, C the error increasing with frequency.

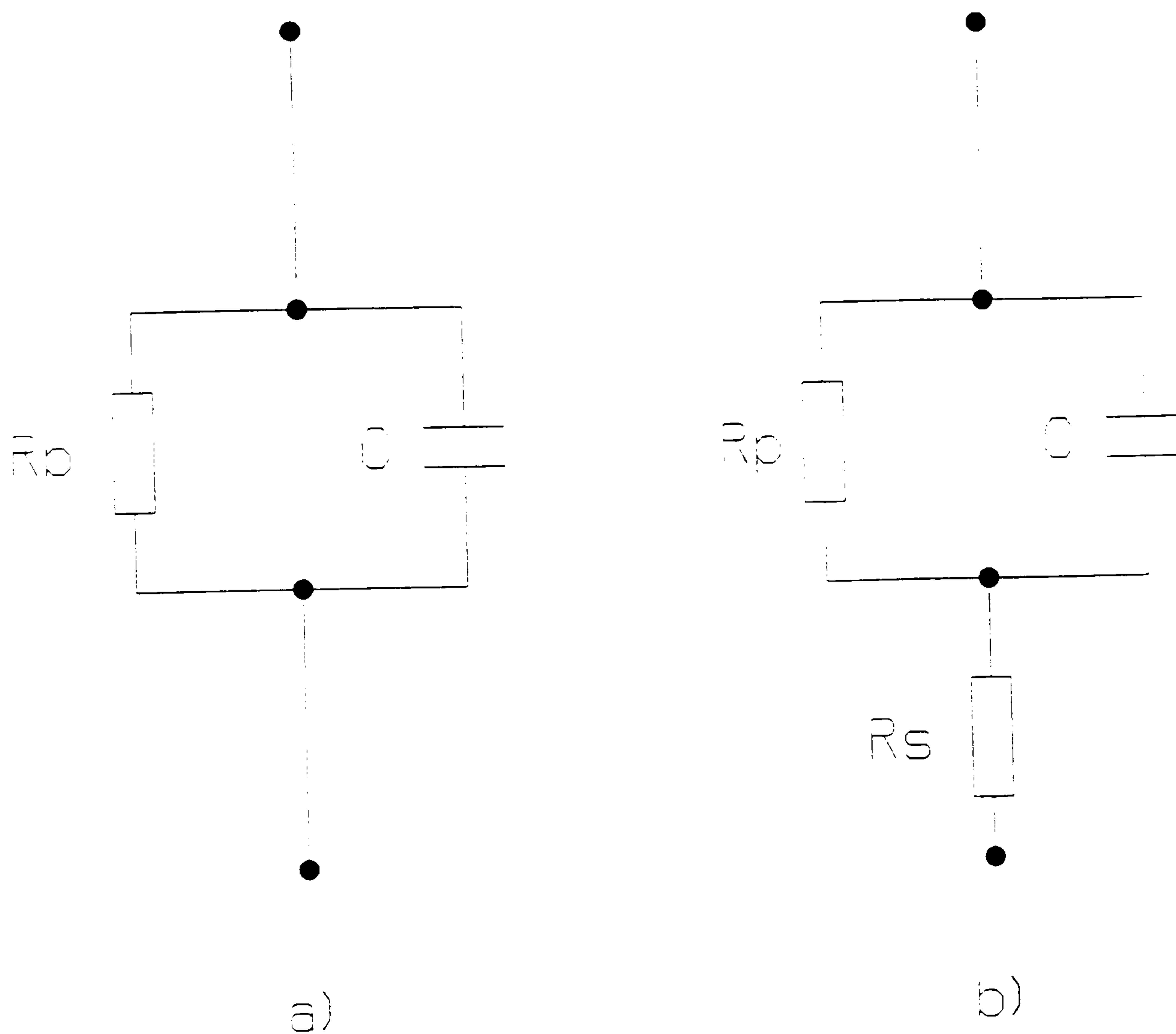

Figure 4.1

Equivalent circuits for: a) parallel resistance.

b) series and parallel resistances.

A number of authors have considered this problem (Blood,1986, Humer-Hager,1988) and have shown that,

$$\frac{C_m}{C}=\frac{1}{[1+(R_s/R_p)]^2+(\omega R_s C)^2} \tag{4.1}$$

where R_p is the parallel resistance and ω is the angular frequency.

The initial work on C-V profiling had to be carried out on non-optimised structures grown on low doped substrates (Mattey et al, 1990) where the ohmic contact was made to the δ layer. Thus, as the layer is depleted an increasing series resistance is presented. The problem was initially solved by the use of a low operating frequency (300 Hz), however errors can then result from the presence of deep states (Blood,1986). It has been shown that the value of R_s, R_p and C may be determined from measurements of admittance at two frequencies (Humer-Hager,1988). For the equivalent circuit of figure 4.1b) with admittance Y and $x=R_p\omega C$,

$$\frac{1}{Y}=R_s+R_p\left[\frac{1}{(\ +x^2)}\right]-iR_p\left[\frac{x}{(1+x^2)}\right]1. \tag{4.2}$$

Splitting Y into real and imaginary components and eliminating R_p then gives,

$$x=\frac{Im\ Y}{(Re\ Y-|Y|^2R_s)}\ . \tag{4.3}$$

$$With\ \omega C = x/R_p\ and\ Im\ Y = |Y|^2 R_p [x/(1+x^2)]\ . \qquad (4.4)$$

$$\omega C = \left[\frac{|Y|^2}{Im\ Y}\right]\left[\frac{x^2}{(1+x^2)}\right] \qquad (4.5)$$

If R_pC is assumed to be independent of frequency, then an expression for R_s is given from the measured capacitances C_{mi}, conductances G_{mi}, and admittances Y_i at frequencies ω_i (i=1,2) can be obtained from equation (4.4).

After determining R_s, C is determined using equation (4.5) and R_p from equation (4.4) (given that $R_p = x/\omega C$). The corrected capacitance value is then used to calculate the apparent carrier concentration,N and depth, d.

4.1c) The automation of C-V measurements

The impedance analyser was interfaced to a BBC Master microcomputer via the IEEE bus. Software was written to automate the C-V measurement. Values of start and stop bias, bias step, oscillator level and frequency were input. One or two frequency measurements could be employed. The data was collected and the values of C and G, corrected where necessary, versus V_b, output to disc for future analysis. The carrier versus depth profile was then produced from equations (4.1) and (4.2), the value of dC/dV_b being determined by differentiating a polynomial fit to the data.

4.2 Transport Measurements.

4.2a) Sample Preparation

Whilst it is possible to make resistivity measurements on samples of arbitrary shape (Van der Pauw, 1957), a bridge shaped specimen enables the separation of the tensor components of the resistivity and allows compliance with international standards for the measurement of resistivity and Hall coefficient (ASTM F 76-73, 1978). It is possible to fabricate Greek cross structures (the preferred geometry for the Van der Pauw technique (Wieder,1979)) by "painting" the cross onto the epilayer surface with wax dissolved in xylene, allowing the wax to harden, and removing the remaining epilayer using a CP4A etch. Contact is then made to the δ layer by smearing Ga-In eutectic over the ends of the cross. This, of course, also makes contact to the substrate however, if the substrate is doped below $\sim 10^{18}$ cm^{-3} it will be highly resistive compared to a "metallic" δ layer at low temperature. This method is limited to highly doped samples and is only really suited to spot measurements at 4.2K.

In view of the previous success of the group in modifying standard MOS processes to produce devices from MBE grown material (Smith et al,1988), it was decided to follow this route to produce Hall bar structures for transport measurements. At the same time provision was made for the fabrication of FET structures using a δ layer as channel (Van Gorkum et al, 1989). A mask set was designed to produce a range of Hall bars, MESFETs and MOSFETs along with a number of other structures on a 3mm x 3mm chip with processing carried out by the Edinburgh Microfabrication Facility.

In order to prevent excessive degradation of the δ layer profile due to

thermal diffusion it is necessary to modify a number of the conventional process steps. Thermal oxidation cannot be used, temperatures of 1000°C for several hours are required. Experiments attempting to reduce this temperature to ~600°C were unsuccessful, producing only 5nm of poor quality oxide after 24 hours. For routine passivation an oxide deposited at 435°C, generally used as a masking layer, has been employed. This is known to be of insufficient quality for a gate oxide (Smith et al,1990). CVD oxidation was used to produce a gate oxide in the first N-channel devices (Van Gorkum et al ,1989), but was unavailable at Edinburgh. However a room-temperature plasma-grown oxide of a quality approaching thermal had been developed at Liverpool University (Taylor et al, 1987), therefore it was decided to attempt to utilise this oxide in combination with the remaining processing at Edinburgh. Initial experiments were unsuccessful due to contamination of the wafers in transit between Edinburgh and Liverpool, this was solved by use of a full RCA clean prior to oxidation.

The other main problem is in implant activation. Ion implanted contact regions are used to form ohmic contact to the δ layer since the depth and concentration of dopant can be accurately controlled hence avoiding contact to the substrate. However, in order to ensure that the implanted species is electrically activated and to anneal the amorphised region, a high temperature anneal at ~1000°C for several minutes is usually employed. Previously, satisfactory activation had been obtained by inserting the wafers into a furnace at 1000°C for ~15s (Smith et al, 1988). Following the installation of rapid thermal process (RTP) facilities at Edinburgh a more repeatable, better characterised anneal at 950°C for 10s with 6s ramp up and down was found to

provide complete activation (DeLima,1990) and was employed for the later layers.

The implant activation has, by far, the most significant impact on the "thermal budget", the remaining processing using a maximum temperature of 435°C for 30 minutes. Analysis of x-ray rocking curves on a number of annealled samples has demonstrated no significant broadening of the δ layer for temperatures of $< \sim 750°C$ (Powell et al,1991). Figure 4.2 shows resolution-limited SIMS profiles taken on a B δ layer before and after annealing in a furnace at 1000°C for 30s using 2.2 keV/O^+ primary ions at normal incidence. Within experimental error, there is no change in the width of the two profiles (the FWHM is ~15nm). This places an upper limit on the FWHM of ~5nm (Mattey et al,1990). Modelling the more recent RTP anneal using the values of the bulk diffusion coefficient predicts a maximum broadening of ~ 1nm (O'Neill, 1991).

The third area of proccessing which had to be addressed was the infilling of the isolation trenches used to define the active area of the δFET devices in order that the aluminium tracks to the bonding pads do not break as they traverse the trench. Rather than use high temperature oxides or nitrides, the use of polyimide was invesigated. Polyimide was spun onto the wafer in solution and baked. It was found that this provided effective planarisation with the added advantage of its excellent dielectric properties. The only disadvantage is the relatively poor adhesion of the aluminium bonding pads to the polyimide which makes probing and bonding more difficult.

On receiving the processed material from Edinburgh, each wafer was

probed using a Wentworth Laboratories MP1000W probe station and Hewlett Packard 4145B parameter analyser to check for ohmic contacts and isolation from the substrate. Satisfactory chips were mounted in ceramic headers using silver loaded epoxy resin and the apropriate devices connected to the leadouts using a Kuliche and Soffa model 4124 thermosonic gold ball bonder.

Besides producing the Hall bar structures used in this study, the first P-channel δMOSFETs have recently been produced using the process sequence developed during this work (Biswas, 1991).

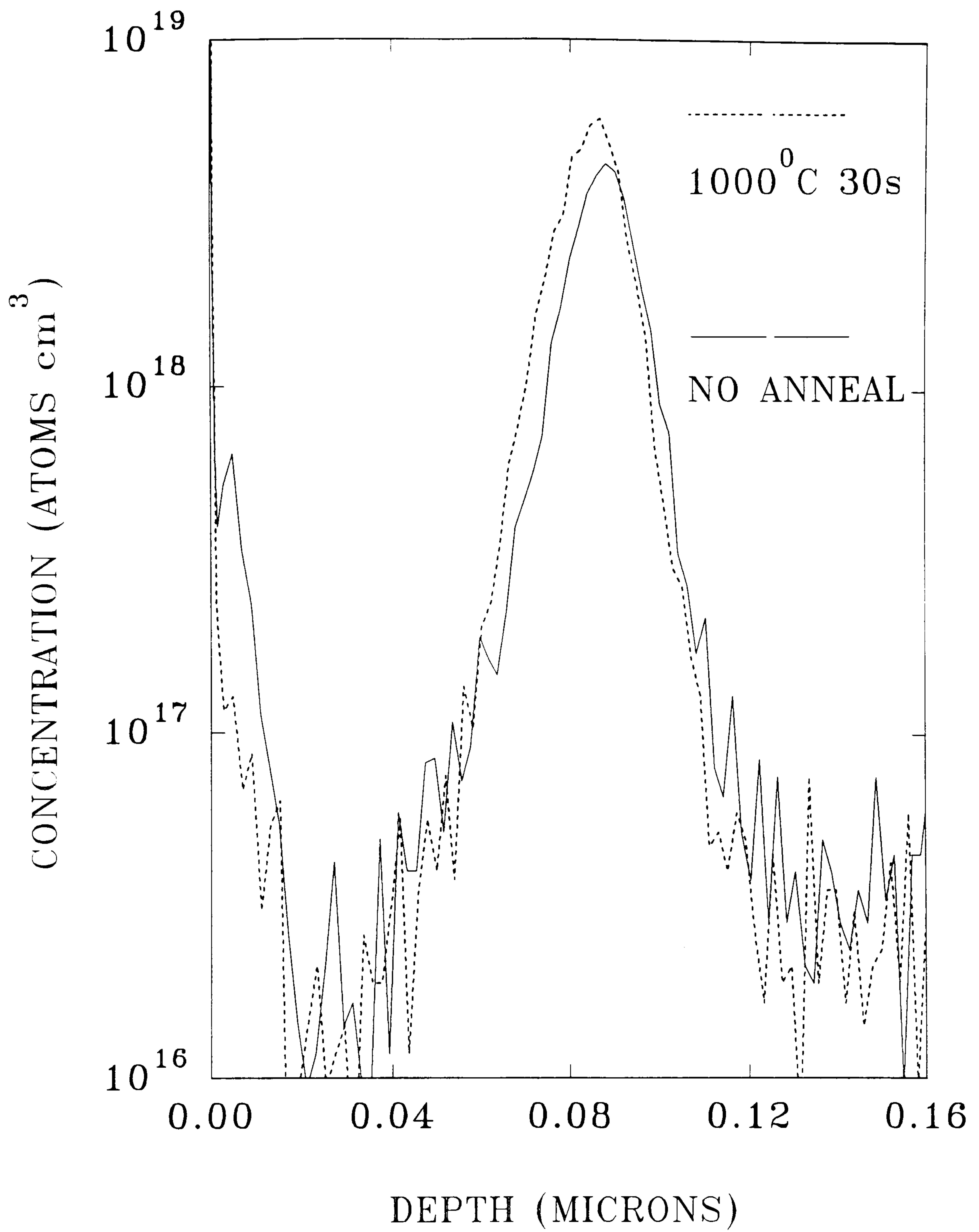

Figure 4.2

SIMS profile of Annealled δ layer.

4.2b) Cryogenics

For the low temperature measurements a commercial closed cycle ^{3}He cryomagnetic system (Oxford Instruments) was used. The insert had a temperature range of 0.3K to 300K with temperature control to +/-.005K at the lower end (rising to +/-0.1K). A magnetic field of 12T was attainable with the magnet at 4.2K, although there was the provision to cool the magnet to 2.2K providing a maximum field of 15T, albeit with a considerable rise in ^{4}He consumption. A top loading system enabled samples to be exchanged without warming up the whole system, although the turn-around time amounted to several hours. The sample space was 20mm in diameter with a field homogeneity of 1 part in 10^3 over 10mm at the magnet centre.

The chip carrier containing the sample was mounted on a copper block containing the calibrated thermometers using a low temperature varnish (GE). The copper block was in turn mounted on the brass block at the end of the insert containing the heater and temperature control sensor.

For measurements on Hall bars constantan wiring connected through a ten-pole seal was used, however this set-up was only suitable for samples of resistance up to $10^7\Omega$. For high impedance measurements (up to $10^{11}\Omega$) the two co-axial lines provided were used for two-probe measurements.

4.2c) Thermometry

The cryostat was fitted with carbon resistors for diagnostics and temperature control. These have the advantages of low cost and, in the case of the Speer resistor fitted to the insert, a relatively small magnetoresistance making

them generally suitable for temperature control in high magnetic fields (a temperature error of <5% has been reported in fields as high as 15T (Oxford Instruments)). The disadvantage of these sensors is their poor reproducibility. However, it was found that the temperture could not be maintained with sufficient accuracy for some magnetoresistance measurements carried out at high fields. In order to overcome this a capactive sensor and bridge with a quoted accuracy of <0.05% in fields of 10T (LakeShore Cryogenics) was used for the high field measurements.

For an accurate determination of the sample temperature suitable calibrated thermometers were used:

For temperatures in the range 0.3K to 6K a germanium resistor (LakeShore cryogenics GR-200A-100) was used. A 38 point calibration against standards based on the ITS-90 above 0.65K and a scale generated using a cerium magnesium nitrate magnetic thermometer in conjunction with NBS superconducting fixed points SRM76 below 0.65K. A series of two fits each using 7th order Chebychev polynomials were supplied:

$$T(x) = \sum a_n t_n(x) \tag{4.7}$$

Where T(x) is the temperature (in Kelvin), a_n represents the Chebychev coefficients, $t_n(x)$ is a Chebychev polynomial and x is a normalized parameter given by,

with Z= $Log_{10}R$ (R is the resistance), Z_u and Z_l represent the limits of Z over the

$$x=\frac{(Z-Z_l)-(Z_u-Z)}{(Z_u-Z_l)} \tag{4.8}$$

range of the fit. The Chebychev polynomials are generated from:

$$t_n=\cos[n \times \arccos(x)] \tag{4.9}$$

The maximum error of the fit is quoted at 0.75mK (LakeShore cryogenics).

The resistance of the sensor was measured using a four-probe technique with current reversal to overcome thermal offsets employing a Keithley model 224 programmable current source and a model 181 nanovoltmeter. The current flowing through the resistor was adjusted to maintain the voltage at about 0.1mV for temperatures below 1K and at around 1mV above this temperature in order to minimise self-heating errors(LakeShore cryogenics). It was found that for low currents ($< \sim 20$nA), the absolute current value was subject to unacceptable error. To overcome this a model 485 picoammeter was used to determine the actual current flowing through the resistor.

For temperatures above 6K a commercially available silicon diode thermometer was used (SMDT, obtained from the Institute of Cryogenics, University of Southampton). A 70 point calibration over the range 1.56K to 300K with a forward-bias current of 10μA was provided by the Cryogenic Facilities Group at Oxford University. A series of five polynomial fits have been calculated (Phillips et al 1989) from which the temperature T(x) is,

$$T(x)=\sum a_n x^n \tag{4.10}$$

with x a normalised voltage,

$$x=\frac{(V-V_l)-(V_u-V)}{(V_u-V_l)} \tag{4.11}$$

where V_u and V_l are the limits of voltage, V, at the extremities of each range.

The voltage was measured using a four-probe technique by a Keithley model 181 nanovoltmeter which combines the necessary high input impedance ($>1G\Omega$) with high resolution (better than $10\mu V$). The $10\mu A$ constant current was provided by a Keithley model 224 current source.

4.2d) Transport measurements

For measurements of resistivity, magnetoresistance and Hall effect the circuit shown in figure 4.3 was used. A Brookdeal model 5209 lock-in amplifier was used both to measure voltage and as an excitation source. The use of such an A.C. technique enabled a high degree of noise immunity to be maintained whilst accomplishing the necessary averaging of the unwanted thermoelectric and thermomagnetic voltages also measured in the Hall efect (Weider, 1979).

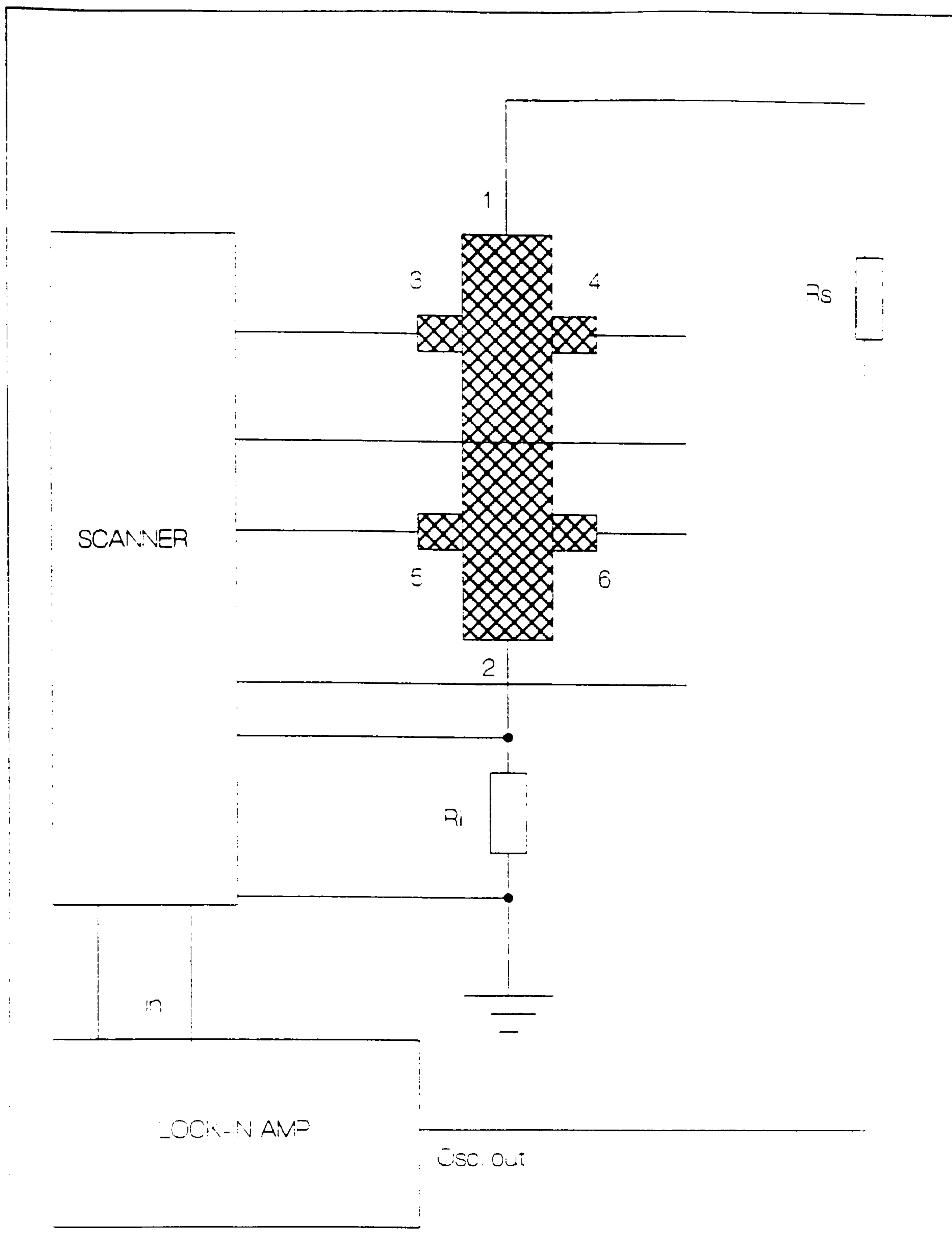

Figure 4. 3

The circuit used to measure resistivity, Hall coefficient and magnetoresistance.

The oscillator output was sourced through a high value resistance, R_s (compared to the sample resistance) in order to provide a constant current, a low frequency, typically 9Hz, being used to provide quasi D.C. conditions. A Keithley model 705 scanner fitted with low-voltage card was used to connect the different Hall bar configurations to the differential input of the lock-in amplifier. A small value resistor, R_i, nominally of resistance 1kΩ, was connected in series with the sample to enable the current flow to be determined.

The sheet resistance, $R_{\square}$, was determined from the voltages $v_{3,5}$ and $v_{4,6}$ (see figure 4.3),

$$R_{\square} = \left(\frac{v_{3,5}+v_{4,6}}{2}\right)\frac{R_i w}{v_i d} \tag{4.12}$$

where v_i is the voltage across the current sensing resistor R_i. The Hall coefficient with magnetic field B was obtained from,

$$R_H = \left[\frac{\left(\frac{v_{6,5}^{+B}-v_{6,5}^{-B}}{2}\right)+\left(\frac{v_{3,4}^{+B}-v_{3,4}^{-B}}{2}\right)}{2}\right]\frac{R_i}{v_i B} \tag{4.13}$$

and the magnetoresistance from,

$$R_{\square B} = \left(\frac{R_{\square}^{+B}+R_{\square}^{-B}}{2}\right) \tag{4.14}$$

The input impedance of the 5209 lock-in amplifier is 100MΩ which limits the sample resistance to <10MΩ, preferably <1MΩ, a condition easily fulfilled for "metallic" samples. However, samples on the insulating side of metal-

insulator transition are considerably more resistive at low temperatures. It was also found that the cryostat wiring and connectors imposed a limit to the sample resistance of $\sim 10^7\Omega$ and that the inert design precluded fitting the six co-axial lines necessary for a full Hall bar measurement. However, two co-axial lines were available and it was considered that the errors imposed by a two-probe measurement would be negligible on high resistance samples, although such an arrangement precludes any measurement of transverse resistivity components. A Keithley 616 electrometer was used for the high impedance measurements. It was found that the sample isolation was limited to typically, $\sim 2\text{x}10^{12}$ Ω, enabling measuremnts to an impedance of about $10^{11}\Omega$.

4.2e) Computer control

In order to ease the colletion of data a BBC Master computer was used with a Procyon IEEE interface to control the instrumentation. Menu-driven software was written to automate resistivity, Hall effect and magnetoresistance measurements, as required. The sample temperature was continuously monitored with selection between the Ge resistor and Si diode according to temperature range, measurements being averaged over ten readings to improve accuracy. The lock-in amplifier and scanner were controlled to select the appropriate configuration and range. Before and after each measurement of sample voltage, the sample current was determined by measuring the voltage across the series resistor, R_i. Finally the data was saved to disc in a format enabling subsequent extraction of any parameter for plotting or further analysis. A hardcopy was provided as back-up.

Chapter 5.

THEORY

5.1 The δ Layer as a 2D System

The ionized impurities in the δ layer will form a "V" shaped quantum well provided that the δ layer sheet density is sufficient that the average impurity spacing is sufficienly less than the Bohr radius, in practice this amounts to a sheet density of $\geq 1\text{x}10^{13}\text{cm}^{-2}$ in Si. Figure 5.1a shows the situation for P-type Si,. holes remain close to the ionised acceptors forming a 2D hole gas with motion quantised perpendicular to the growth direction. At lower doping levels the random impurity distribution in the plane of the δ layer renders this description invaild.

In order to determine accurately the subband structure and occupation it is necessary to solve self-consistently Poisson's and Schrodinger's equations. This is difficult to achieve in practice, although a number of authors have produced results for N-type δ layers in Si using techniques of varying degrees of sophistication. The approximate subband energies may be obtained following the simple analytical method developed by Schubert et al (1986) for GaAs. The charge distribution, $N_a(x)$ is described by a Dirac δ function:

$$N_a = N_a^{2D}\delta(x) \tag{5.1}$$

Where N_a^{2D} is the δ layer sheet doping density. The shape of the top of the

valence band is then obtained by solving Poisson's equation to give,

$$\frac{dE}{dx} = -\frac{e^2}{2\varepsilon_r\varepsilon_0} N_a^{2D} \qquad x>0 \tag{5.2}$$

with the hole energy E. The de Broglie wavelength is then matched to the well width:

$$\lambda_{dB} = \frac{h}{(2m^* E)^{1/2}} \tag{5.3}$$

$$(n+1)\lambda_{dB} = \left(\frac{2\varepsilon_r\varepsilon_0}{e^2 N_a^{2D}}\right) E \tag{5.4}$$

With n=0,1,2.... Thus the subband energies amount to,

$$E_n = \frac{1}{4}\, 2^{-1/3}\, (n+1)^{2/3} \left[\frac{e^2 h N_a^{2D}}{\varepsilon_r\varepsilon_0 (m^*)^{1/2}}\right]^{2/3} \tag{5.5}$$

and the real space extent of the subbands to,

$$x_n = \frac{(n+1)}{2} \left[\frac{h}{(2m^* E_n)^{1/2}}\right]^{2/3} \tag{5.6}$$

This approach gives similar values for the subband energies to calculations based on the WKB approximation, however, since it ignores the effect of free carriers, the higher subband energies are significantly overestimated.

A more accurate solution was obtained by following the approach of Schubert et al (1986) who propose a simple polygonal model to give an analytic

description of the effect of free carriers. The triangular well is retained with the band bending due to the free carriers assumed to occur at the points x_i where the ith subband intersects the potential well, as shown in figure 5.1b. The subband separation is then given by:

$$E_i - E_{i-1} = \left(\frac{e^2}{2\varepsilon_r\varepsilon_0}\right)\left[N_A^{2D} - \sum_{j=0}^{i-1} n_j\right](x_i - x_{i-1}) \tag{5.7}$$

where the values of x_i are obtained from matching the de Broglie wavelength (equation 5.3) to the well width as above. The carrier density, n_i, in the ith subband may be obtained as a function of the Fermi energy E_F using the density of states,

$$n_i = \left[\frac{m^*}{\pi\hbar^2}\right](E_F - E_i) \tag{5.8}$$

A computer program was written to calculate the subband structure for a given carrier sheet density using equations 5.7 and 5.8. Initially the bare subband energies are obtained from equation 5.5 and the Fermi energy is the set to the bottom of the lowest subband. The Fermi energy is then incremented in 1meV steps and the subband energies recalculated for the given subband occupation. The program is terminated when the subband occupation (the term under the summation sign in equation 5.7 is equal to the acceptor sheet density.

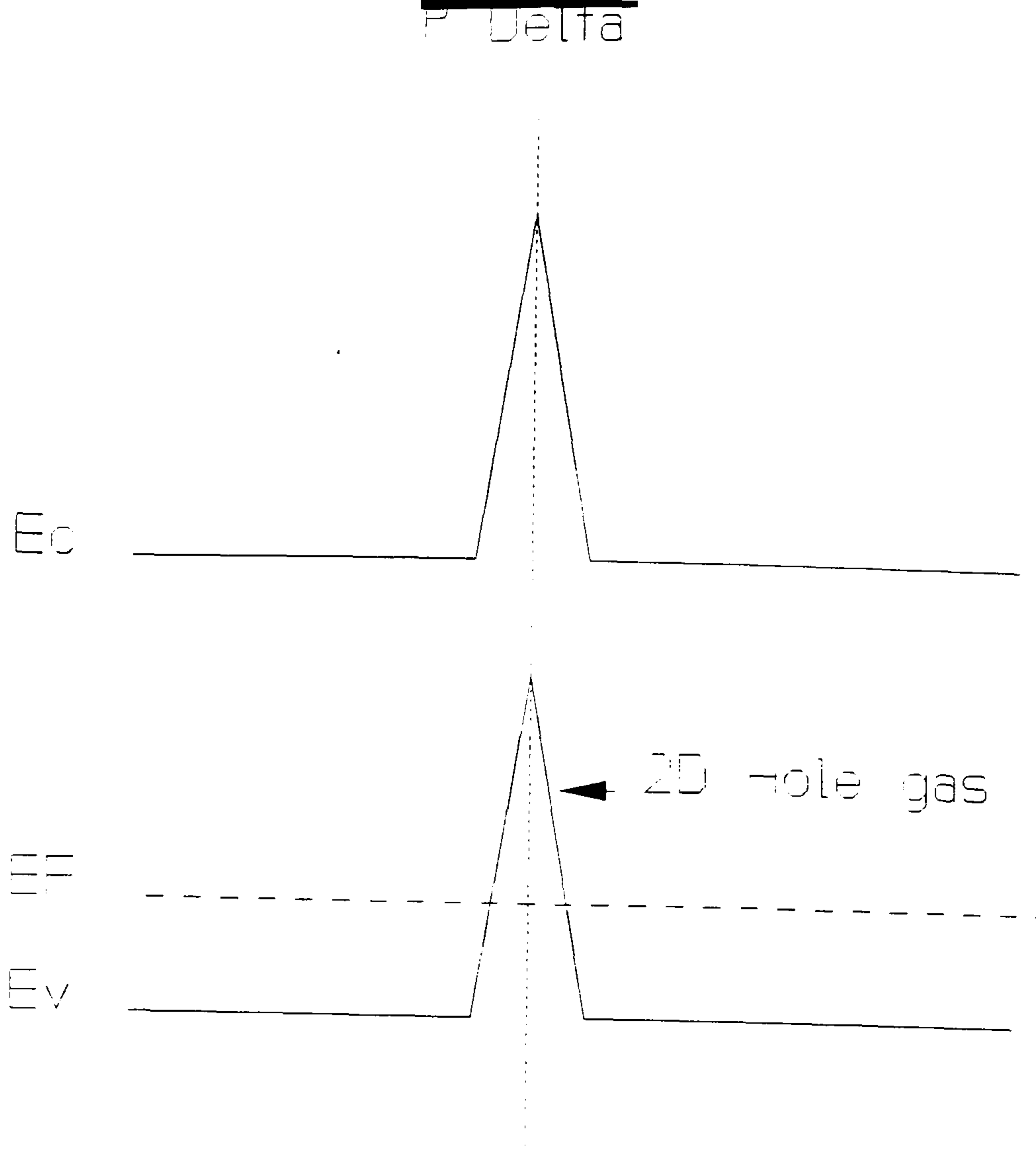

a) "V" shaped quantum well formed by δ layer.

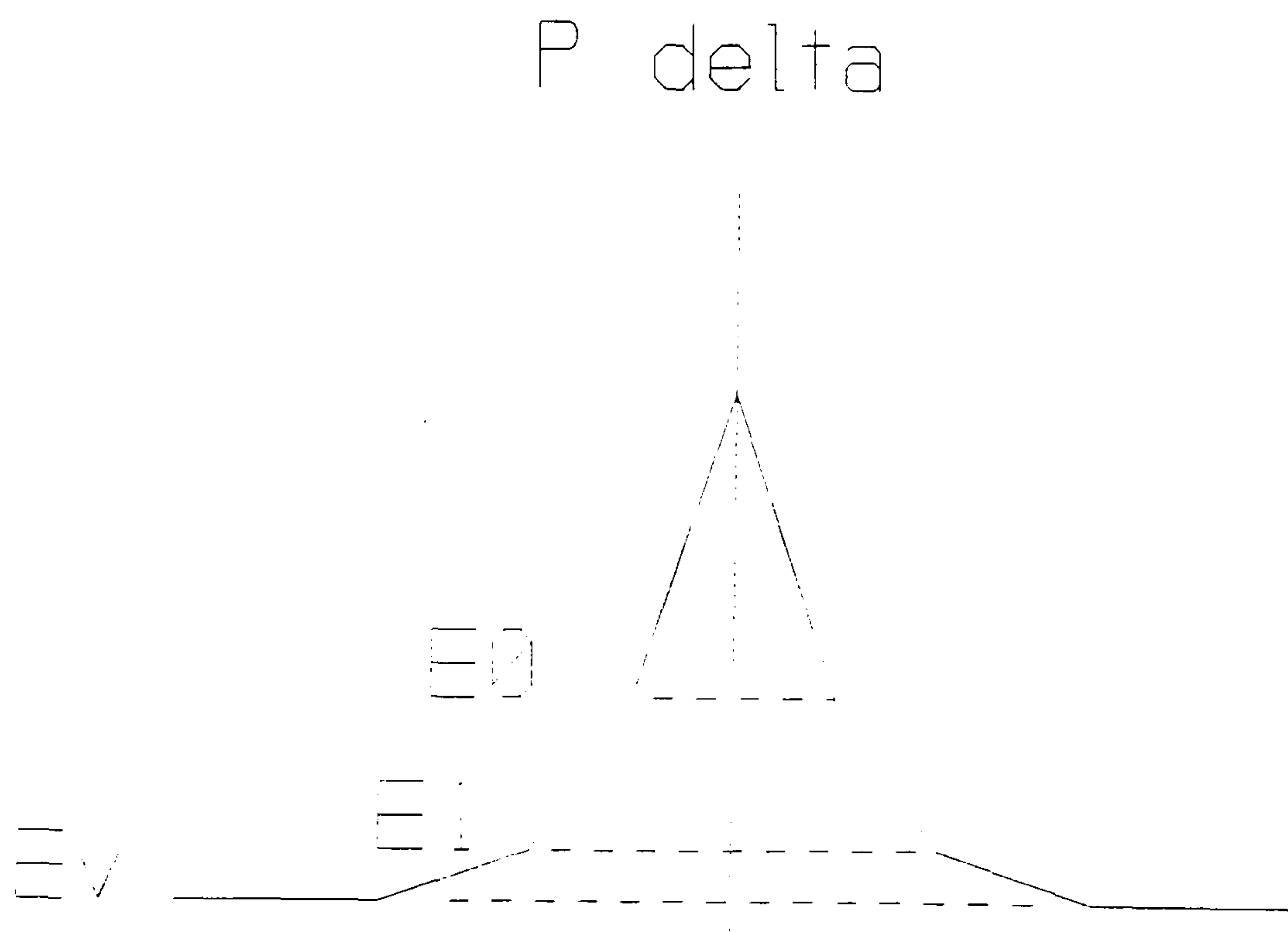

Figure 5.1

b) Polygonal well.

5.2 C-V Profiling

Conventionally, the doping profile of a semiconductor may be obtained from the dependence of the depletion capacitance per unit area, C, of a Schottky contact on the applied reverse bias, V. Within the depletion approximation, the doping concentration, n(x), is given by the well-known equation:

$$n(x)=\frac{-C^3}{e\varepsilon_r\varepsilon_0}\left(\frac{dC}{dV}\right)^{-1} \tag{5.9}$$

With e equal to the electronic charge, the semiconductor relative permitivity ϵ_r and the dielectric constant ϵ_0. The depth, x, of the depletion edge is determined from C,

$$x=\frac{\varepsilon_r\varepsilon_0}{C} \tag{5.10}$$

As was first pointed out by Kennedy et al (1968), n(x) is not, in general, the doping profile, but is the profile of majority carriers. If the doping concentration is constant with depth, then the majority carrier profile will be identical to the doping profile assuming complete activation and the absence of significant trap states. However, for changes in doping profile the carrier profile will change more slowly due to carrier diffusion. The characteristic length scale for the decay of carrier concentration at a change in doping concentration is the Debye-Hückel screening length, L_D, given by,

$$L_D=\left(\frac{\varepsilon_r\varepsilon_0 kT}{e^2N}\right)^{1/2} \tag{5.11}$$

where N is the doping concentration. Thus near an abrupt change in doping

concentration at x_0 (Blood,1986),

$$n(x) \approx e^{\left(\frac{-(x-x_0)^2}{2L_D^2}\right)^{1/2}} \tag{5.12}$$

In the case of degenerate doping the appropriate length scale is the Thomas-Fermi screening length, L_{TF}, given by,

$$L_{TF}=\left(\frac{2}{3}\frac{\varepsilon_r\varepsilon_0(E_F-E_C)}{e^2N}\right)^{1/2} \tag{5.13}$$

Given that L_D is ~4nm in Si at 300K with a doping concentration of $1x10^{18}cm^{-3}$, it is clear tha the C-V profile from a δ layer is likely to be significantly broadened as compared to the doping profile, typically of FWHM <2nm.

The C-V profiles obtained from Sb δ layers in Si have been modelled classically by Van Gorkum et al (1989) and by Wood and O'Neill (1991). The doping profile was assumed to be "top hat" shaped and Poisson's equation solved in one dimension perpendicular to the δ layer using a finite difference technique. The total space charge was calculated from the surface electric field using Gauss' law, the theoretical C-V profile was then used with equations 5.9 and 5.10 to obtain the apparent doping profile which was then compared with experiment.

For very narrow layers or for high doping levels it seems likely that the quantum confinement of the carriers will become important. This has been considered by Schubert et al (1986, 1990) for δ layers in GaAs and by Wood and O'Neill (1991) in Si.

Schubert et al (1986) assert that the width limitation cannot be due to the Debye-Hückel screening length (equation 5.11) since only a very small decrease

in profile width was seen in lowering the temperature from 300K to 77K. The origonal model has been extended to include higher order subbands (Schubert et al,1990) using variational wavefunctions and the general result obtained is that for a quantum confined system the change in position expectation value of the ground state on application of a depleting bias, and hence the resolution of the C-V profile, is comparable to the spatial extent of the ground state wavefunction.

Wood and O'Neill (1991) have investigated the apparent contradiction of the classical and quantum approaches. In the case of N-type δ layers in Si they found that the two approaches can be reconcilled provided all occupied subbands are taken into account. The classical approach being more appropriate for lower sheet densities (in practice $<3x10^{12}cm^{-2}$) where the subband energies lie very close together leading to the occupation of a large number of subbands.

5.3 Transport in 2D Systems

5.3a) Strong Localisation and the Metal-Insulator Transition

The concept of strong localisation was introduced by Anderson (1958) and elucidated in a number of papers by Mott (see for example Mott and Davies, 1978). Within the tight-binding approximation Anderson considered the consequences for a band of width B if a random potential V_0 is added to a crystalline array of potential wells of depth V (with V_0 in the range $\pm V$) as shown in figure 5.2. Anderson showed that above a critical value of V_0/B the electron wavefunctions decay exponentially with distance x as $e^{-\alpha x}$ rather than being the familiar extended Bloch states. The precise value of $(V_0/B)_{crit}$ is difficult to calculate and depends on the co-ordination number, z, but is thought to be ~ 2 for z=6 (Mott,1974).

Mott (eg see Mott and Davies, 1978) pointed out that if the disorder is insufficient to localise all the states in a band a mobility edge, E_c, exists separating localised states in the band tail from extended states. If the Fermi energy, E_F, lies below E_c the zero temperature conductivity is zero. Moreover, as E_F crosses E_c there is a discontinous transition (the Anderson transition) to a conductivity σ_{min}, the minimum metallic conductivity given by (in 2D),

$$\sigma_{min} = \frac{Ce^2}{\hbar} \qquad (5.14)$$

where the value of C depends on $(V_0/B)_{crit}$ but is ~ 0.1 (Pepper,1985).

At finite, but low, temperatures when E_F lies in localised states conduction is due to hopping between neighbouring sites, or at the lowest temperatures variable range hopping between sites close in energy to E_F. In this regime the hopping probability ,P (proportional to σ) is

$$P \propto e^{-\left(2\alpha R+\frac{\Delta E}{kT}\right)} \tag{5.15}$$

where R is the distance between sites, α is the inverse Bohr radius and ΔE is some mean energy required to make a hop. In 2D $\Delta E=[\alpha R^2 N(E_F)]^{-1}$ and the optimum inter-site distance may de obtained by putting $dP/dR=0$ giving,

$$P \propto e^{-\left(\frac{3\alpha^2}{N(E_F)kT}\right)^{1/3}} \tag{5.16}$$

Thus Ln σ is proportional to $T^{-1/3}$ for variable range hopping in 2D. In 3D the temperature exponent is 1/4. If the electron-electron is significant a gap (the Coulomb gap) in the density of states results at E_F and a temperature exponent of 1/2 is predicted (Efros and Schlovskii, 1984).

In the case of p-type semiconductors the conductivity at temperatures above the variable range hopping regime is activated and,

$$\sigma(T) = \sum_{i=1}^{3} \sigma_i e^{\frac{-\epsilon_i}{kT}} \tag{5.17}$$

At high temperatures conductivity occurs in the valence band with activation energy ϵ_1 then, as the temperature is reduced, via doubly occupied acceptor states in an upper Hubbard (A^+) band with activation energy ϵ_2 and finally, with activation energy ϵ_3 due to nearest neighbour hopping from a neutral

impurity to an ionised impurity in the lower Hubbard (A^0) band (eg see Mott and Davies, 1979). The activation energy ϵ_2 is not observed for low doping densities.

For a wide variety of materials the critical site concentration, n_c for the onset of metallic behaviour is given by the Mott critereon,

$$n_c^{1/3} a_H^* = 0.26 \pm 0.05 \tag{5.18}$$

where a^*_H is the effective Bohr radius. The value of the numerical constant was obtained by Edwards and Sienko (1978) from consideration of experimental data with a^*_H between .1nm and 100nm, from simple theoretical arguments Mott's origonal value was 0.25.

The metal-insulator transition may also be induced by a magnetic field, the effect of which is to shrink the wavefunctions (ie. the electronic orbits), thus a positive magnetoresistance will result for metallic samples leading, eventually, to a transition to an insulating state (Mott, 1978).

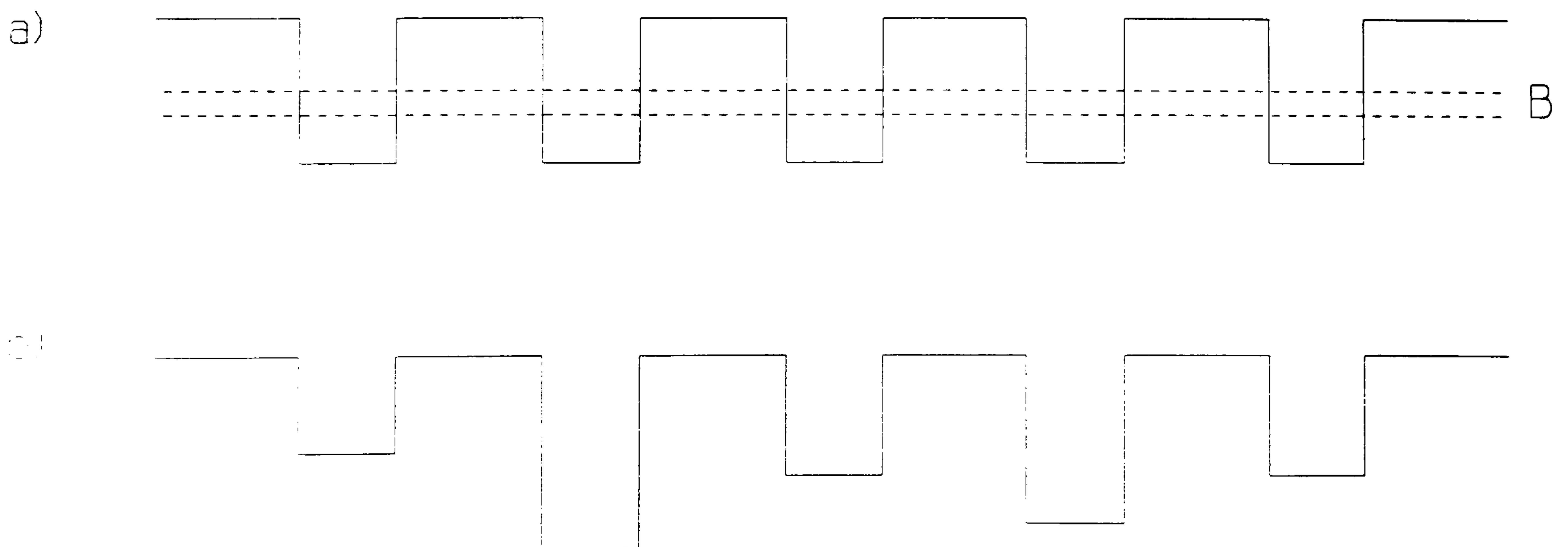

Figure 5.1

Random potential energy proposed by Anderson

a) $V_0=0$

b) V_0/B large

3.3b) Scaling Theory and Weak Localisation

The scaling theory proposed by Abrahams, Anderson, Liccardello and Ramkrishnan (AALR,1979) advanced the understanding of the localisation problem considerably. They considered the behaviour of a d dimensional system of hypercubes of size L^d as its size is scaled.

The separation of energy levels within each cell and hence the energy gap, ΔE between cells is given by

$$\Delta E = \frac{dE}{dn} = \frac{1}{L^d\, N(E)} \qquad (5.19)$$

where N(E) is the density of states (Licardello and Thouless, 1975). The energy of a localised state (ie one where the amplitude of the wavefunction decays exponentially) will obviously be insensitive to the boundary conditions, provided the system is large compared to the localisation length, ζ. Hence the change in energy δE in going from periodic to antiperiodic boundary conditions will be small compared to that for extended states which will be of order ΔE. Thus $\delta E/\Delta E$ is a measure of the localisation (analogous to Anderson's V_0/B)- if $\delta E/\Delta E$ decreases as the size of the system is increased, the system is localised otherwise the states remain extended.

The conductance of the system G(L) is given by,

$$G(L) = \sigma L^{d-2} \qquad (5.20)$$

if the mean free path, l< <L, the conductivity is related to the diffusion constant, D by the Einstein relation hence,

$$G(L) = De^2 N(E) L^{d-2} \qquad (5.21)$$

The electron will thus diffuse across a cell in a time $t = L^2/D$ and the energy uncertainty is,

$$\delta E = \frac{\hbar}{t} \qquad (5.22)$$

Therefore,

$$\frac{\delta E}{\Delta E} = \frac{\delta E}{(dE/dn)} = G(L)\frac{\hbar}{e^2} = g\ L) \qquad (5.23)$$

where g(L), the Thouless number, describes the scaling behaviour. AALR (1979) defined a smooth function ß,

$$\beta = \frac{d Ln g(L)}{d Ln L} \qquad (5.24)$$

The asymptotes of which may be determined from physical arguments:

For ohmic conduction, the conductivity is a material constant, independent of L for L> >l hence,

$$g(L) = \sigma L^{d-2} \quad and \quad \beta_{g \to \infty} = d-2 \qquad (5.25)$$

For exponential localisation, with ζ< <L the conductance behaves as,

$$g = g_0 e^{-\frac{L}{\zeta}} \quad and\ hence \quad \beta_{g\to 0} = Ln\left(\frac{g}{g_o}\right) \tag{5.26}$$

Figure 5.3 shows the behaviour of ß between these extremes as determined by AALR (1979).

In 3D two regimes exist separated by a critical point g_c at ß=0. For $g>g_c$ the system is metallic as ß approaches unity, for $g<g_c$ the system is localised. Hence g_c may be identified with Mott's mobility edge (see Chapter 5.3a). However, there is no discontinous transition to g=0 and the concept of the mimimum metallic conductivity is not supported.

In 2D (and 1D) ß is always negative suggesting the absence of any truly extended states.

The conductivity in 2D has been calculated using perturbation theory in the limit of weak disorder ie. $k_f l >> 1$ (Lee and Ramakrishnan, 1985) to give,

$$\sigma(L) = \sigma_B - \left(\frac{e^2}{\pi^2 \hbar}\right) Ln\left[\frac{L}{l}\right] \tag{5.27}$$

where σ_B is the classical Boltzmann conductivity given by,

$$\sigma_B = \frac{ne^2\tau}{m^*} \tag{5.28}$$

Physically this weak localisation correction to the classical conductivity arises from quantum interference effects first elucidated by Altsuler and Aronov (1985). Figure 5.4 shows an electron diffusing round a closed path of elastic scatterers. If the probability amplitude of the electron traversing the path clockwise is Ψ_1 and that of the electron traversing the path anticlockwise is Ψ_2, the probability, W, of the electron returning to the origin is given by,

$$W=\left[\sum_{1}^{2}\psi_i\right]^2 \qquad (5.29)$$

$$ie. \qquad W=[\psi_1]^2+[\psi_2]^2+[\psi_1^*\psi_2]+[\psi_1\psi_2^*]$$

Since phase is maintained during elastic scattering, ,Ψ_1 and Ψ_2 are coherent each referring to the same path but traversed in opposite directions.

$$Hence \qquad W=4[\psi]^2 \qquad (5.30)$$

Which is equal to twice the classical probability ($2[\Psi]^2$). This tendency to localisation will be reduced by any inelastic process. If τ_ϵ is the inelastic scattering time and τ is the mean free time the conductivity is given by (from equation 5.27,

$$\sigma=\sigma_B-\left(\frac{e^2}{2\pi^2\hbar}\right)Ln\left[\frac{\tau_\varepsilon}{\tau}\right] \qquad (5.31)$$

If τ is independent of temperature T and τ_ϵ depends on temperature as T^{-p}, the conductivity is then,

$$\sigma=\sigma_B-\left(\frac{pe^2}{2\pi^2\hbar}\right)Ln\,T \qquad (5.32)$$

Application of a magnetic field destroys the time reversal symmetry of the wavefunctions leading to the destruction of the interference and hence a negative magnetoresistance. A magnetic de-phasing time τ_m can be defined where a phase change of one radian is induced by the magnetic field, B,

$$\tau_m = \frac{\hbar}{4eBD} \tag{5.33}$$

Provided $\tau_m < \tau_\epsilon$, τ_m should replace τ_ϵ in equation 5.31, leading to,

$$\Delta\sigma(B) = \left(\frac{e^2}{2\pi^2\hbar}\right) Ln\left[\frac{eD\tau_\varepsilon B}{\hbar}\right] \tag{5.34}$$

for the approximate change in conductivity with magnetic field.

The electron spin is neglected in the above argument, however in the presence of spin-orbit coupling the spin no longer a good quantum number and may undergo a change of direction during scattering. The spin dependent term consists of two parts - the triplet state where the two electron wavefunctions carry parallel spins (magnetic quantum number m=-1,0,+1) and the singlet state where the electron wavefunctions carry antiparallel spins. Following Alshuler and Aranov (1985) representing the singlet state by Ψ_{00} and the triplet states by Ψ_{1m}, the interference term I is given by,

$$2I = \left(\sum_{m=-1}^{m=+1} [\psi_{1m}]^2 - [\psi_{00}]^2\right) \tag{5.35}$$

The spin-orbit coupling is dependent on the angle between the electron spin and its momentum. Since the two wavefunctions are equivalent to the electron traversing the path in opposite directions, each scattering centre is approached with opposite velocities (and hence momenta), thus the two types of spin term will be affected differently.

In the case of the singlet state with opposite spins, the spin-orbit interaction will have the same effect on each wavefunction and the two waves will

be in phase at the origin.

In the case of parallel spins, the spin direction will be changed by equal, but opposite, amounts at a scattering centre. Thus after a time τ_{so} (the spin-orbit scattering time), the spins will be randomized and the wavefunctions will tend to cancel each other out at the origin. If $\tau_{so} > \tau_{\epsilon}$ the constructive interference of the triplet state will be destroyed, the interference term becomes $-\frac{1}{2}[\Psi_{00}]^2$ (see equation 5.35), and the correction to the classical conductivity becomes negative-weak antilocalistion. The magnetoresistance will therefore be positive, at least for low fields, at high fields the magnetic de-phasing time, τ_m will become less than τ_{so} and the spin-orbit interaction does not have time to occur, thus the magnetoresistance becomes negative. This effect has been used to determine τ_{so} experimentally (Bergmann, 1985).

It should be noted that in the weak localisation regime the temperature dependence of the Hall mobility is the same as that of the conductance (Fukuyama, 1980) thus $\Delta R_H/R_H=0$ (where R_H is the Hall coefficient).

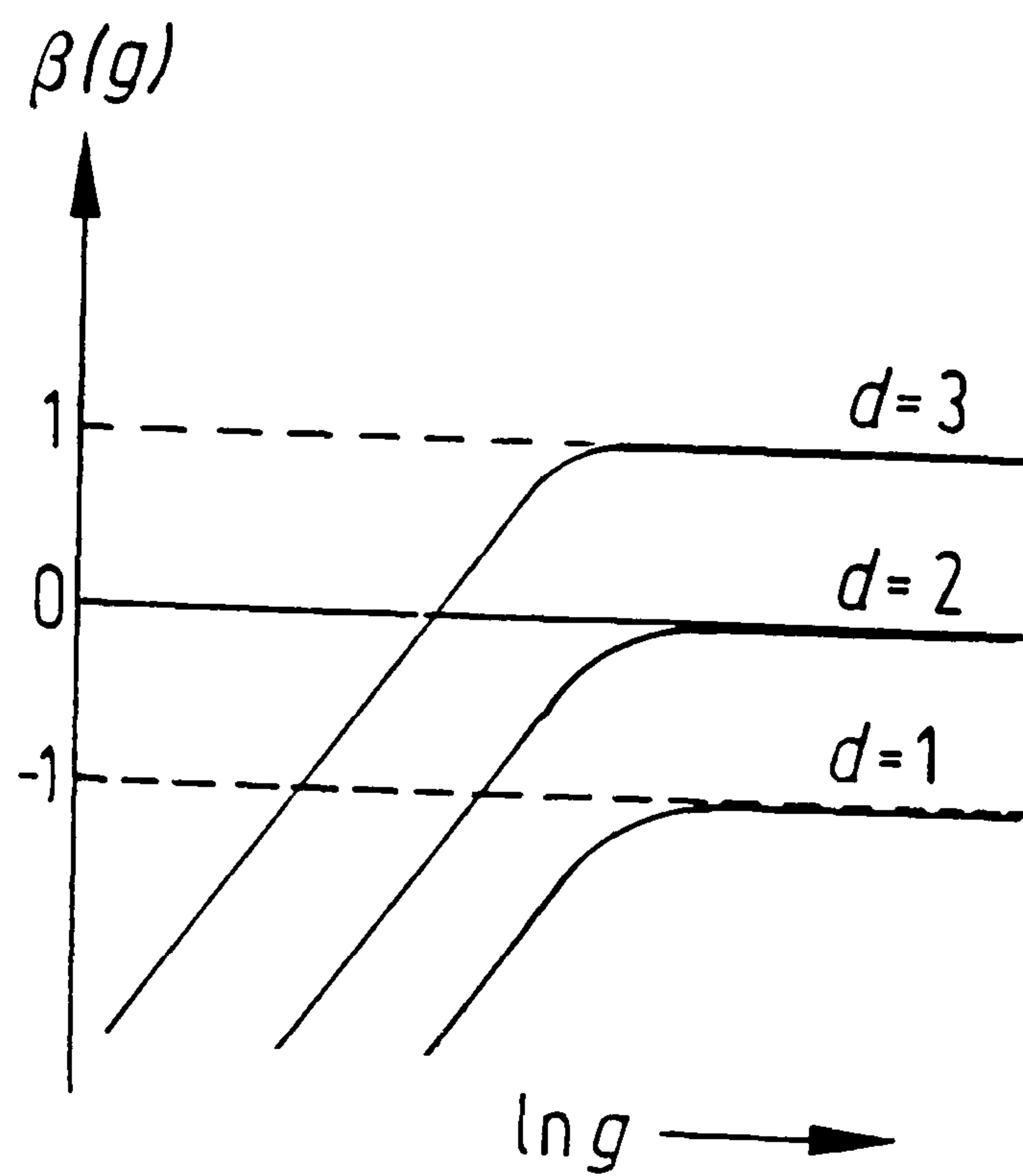

Figure 5.2

Scaling behaviour of conductance (after Kramer et al, 1985).

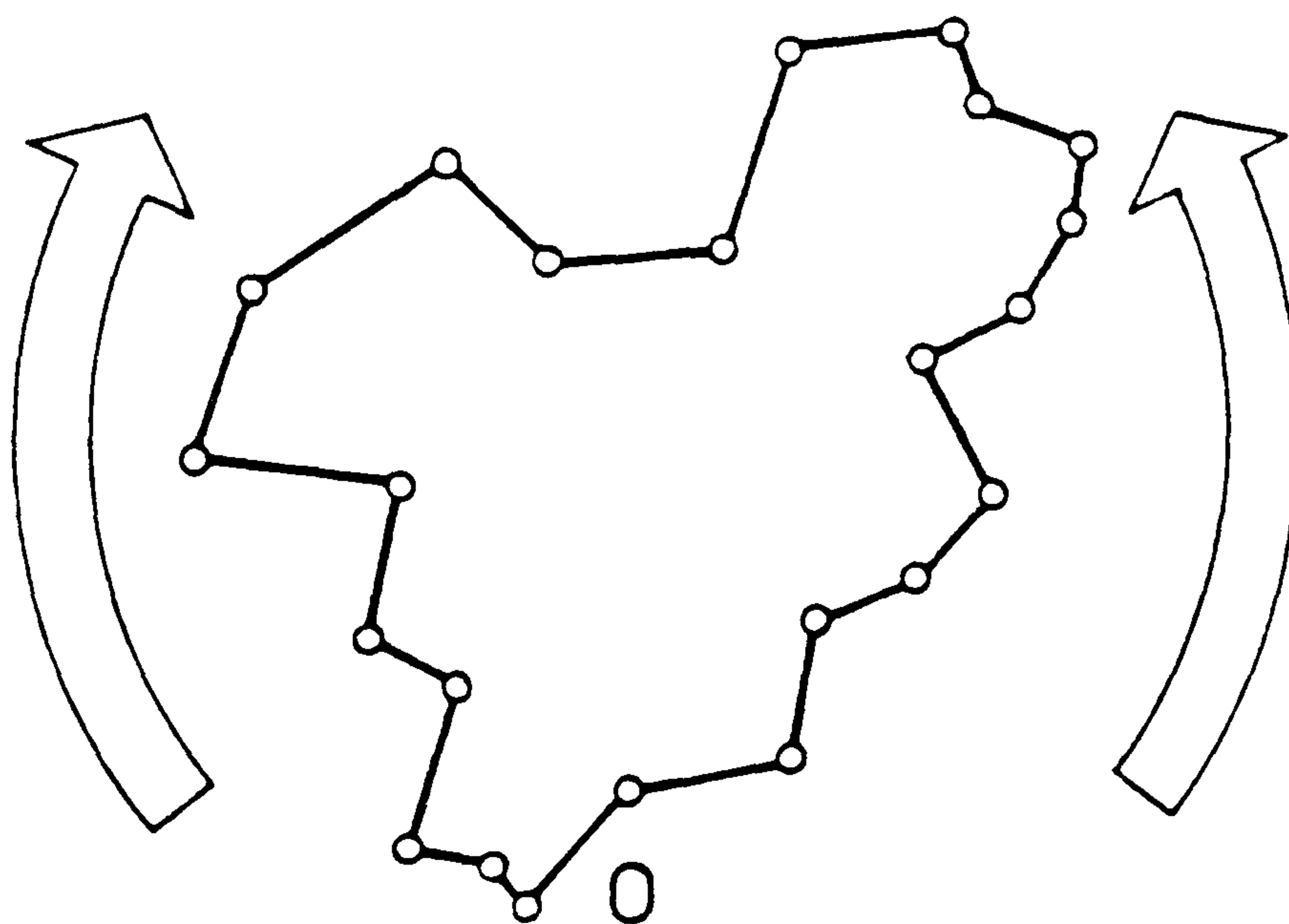

Figure 5.3

Closed path of an electrom diffusing under the influence of elastic scattering (after Dugdale 1987)

5.3c) Electron-Electron Interactions

The above picture ignores electron-electron interactions. Shortly after the logarithmic correction to the Boltzmann conductivity due to weak localisation was discovered, Alshuler et al (1980,1981) and Fukuyama (1980) showed, using diagrammatic perturbation theory, a similar correction could arise from electron-electron interactions in a disordered system.

Bergmann (1987) provided a physical description of the process by which the electron-electron interaction may be enhanced in the presence of disorder. The process involves the interference of two electrons, if the energy difference is of the order of kT, the thermal coherence time, τ_T may be written as,

$$\tau_T \sim \frac{\hbar}{kT} \tag{5.36}$$

Provided $\tau_T > \tau_0$, the elastic scattering time, it is possible that an electron elasically scatterred round a closed path as in Chapter 5.3b may interfere with another electron. Bergmann (1987) coined the phrase 'electron hologram' for the charge pattern established round such a closed path (since it is a record of the phase change associated with traversing the path). It is possible that the second electron will traverse the same path and have the phase change it suffered in traversing the path exactly compensated by the electron hologram. Thus the electron-electron interaction can enhance one electron wavefunction by such holographic processes.

Alternatively one may consider the electron-electron interaction to be enhanced since the electrons remain spatially closer together in the presence of

such elastic scattering process than would plane wave states.

The net effect of the interaction is to produce a Coulomb gap in the density of states at the Fermi energy.

Fukuyama (1980) described the interaction in terms of coupling constants g_i where i=1 and 2 describe the exchange terms ie. those with parallel spin which reduces the Coulomb interaction (due to the Pauli principle) and i=3 and 4 describe the Hartree terms which include the Coulomb interaction but ignore spin effects. The conductivity correction for a single valley amounts to:

$$\delta\sigma_i = \sigma_B \lambda g Ln\left[\frac{4\pi kT\tau}{\hbar}\right] \tag{5.37}$$

where $\lambda(= h/4\pi^2 E_F \tau)$ is a disorder parameter and the g_i depend on the nature of the interactions. According to Fukuyama (1981) $g_1=1$ and $g_2=g_3=g_4=F/2$ for a screened Coulomb interaction where F is a screening parameter.

The magnetoresistance due to interactions arises from orbital and Zeeman spin-splitting effects (Lee and Ramakrishnan, 1985). At low fields the oribtal contibution dominates. Spin-splitting effects become important, giving a positive magnetoresistance due to the suppression of anti-parallel spin interactions once the Zeeman spin-splitting becomes comparable to kT.

5.3d) Corrections due to weak localisation and electron-electron interactions.

Both weak localisation and electron-electron interactions are likely to be present in any real system. The diffusion constant, D, is affected by the weak localisation and the density of states at the Fermi energy, $N(E_F)$ is affected by the

electron-electron interactions. Since these two are related to the conductivity by $\sigma = e^2 D N(E_F)$, the net effect is additive,

$$\frac{\Delta\sigma}{\sigma} = \frac{\Delta D}{D} + \frac{\Delta N(E_F)}{N(E_F)} \tag{5.38}$$

Although both have a logarithmic temperature dependence (in 2D), it is possible to separate the two effects by considering the behaviour of both R and R_H (Uren et al,1980).

Chapter 6.

RESULTS AND DISCUSSION

6.1 Structural Characterisation

Figure 6.1 shows a microdensitometer plot obtained from a bevelled and stained B δ layer which is delineated as a dark line the width of which suggests a δ layer width ~2nm. Although it is not clear exactly what this line represents it is interesting to note that such a crude technique can be applied to such high resolution structures. More quantitative results were obtained from SIMS, TEM and XRD analysis.

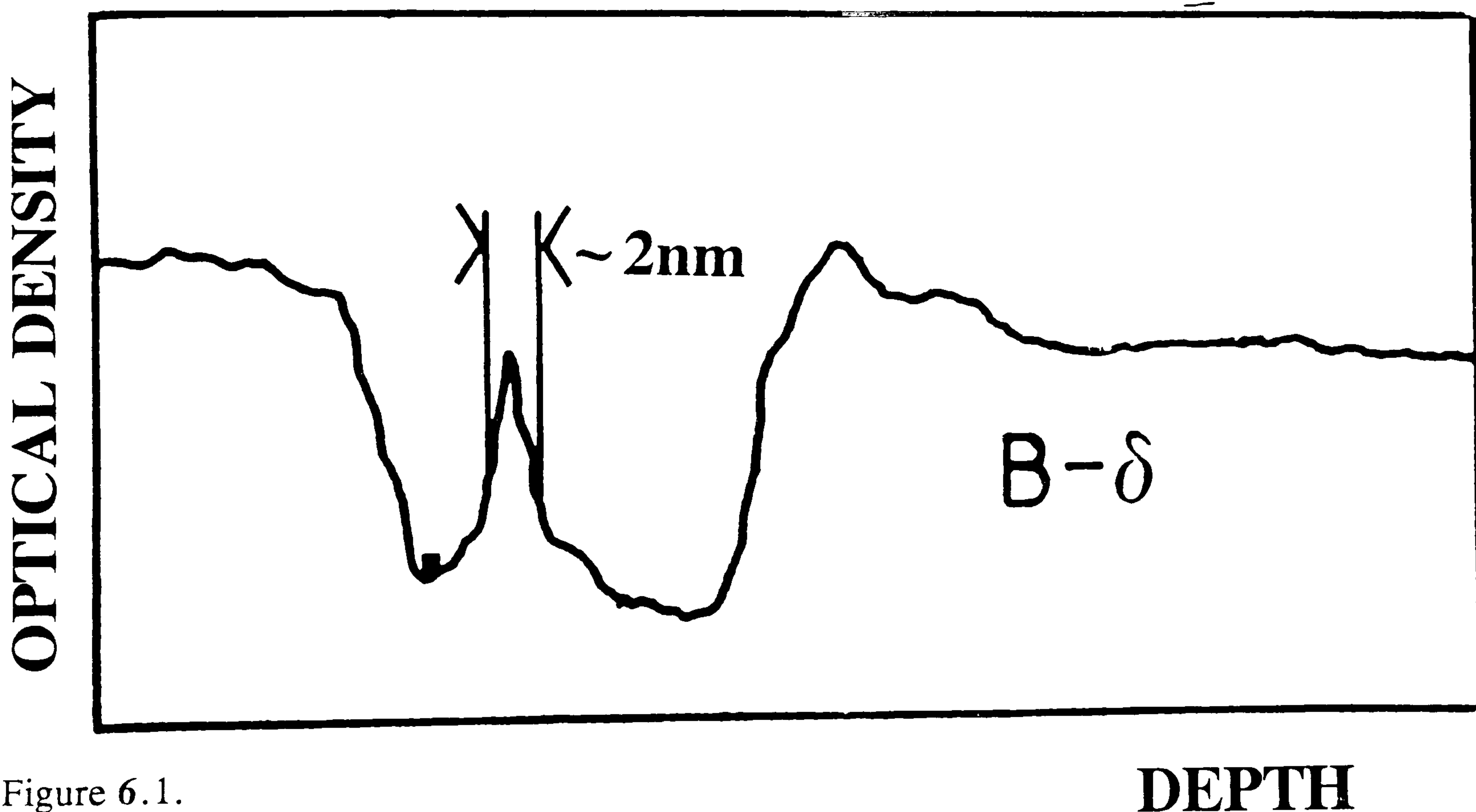

Figure 6.1.

Optical density plotted versus depth along a bevel of angle 0.13° of a stained B δ. The apparent width of the δ layer is ~2nm.

6.1a) SIMS Analysis

Figure 6.2 shows a SIMS depth profile of a sample of nominal sheet density $1x10^{13}cm^{-2}$ taken using extremely low energy primary ions (450 eV/0^+). The measured areal dopant density is $1x10^{13}$ cm^{-2}, in good agreement with the growth schedule and the FWHM is 3.6nm. Also plotted on figure 6.2 is the reconstructed profile at zero impact energy which has FWHM of 2.7nm and was obtained as follows:

A series of SIMS profiles of the δ layer taken with primary ion energy, E_p, in the range 450 eV/0+ to 1.7 keV/0+ showed increasing asymmetry and broadening of the δ profile due to atomic mixing and beam incorporation along with the differential shift (see Chapter 3.2a).

Figures 6.3 and 6.4 show the dependence of the leading and trailing slopes, FWHM, peak concentration and position on E_p. If the broadening and shifting processes are all linearly dependent on energy, these data may be extrapolated to $E_p = 0$ and the reconstructed profile shown in figure 6.2 obtained. However, this reconstruction constrains the profile shape to exponential up and down slopes meeting at a cusp. It is impossible to determine how close this is to the true profile. It is likely that density renormalisation effects (Collins et al, 1985), not intrinsically dependent on E_p, give rise to residual broadening which makes the reconstruction a worst case.

To investigate this further a series of profiles of a shallow (5 keV) boron implant in Si was taken over the same energy range as the delta. Assuming that the decay slope on the δ profile was entirely limited by mixing and incorporation effects, the slope values at each energy were used to correct the decay slope of

the implant profile and extract its true magnitude. This process was found to give an implant profile independent of E_p, showing that, even at 450 eV/0+, the δ profile was entirely due the SIMS process. Hence the true width of the δ layer is narrower than that obtained from the profile at E_p = 450eV by an unknown amount, probably by at least a factor of 2, i.e. the true width is $\leq$ 2nm.

Subsequently δ layers have played an important role in attempting to elucidate the mass transport processes inherent in the SIMS technique and it is thought that they could offer advantages as calibration standards compared to ion implants (Dowsett et al, 1991).

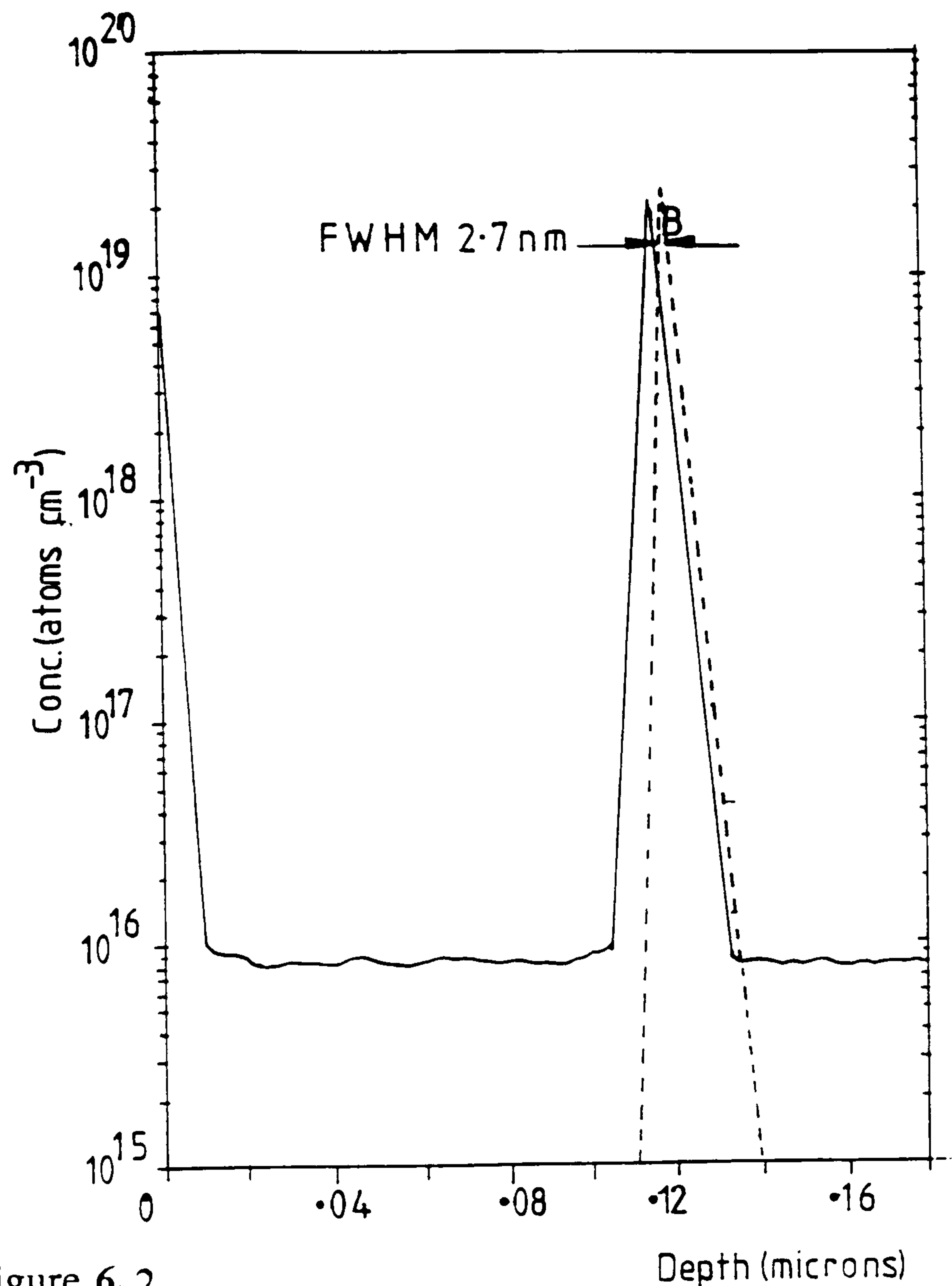

Figure 6.2.

SIMS profile of a B δ layer obtained using 450eV/O^+ ions at normal incidence (full line) and the reconstructed profile at zero impact energy (broken line).

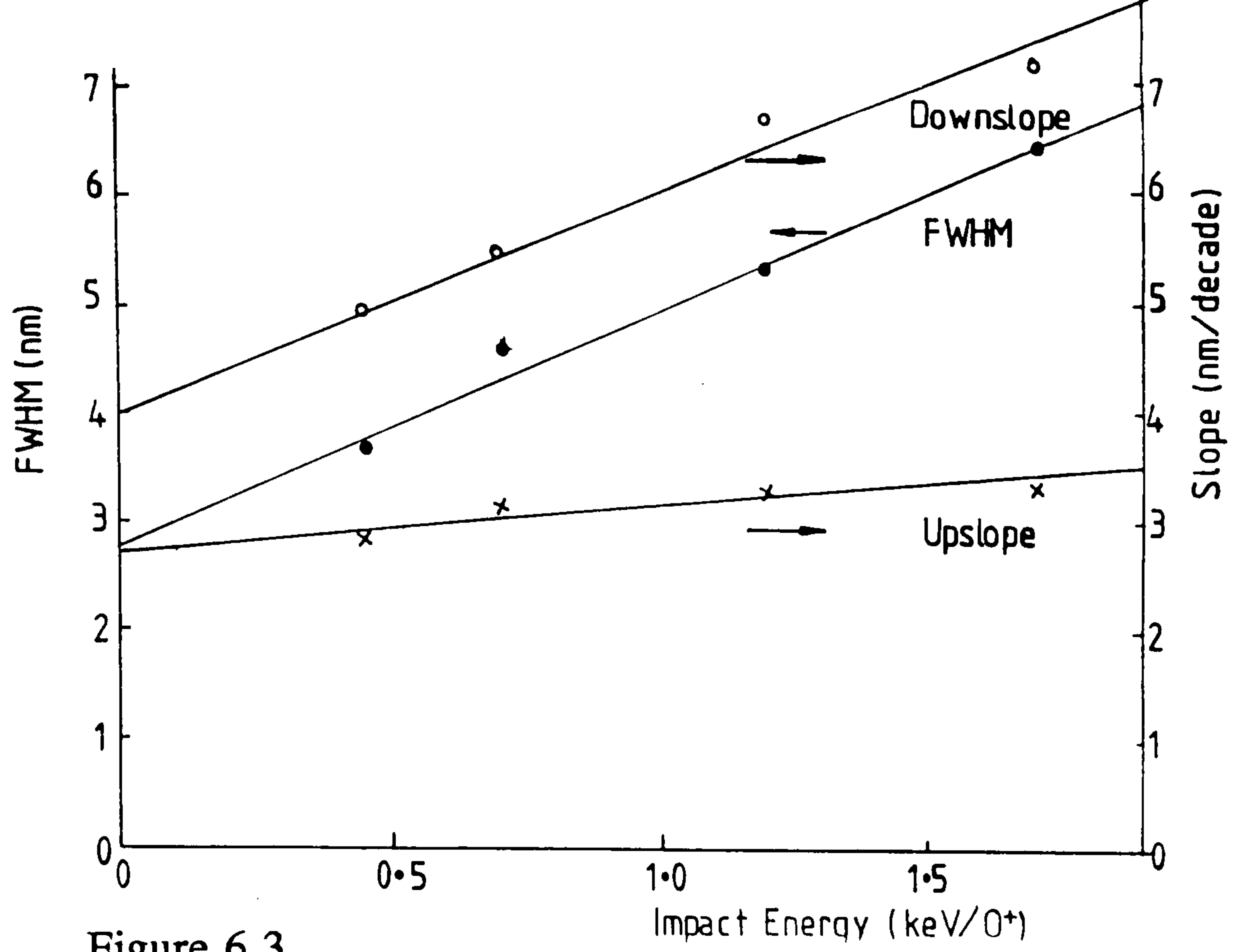

Figure 6.3

Extrapolation of SIMS data to $E_p=0$.

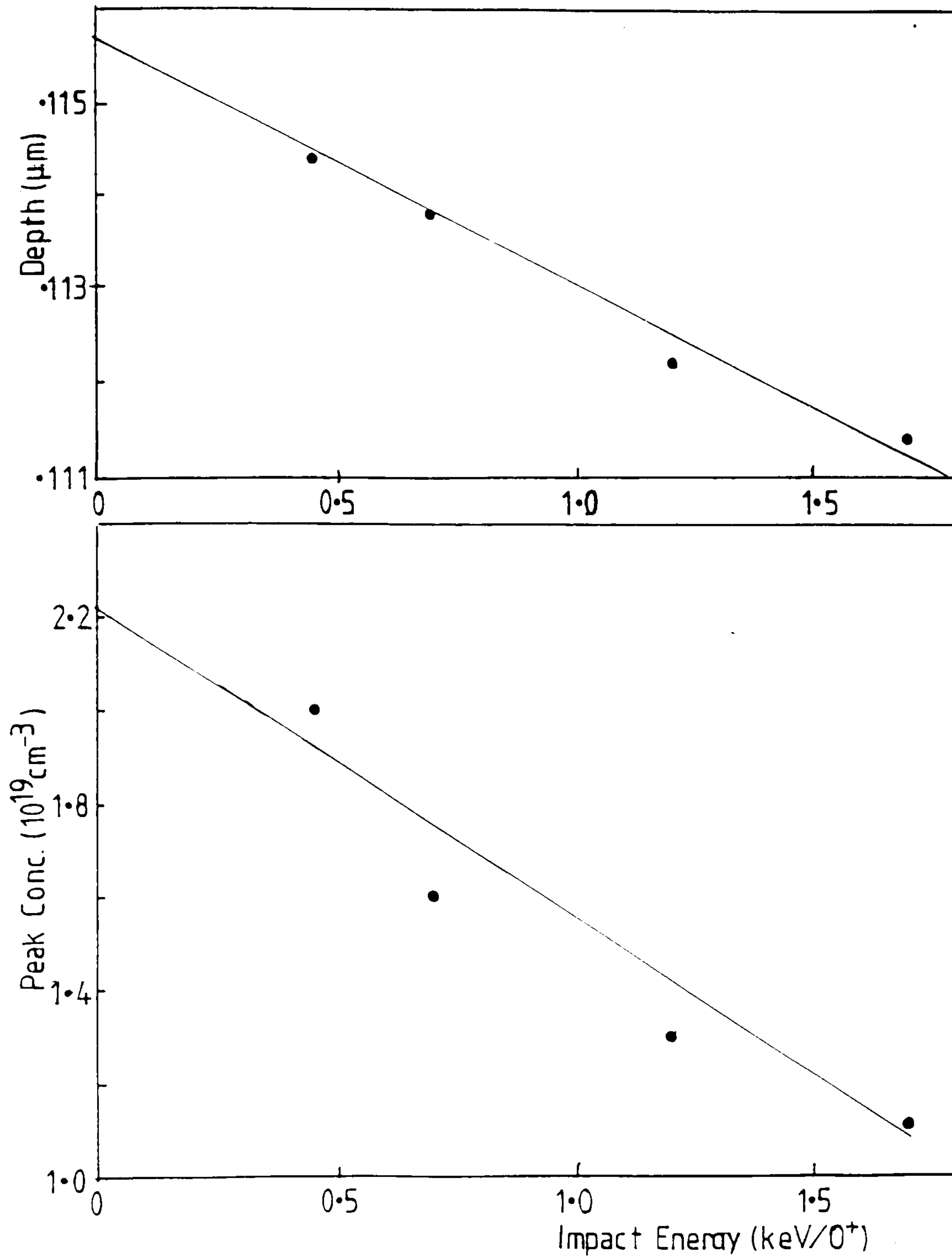

Figure 6.4

6.1b) XTEM

To provide further information on the δ layer width cross-sectional TEM was used. Preliminary analysis was performed on a B δ layer of areal density $1x10^{13}$ cm^{-2} (Mattey et al, 1990a). The δ layer was seen as a dark line of width ~2nm in a bright field two-beam g=400 image. However some structure was evident, possibly due to precipitation (although Hall measurements suggested complete activation). The contrast mechanism was also the subject of some uncertainty (Whitehurst, 1989). Figure 6.5 shows the micrograph obtained from a sample of the maximum sheet density ($3.8x10^{14}cm^{-2}$) examined in the (110) direction using a many-beam overfocus condition to obtain sufficient contrast. The surface texture contrast is due to the ion beam milling used in the sample preparation. The apparent width of the δ layer is 2nm, however it is thought that this is greater than the true width due to lack of contrast, stress in the film and Fresnel effects (Powell, Mattey, Kubiak, Parker, Whall and Bowen, 1991). There is no evidence of any preciptates nor of any defects nucleating at the δ layer which places an upper limit of $10^{5}cm^{-2}$ on the dislocation density.

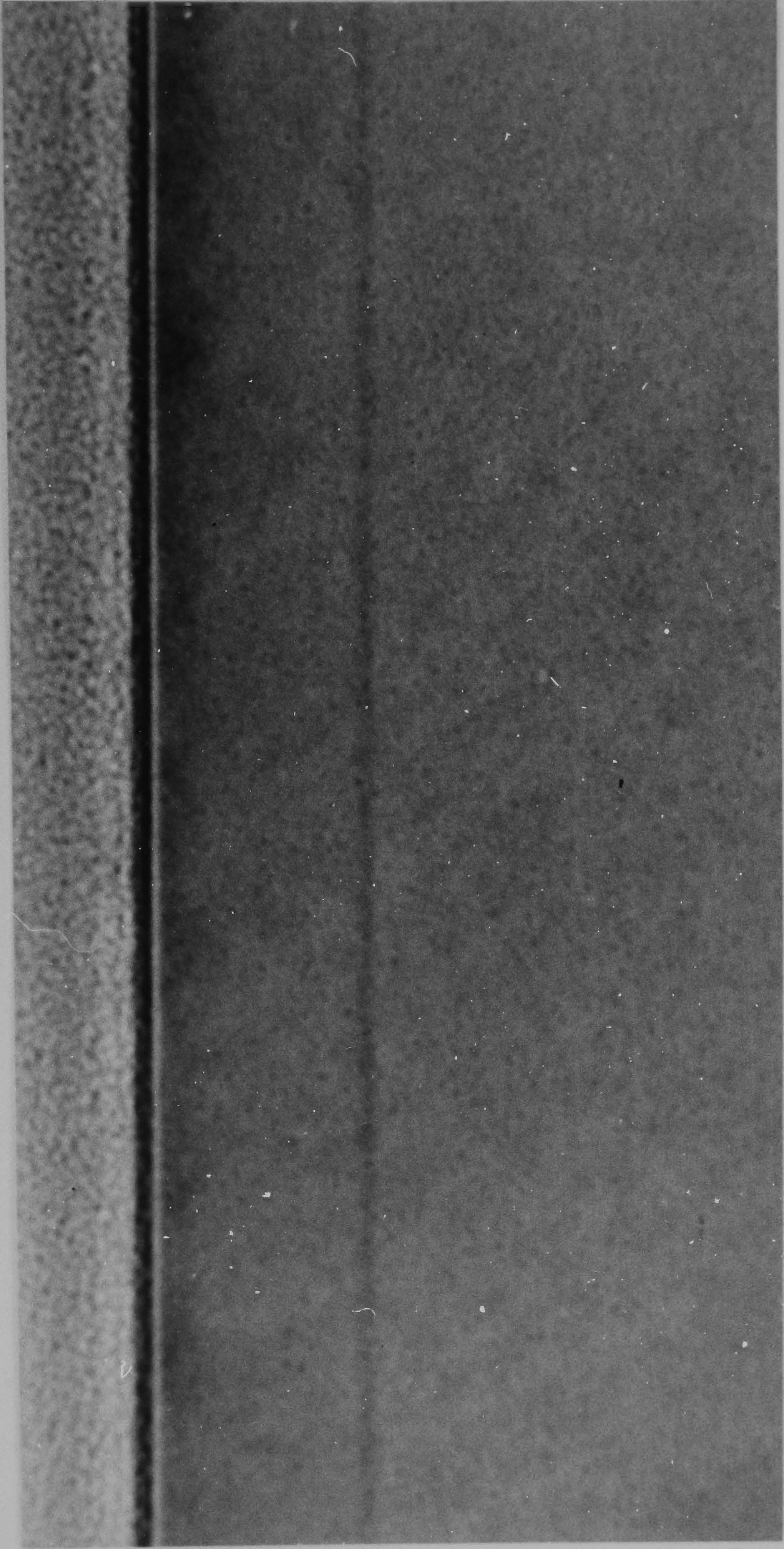

B δ Layer

Figure 6.5.

TEM image of a δ layer of sheet density $3.5 \times 10^{14} cm^{-2}$.

6.1c) Double Crystal XRD

More recently double crystal XRD was undertaken on a sample of sheet density $3.8x10^{14}cm^{-2}$ (Powell, Mattey, Kubiak, Parker, Whall and Bowen,1991). Figure 6.6 shows the rocking curve obtained in the (113) direction, the (004) rocking curve was also obtained to enable the unambiguous determination of the degree of strain. The five peaks result from interference between the diffracted beams from the δ layer and cap and the diffracted beam from the underlying Si. The sharpness of the peaks is indicative of good crystalline quality which suggests that the B layer is pseudomorphic ie. tetragonally contracted in the growth direction (100). The depth of the δ layer was determined from the fringe separation and found to be 51 ± 2nm, in good agreement with the growth schedule and the values obtained from SIMS and TEM. Also shown in Figure 6.6 is the simulated rocking curve for the structure shown in the inset, from this and further simulation it is possible to place an upper limit of 1nm on the width of the δ layer, suggesting that this is the thinnest δ layer reported to date. The lattice contraction in the (100) direction was found to be 0.031 ± 0.002nm which, given the sheet density, enables the calculation of a value of $5.6\pm0.7x10^{-23}cm^3$ for the lattice contraction per B atom. This value is in agreement with that obtained for activated B suggesting that the δ layer is fully activated.

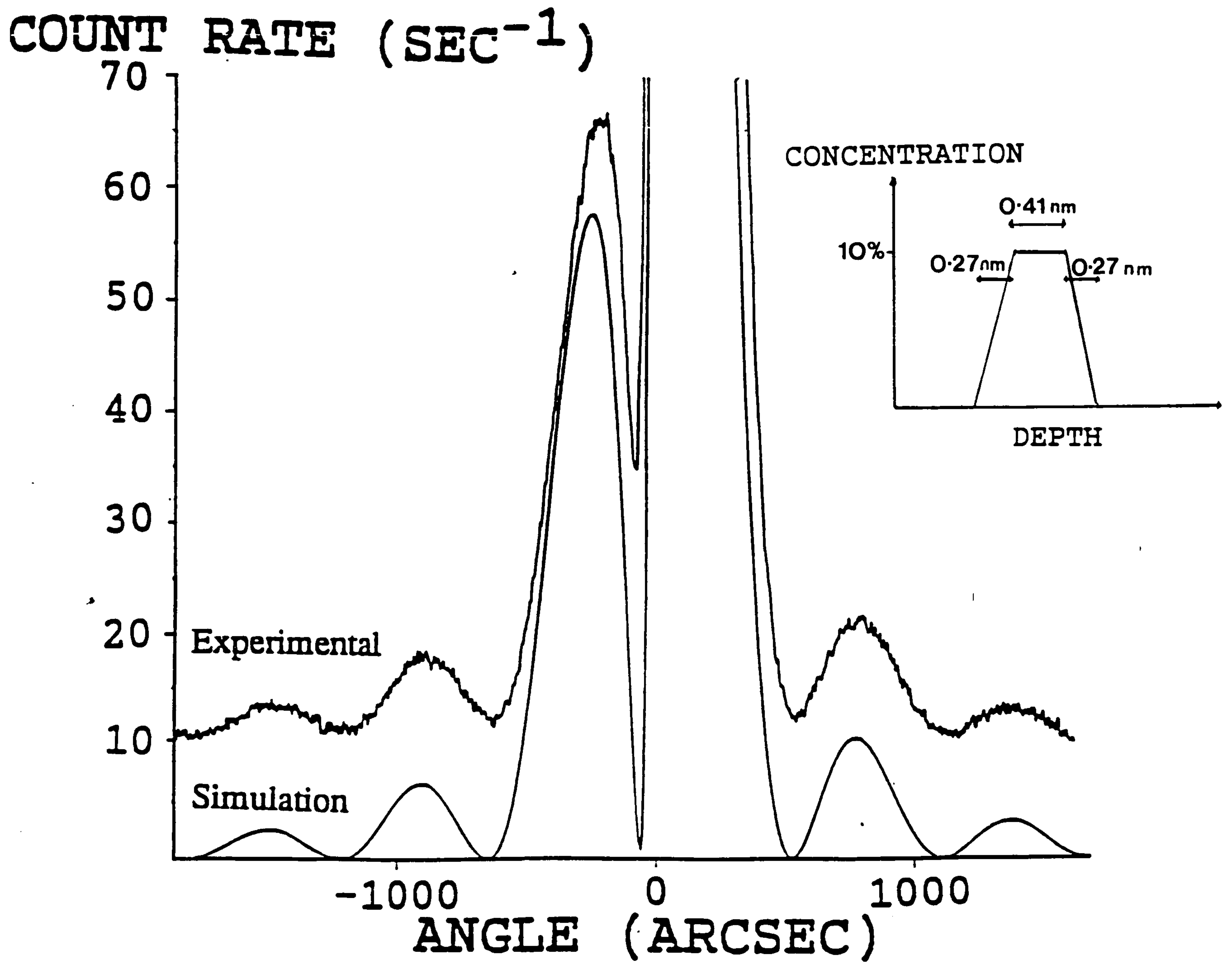

Figure 6.6

XRD Rocking curve for a B δ layer of sheet density $3.5 \times 10^{14} cm^{-2}$.

6.2 Electrical Properties

6.2a) C-V Measurements

To investigate further the structure of the δ layer C-V measurements were undertaken. The sample configuration shown in figure 6.7 was used to minimise the effects of series resistance as the δ layer is depleted (Van Gorkum, 1986). The two frequency technique (Chapter 4) was used to determine the true capacitance in the presence of any effects due to residual series and parallel resistances. Measurements were carried out at numerous frequencies of up to 5MHz to check the validity of this approach and to justify the assumption that the effect of deep states could be ignored.

Initially sputtered Al was used as a Schottky barrier with no post-deposition anneal. Figure 6.8. shows a typical I-V characteristic, plots of C versus V and the resulting values of N versus d for a sample of nominal sheet density $2x10^{12}cm^{-2}$ are shown in figures 6.9. and 6.10 respectively. It is clear that the δ layer is depleted at zero bias, presumably due to the presence of hole trapping states at the metal/semiconductor interface. In order to profile this structure it was necessary to drive the junction into forward bias, with consequent increase in parallel conductance. The Al contacts were also subject to ageing, possibly due to field enhanced diffusion of the Al into the Si, or vice-versa (Sze, 1981). Any attempt at post-depostion anealling, whilst reducing the depletion due to interface charge, tended to increase the ageing effects.

Despite the extensive literature on the subject (eg. Rhoderick, 1978) great difficulty was experienced in producing reliable Schottky barriers on MBE-Si. Sputtered Mo, Pt and evaporated Al and Au:Sb were investigated in combination with a number of pre-deposition cleans with little success. Sputtered titanium was found to exhibit the same behaviour as Al with no post-depostion anneal, however a stable Schottky barrier was obtained following a ten second anneal at 550°C, presumably due to the formation of a titanium silicide. Figures 6.11. and 6.12. show the C-V characteristic and the resulting profile for a sample of nominal sheet density $2x10^{12}cm^{-2}$. The areal density of the C-V profile of $\sim 1.5x10^{12}cm^{-2}$ compares favourably with the intended sheet density. The FWHM of 2.4nm is in agreement with the quantum mechanical description of this system which predicts a FWHM of $\sim$3nm as opposed to $\sim$8nm predicted by the classical description (Wood). This result is of interest since it was expected that the observed profile would correspond to the larger (classical) predicted width.

The apparent discrepancy between the intended depth of 50nm and the apparent depth of $\sim$32nm observed from the C-V profile is thought to be due to the consumption of silicon in the formation of the silicide Schottky barrier. Figure 6.13 shows a SIMS profile taken through the test structure and confirms that this is the case.

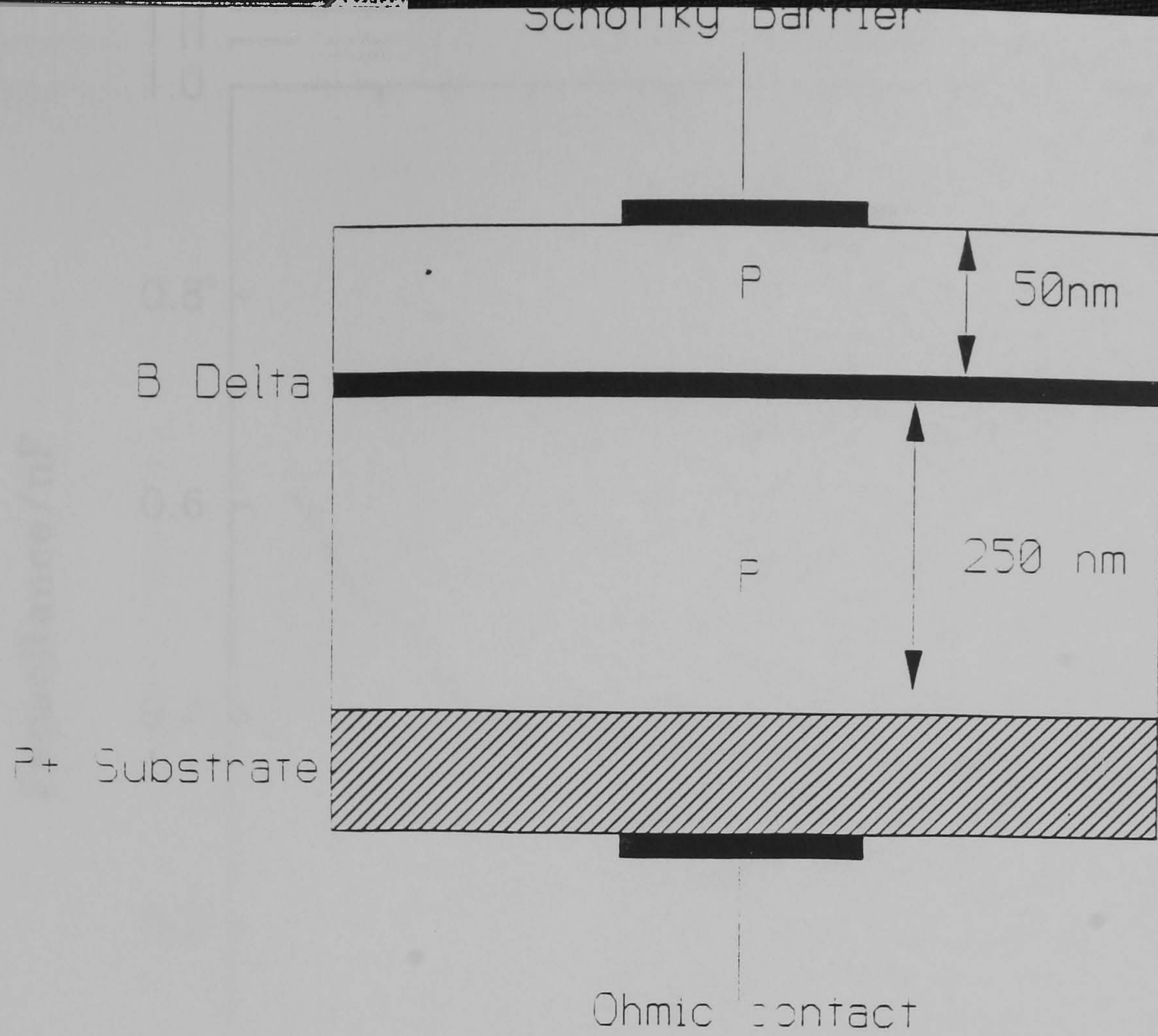

Figure 6.7

Structure used for C–V measurements

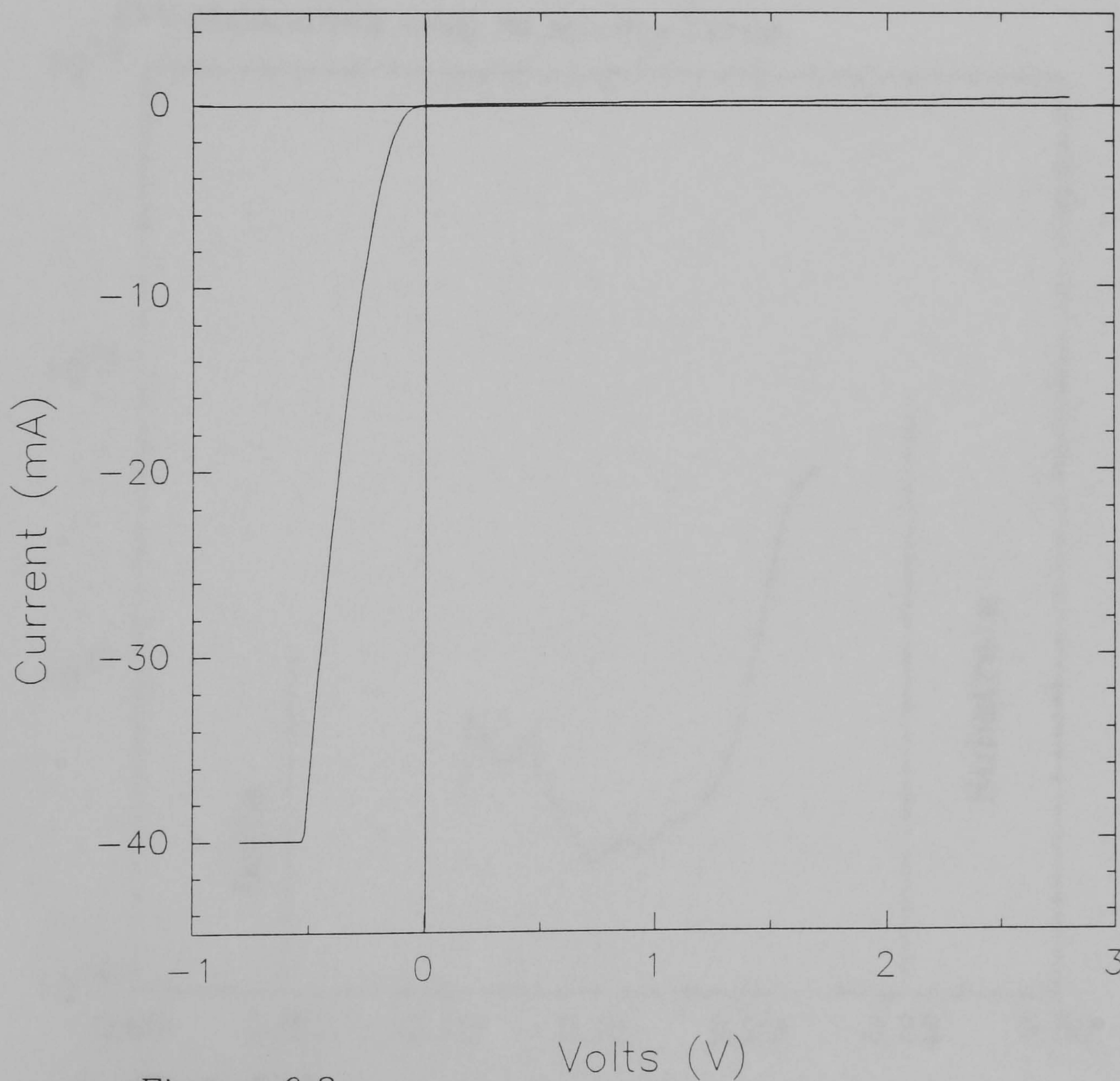

Figure 6.8

I–V characteristic for Al Schottky barrier.

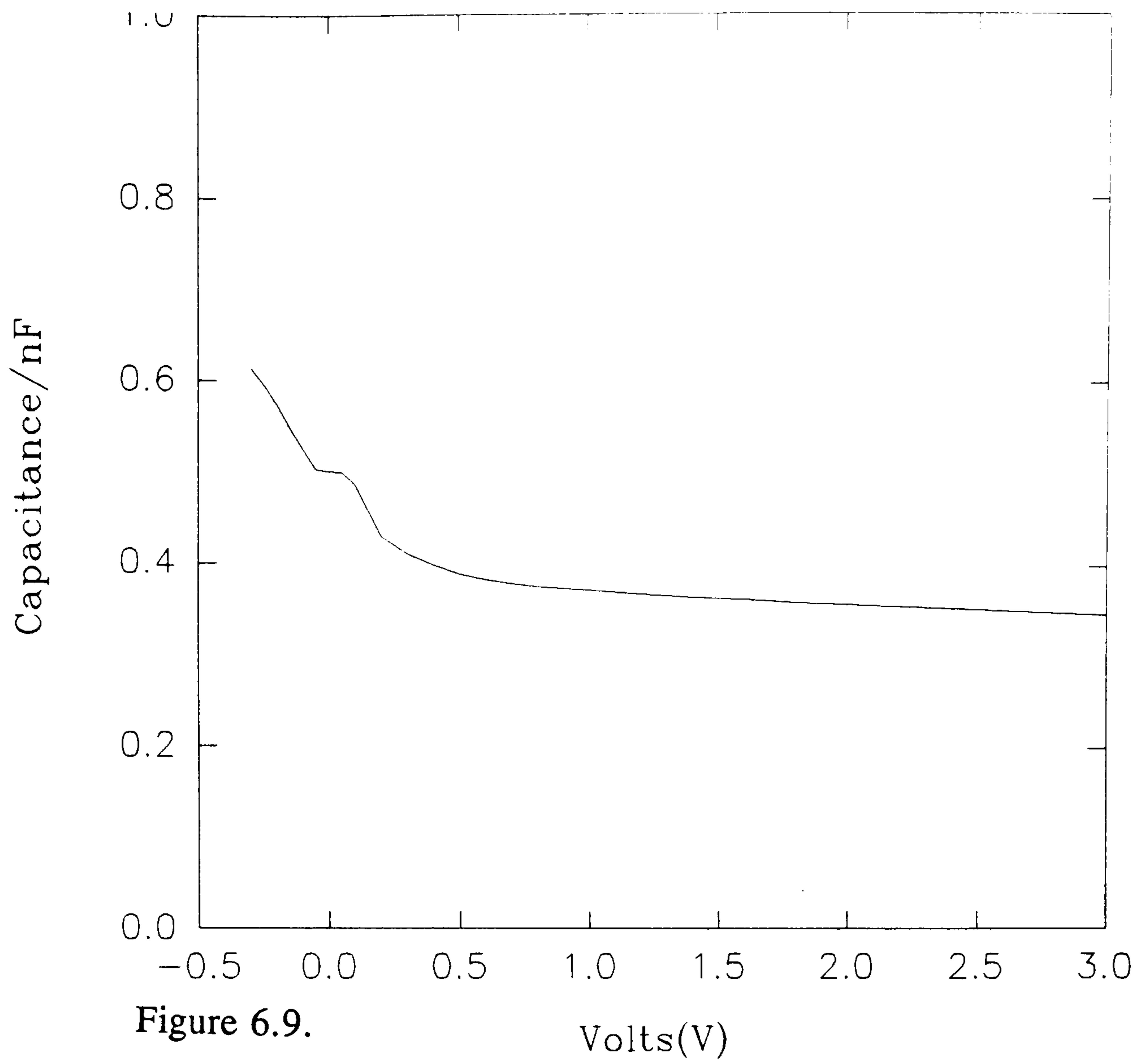

Figure 6.9.

C-V characteristic using Al Schottky barrier.

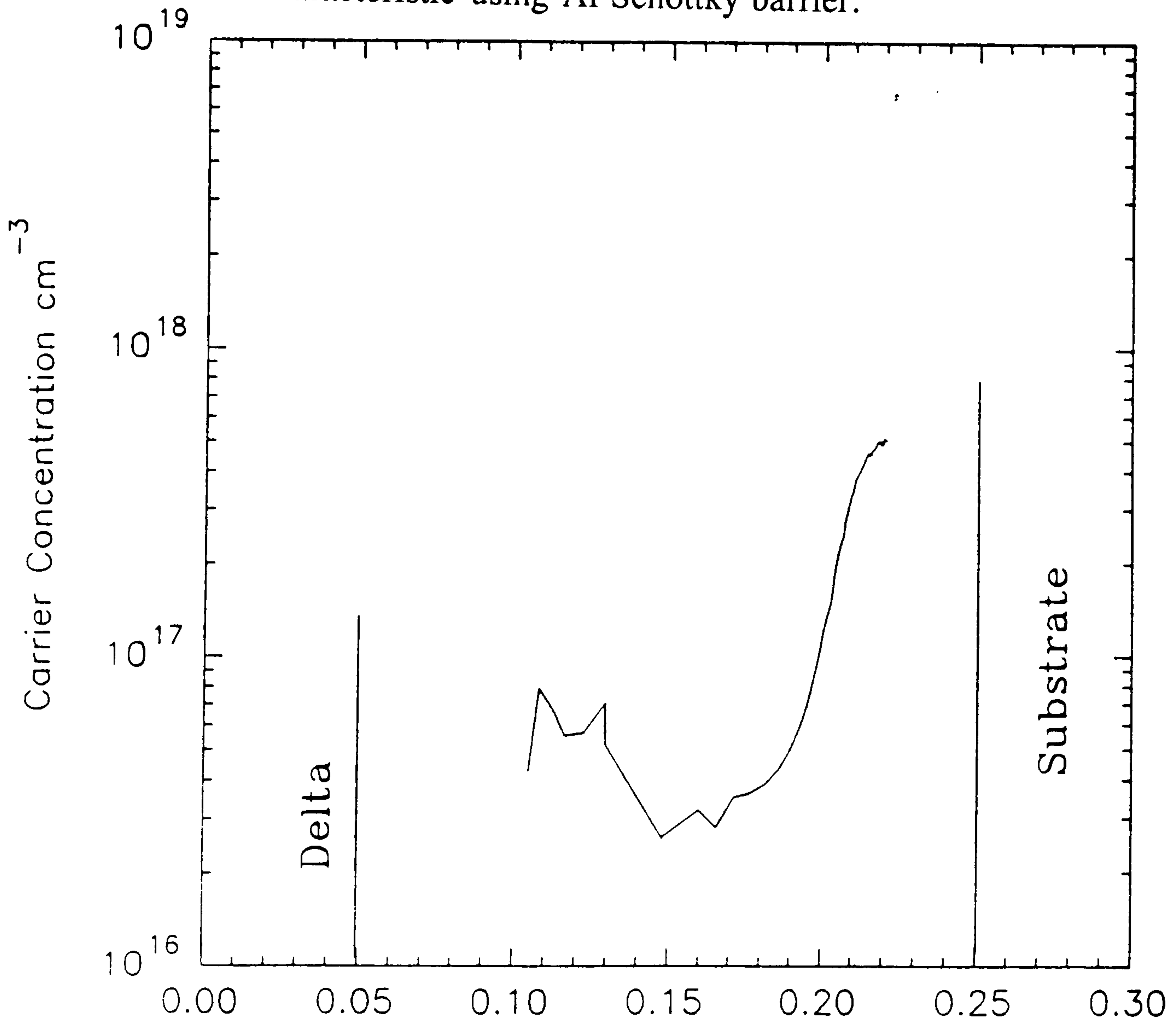

Figure 6.10.

Carrier profile obtained from figure 6.9.

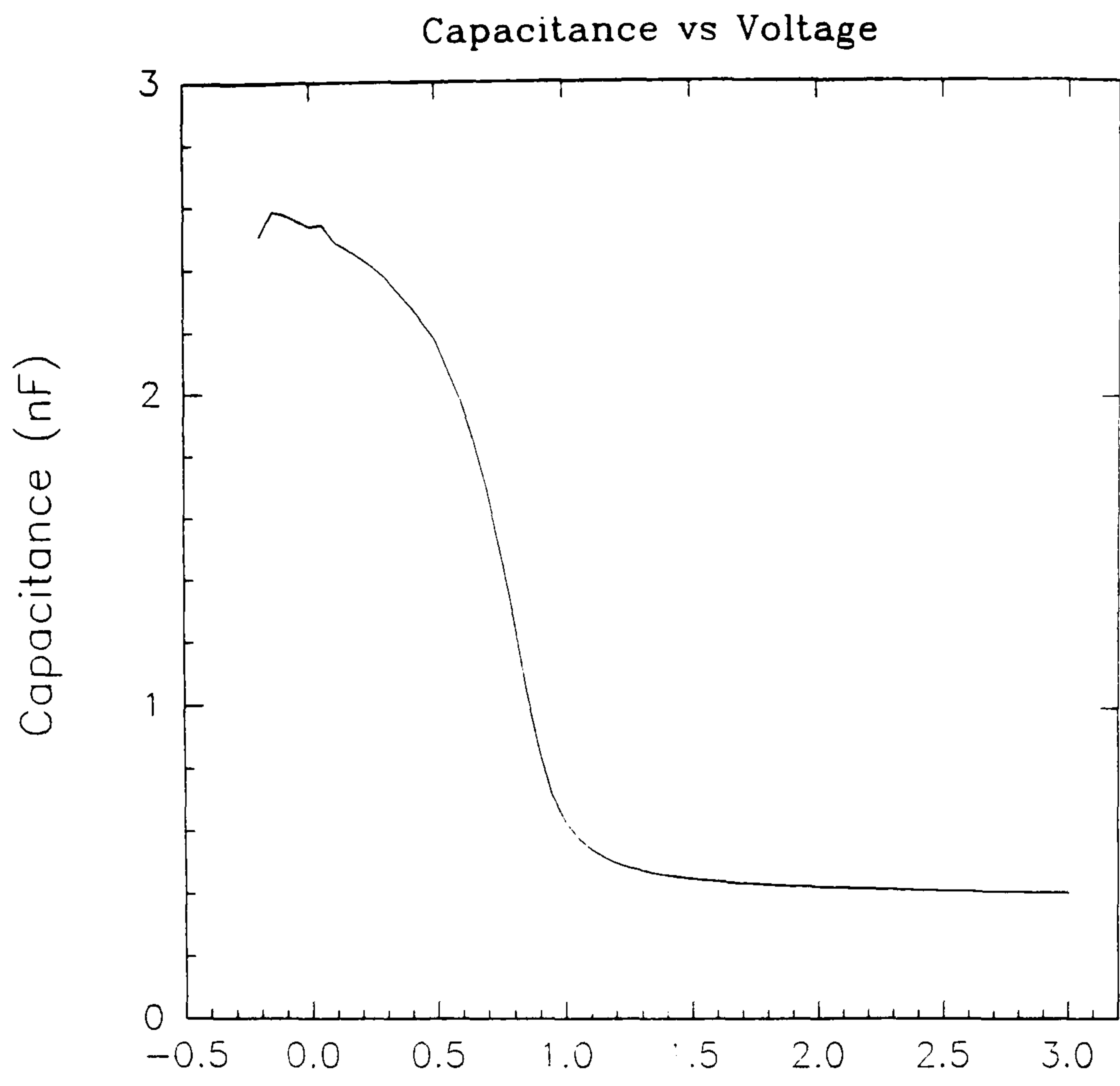

Figure 6.11.

C-V characteristic using Ti Schottky barrier.

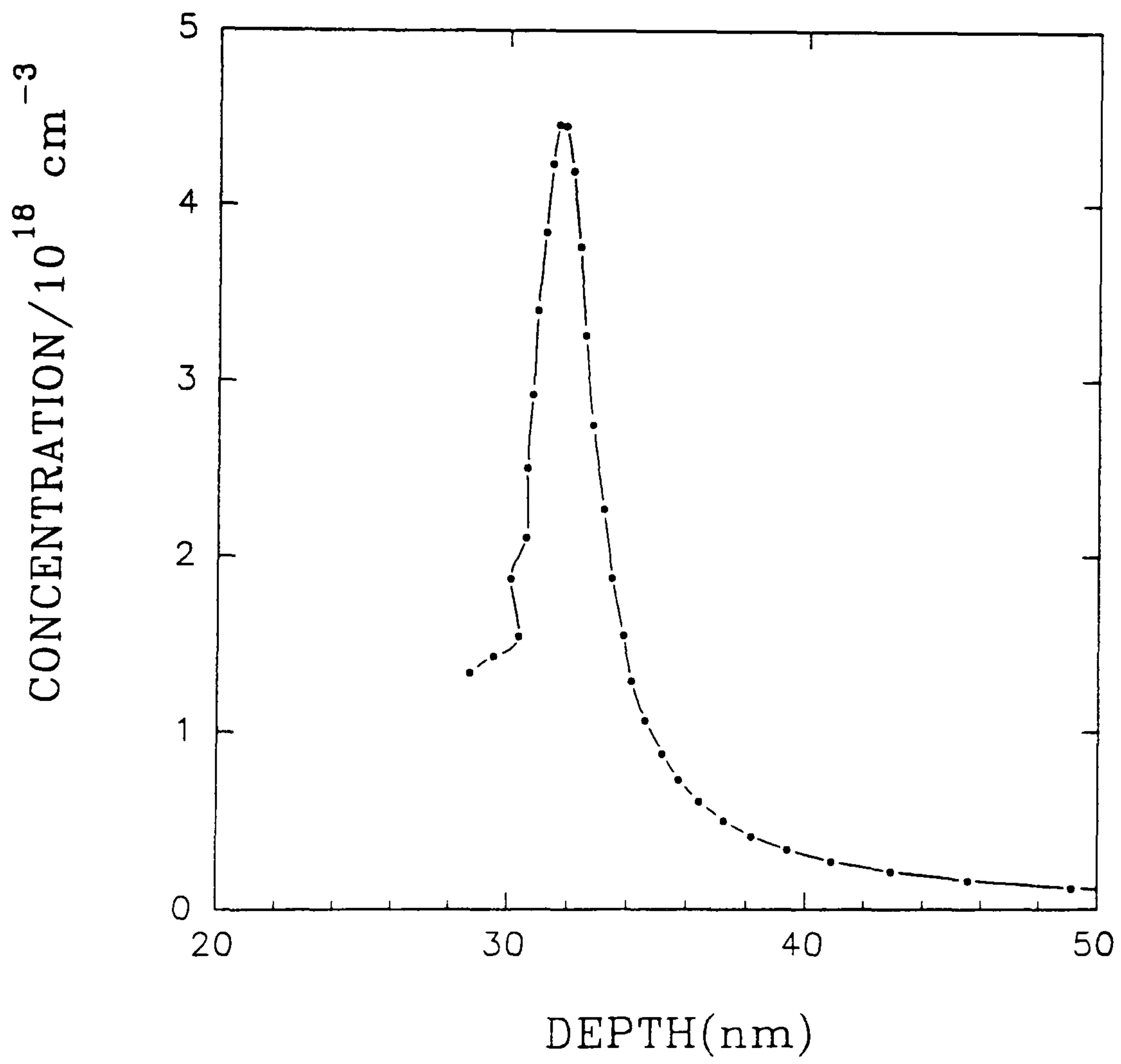

Figure 6.12.

Carrier profile obtained from figure 6.11.

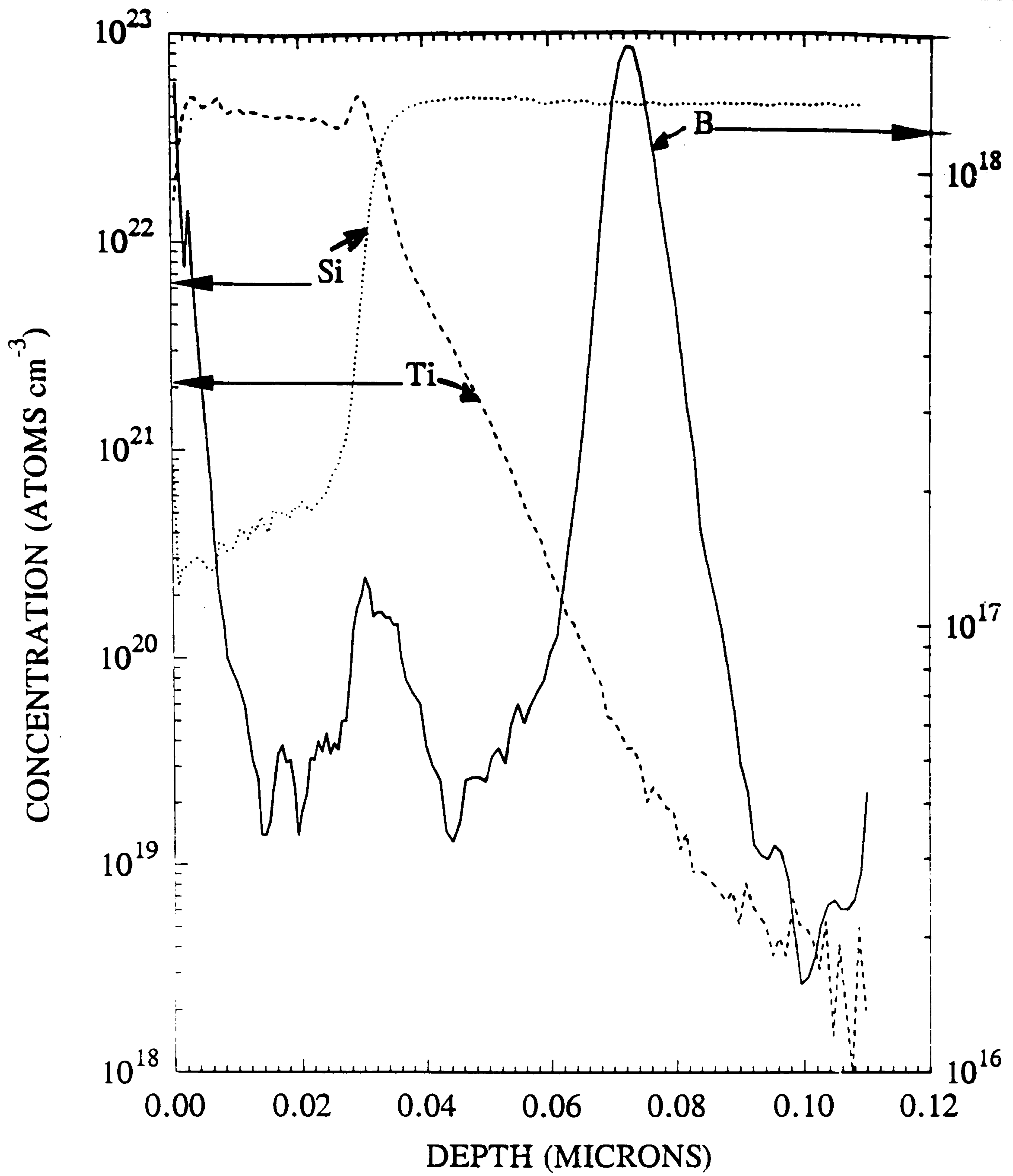

Boron delta 20/7 with Ti cap. Sheet concentration $2x10^{12}$ cm^{-2}
FWHM 8.5 nm. EVA 2000 SIMS primary ions 5 keV, 200 nA O_2^+

Figure 6.13.

SIMS profile of sample used for C-V measurements showing relative depth of δ layer.

6.2b) Transport Properties

The degree of activation of the B δ layers was investigated using Hall measurements carried out at 4.2K (to freeze out parallel conduction paths) on in-house processed Greek cross structures. It was found that complete activation was obtained for sheet densities up to $(3.5\pm0.4)x10^{14}cm^{-2}$. However, interpretation of the Hall measurements is complicated by the multi-subband conduction, although Eisele (1989) has argued that the measurement leads to a minimum value. The problem of the multi-subband conduction is discussed in more detail below.

For a more thorough investigation of the transport properties Hall bars of size 30μm x 310μm were fabricated from structures containing p^+ δ layers in a p^- ($10^{16}cm^{-3}$) background. To ensure that the measured properties were due to the δ layer and not to any other effect, for example a surface inversion layer, test structures containing two δ layers and with no δ layer were measured. All measurements were carried out with an electric field of less than $\sim 1Vm^{-1}$.

Figures 6.14, 6.15 and 6.16 show the resistance and Hall coefficient plotted verus T for B δ layers of sheet density in the range $1.8x10^{13}cm^{-2}$ to $7.6x10^{13}cm^{-2}$. The logarithmic dependence between $\sim$0.5K and $\sim$20K is consistent with the behaviour of a 2D hole gas of weakly localised carriers (see Chapter 4.). The behaviour above 20K is thought to be primarily due to the occurence of parallel conduction paths.

According to theory (see Chapter 4), $R_{\square}$ is sensitive to both localisation and interaction effects whilst R_H is sensitive only to the interaction mechanism.

For a single subband (the relevance of these expressions to multi-subband conduction is discussed below),

$$\frac{\delta R_{\square}}{R_{\square}} = -R_{\square}\frac{((1-{}^{3}/_{4}F^{*})-\alpha p)e^{2}}{2\pi^{2}\hbar}\ln\frac{kT\tau}{\hbar} \tag{6.1}$$

where F^{*} is a renormalised screening parameter, τ is the elastic scattering time, p is the temperature expononent of the phase breaking rate (ie. τ_{ϕ} proportional to T^{p}) and α is a phenomenological factor depending on the spin-orbit scattering rate. $\alpha=1$ for no spin-orbit scattering, $\alpha=-1/2$ for strong spin-orbit scattering (Altshuler et al, 1981). The Hall coefficient is given by,

$$\frac{\delta R_{H}}{R_{H}} = -2R_{\square}\frac{e^{2}}{2\pi^{2}\hbar}\left[(1-{}^{3}/_{4}F^{*})\ln\frac{kT\tau}{\hbar} - \frac{F^{*}}{2}G\left(\frac{g\mu_{B}B}{kT}\right)\right] \tag{6.2}$$

where the term containing G is due to the Zeeman spin splitting in the finite magnetic field necessary to measure the Hall coefficient. The function $G(X)\geq 0$ has two limits of interest (Burdis and Dean, 1988):

$$G(X)\rightarrow 0.091X^{2} \quad as \quad X\rightarrow 0 \tag{6.3}$$

$$G(X)\rightarrow \ln\frac{X}{1.3} \quad as \quad X\rightarrow\infty \tag{6.4}$$

The Zeeman contribution is normally ignored, but the present results were obtained using a relatively high magnetic field of 0.5T, hence its effect should be considered. Taking a median effective mass of $(0.5+0.16)m_{0}/2$, corresponding to the mean of the heavy and light hole effective masses, $g\mu_{B}B/k \sim 2K$ and

neglecting the Zeeman contribution results in an error of <5% in F^*.

Values of $R_\square$, the measured sheet density, N_s ($=1/eR_H$), μ and the extracted parameters F^* and αp at a temperature of 4K are presented in Table I.

Since it is expected that $p \geq 1$ (Fukuyama and Abrahams, 1983, Altshuler et al, 1982), the fact that $\alpha p \leq 0.34$ suggests the presence of spin-orbit scattering in these samples. As αp decreases and becomes negative as N_s increases it seems that the spin-orbit scattering is associated with the boron concentration in the δ layer.

The saturation of $R_\square$ may be due to the dominance of spin-orbit scattering at low temperatures, however this mechanism probably cannot account for the saturation of R_H which is associated with interaction effects. Furthermore, the behaviour of R_H cannot be due to the Zeeman interaction term (equation 6.2) which is of the wrong sign. This phenomenon may be explicable in terms of electron heating due to a long electron-phonon scattering time at low temperatures (Bishop et al, 1982).

The value of $F^* \sim 0.9$ is not inconsistent with typically measured values and is approximately independent of sheet density in agreement with the predictions of Fukayama (1981). The present system is qualitatively different from that of Kichigin et al (1984), where very strong spin-orbit scattering in a InSb/GaAs heterojunction led to a value of $\alpha p=-0.5$ and a negative value of F^* ~ -0.48, suggesting that this parameter may be fundamentally altered by the presence of strong spin-orbit scattering.

It is not expected that the multi-subband nature of the δ layers will affect

the argument, as it has been shown (Kearney and Butcher, 1988, Iwabuchi and Nagaoka, 1989) that multi-subband systems can be treated through an effective renormalisation of the diffusion constant and the magnitude (but not the sign) of the prefactor α. A similar conclusion is reached, incidentally, for multi-valley systems, where this time $g_v\alpha$(g_v is the valley degeneracy) varies with the intervalley scattering rate, $1/\tau_v$, but always remains greater than unity. However, an idea of the subband structure, including the wavefunction widths may be obtained from the polygonal model discussed in Chapter 5.1. There is some uncertainty as to the appropriate effective masses and band non-parabolicities in the confining potential of the δ layer, the situation being further complicated by the presence of strain. Nevertheless, taking the bulk effective masses at 4K as 0.531, 0.234 and 0.153 for the heavy, spin-orbit split and light hole subband respectively (EMIS,1989), those subband minima lying below the Fermi energy are shown as a function of doping sheet density in figure 6.17. Hence the values of effective diffusion constant $D=(R_{\square}e^2N(E_F))^{-1}$ shown in Table I were calculated and values of $k_Fl=(4\pi m^*D)/h$ estimated (k_F is the Fermi wavevector and l is the elastic mean free path).

The conventional theories of weak localisation and interaction effects (Lee and Ramakrishnan, 1985) are derived under the assumption that $k_Fl >> 1$. Morgan et al (1985) have argued that the predictions should also be useful for somewhat lower values $k_Fl > 1$, however in the present case $k_Fl \sim 1$. Despite these low values of k_Fl the resistance and Hall data are indicative of metallic conduction and should be contrasted with the activated transport discussed below.

Table I.

$R_{\square}$/kΩ (4K)	N_s/cm^{-2} (4K)	μ/cm^{2}V^{-1}s^{-1} (4K)	F^*	αp	D/m^{-2}s^{-1}	$k_F l$	Width/nm
3.69	7.6×10^{13}	22	0.96	-0.14	1.2×10^{-4}	1.11	2.8
6.76	2.3×10^{13}	41	0.85	0.01	7.5×10^{-5}	0.69	3.4
9.4	1.8×10^{13}	38	0.88	0.34	6.6×10^{-5}	0.61	3.8

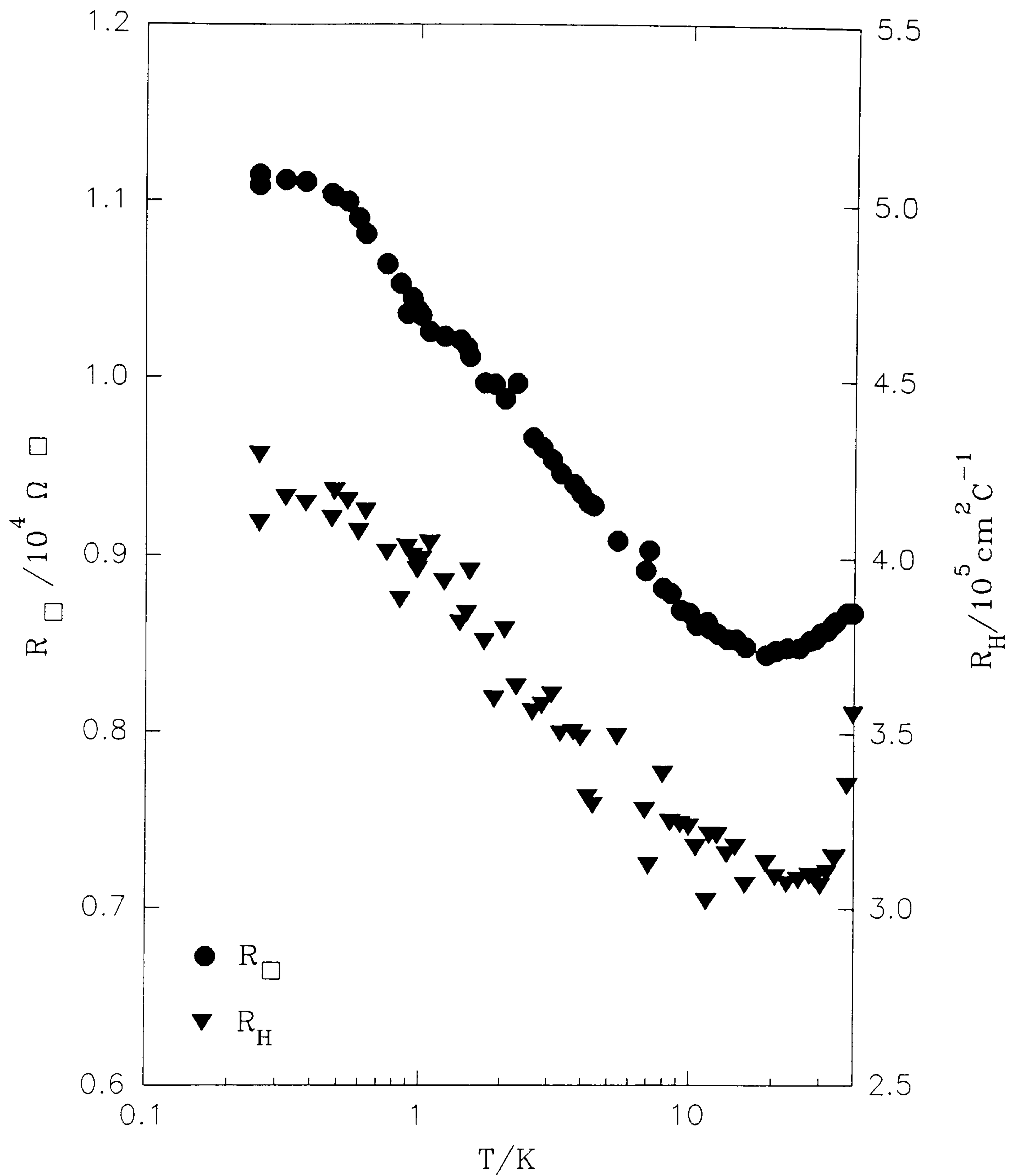

Figure 6.14.

Resistance, $R_{\square}$, and Hall coefficient, R_H, of a sample of sheet density $1.8 \times 10^{13} cm^{-2}$ plotted versus Log T in the temperture range 0.3K to 30K.

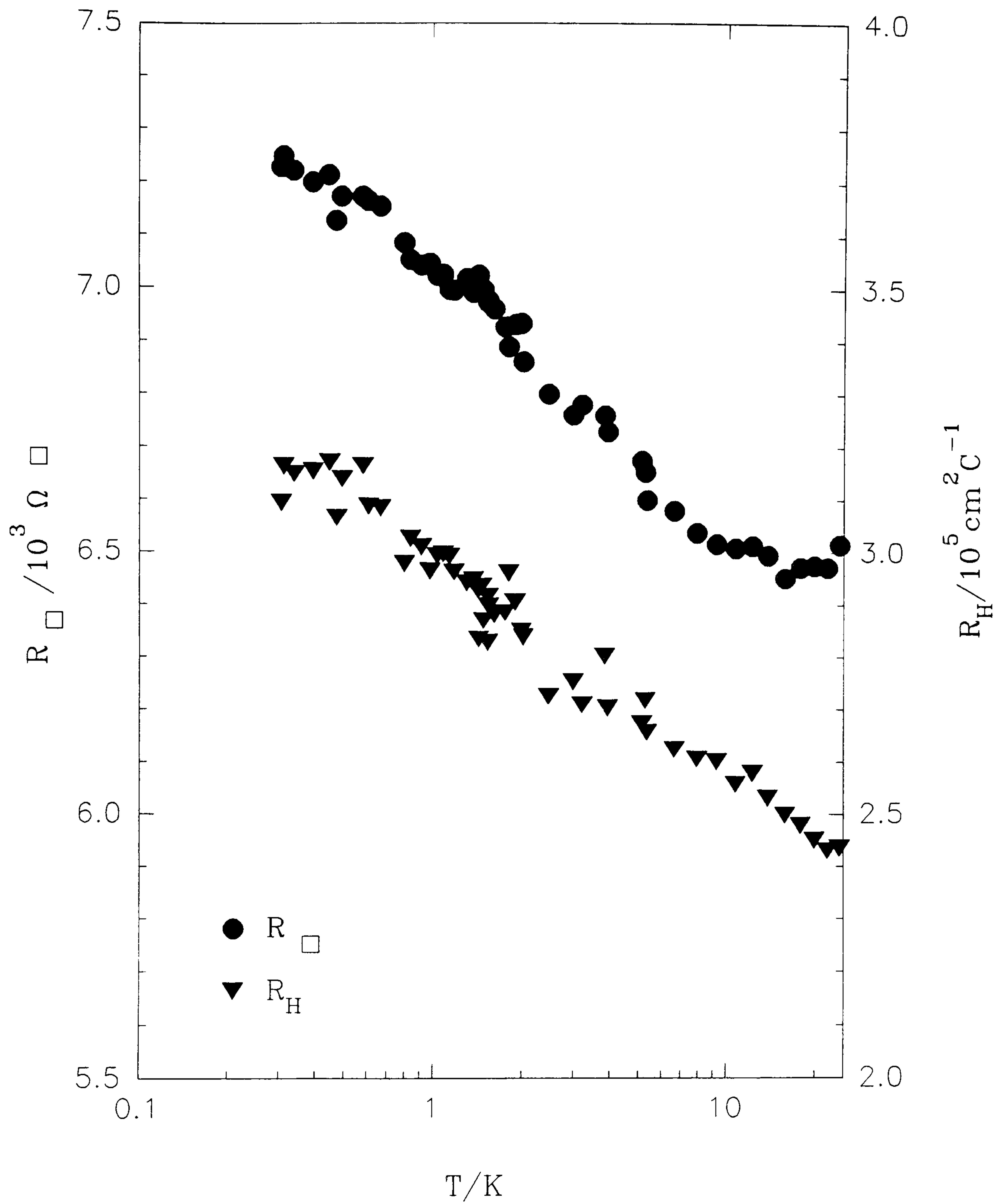

Figure 6.15.

Resistance, $R_{\square}$, and Hall coefficient, R_H, of a sample of sheet density $2.3\text{x}10^{13}\text{cm}^{-2}$ plotted versus Log T in the temperature range 0.3K to 30K.

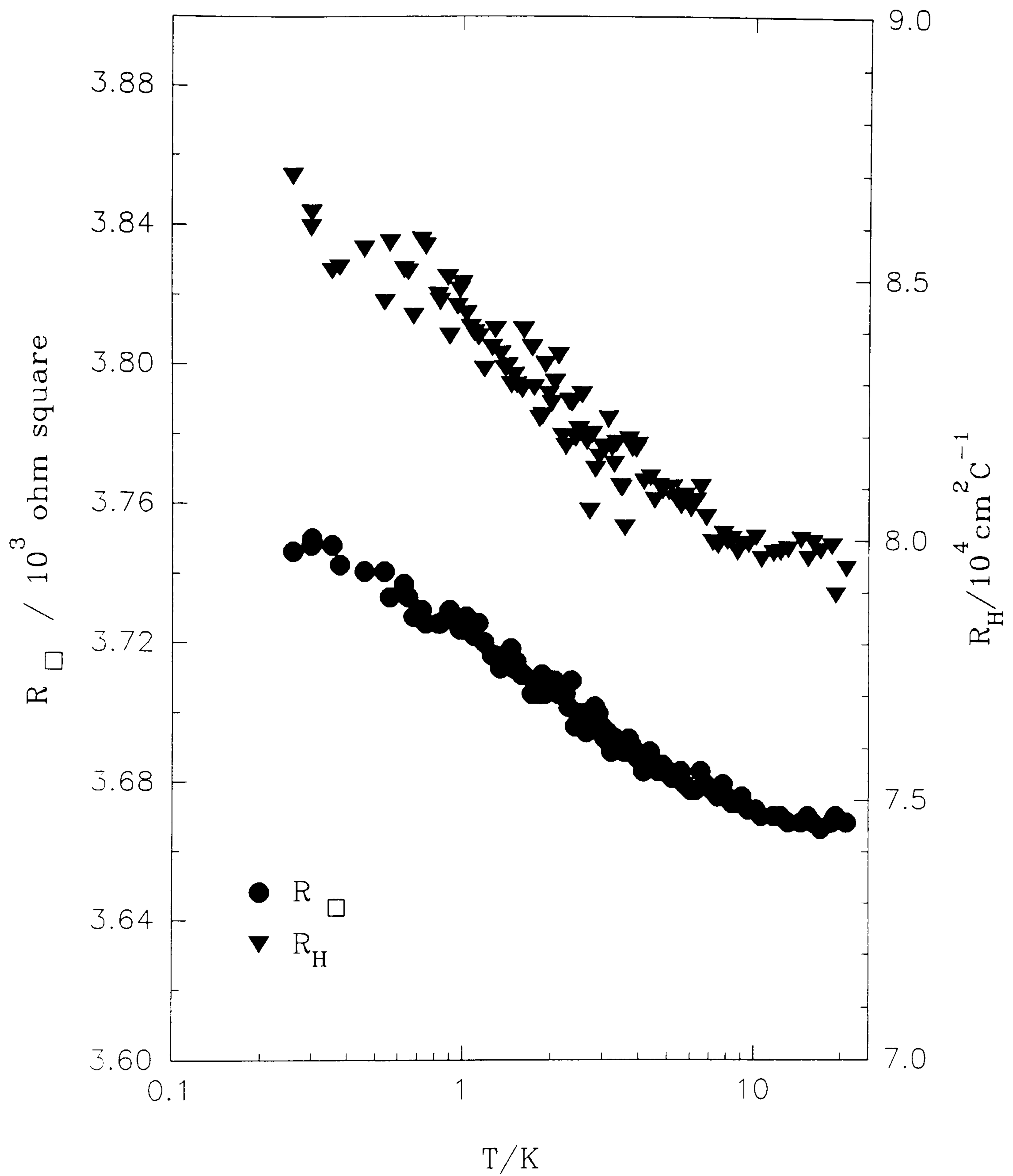

Figure 6.16

Resistance, R □ , and Hall coefficient, R_H, of a sample of sheet density $8x10^{13}cm^{-2}$ plotted versus Log T in the temperature range 0.3K to 30 K.

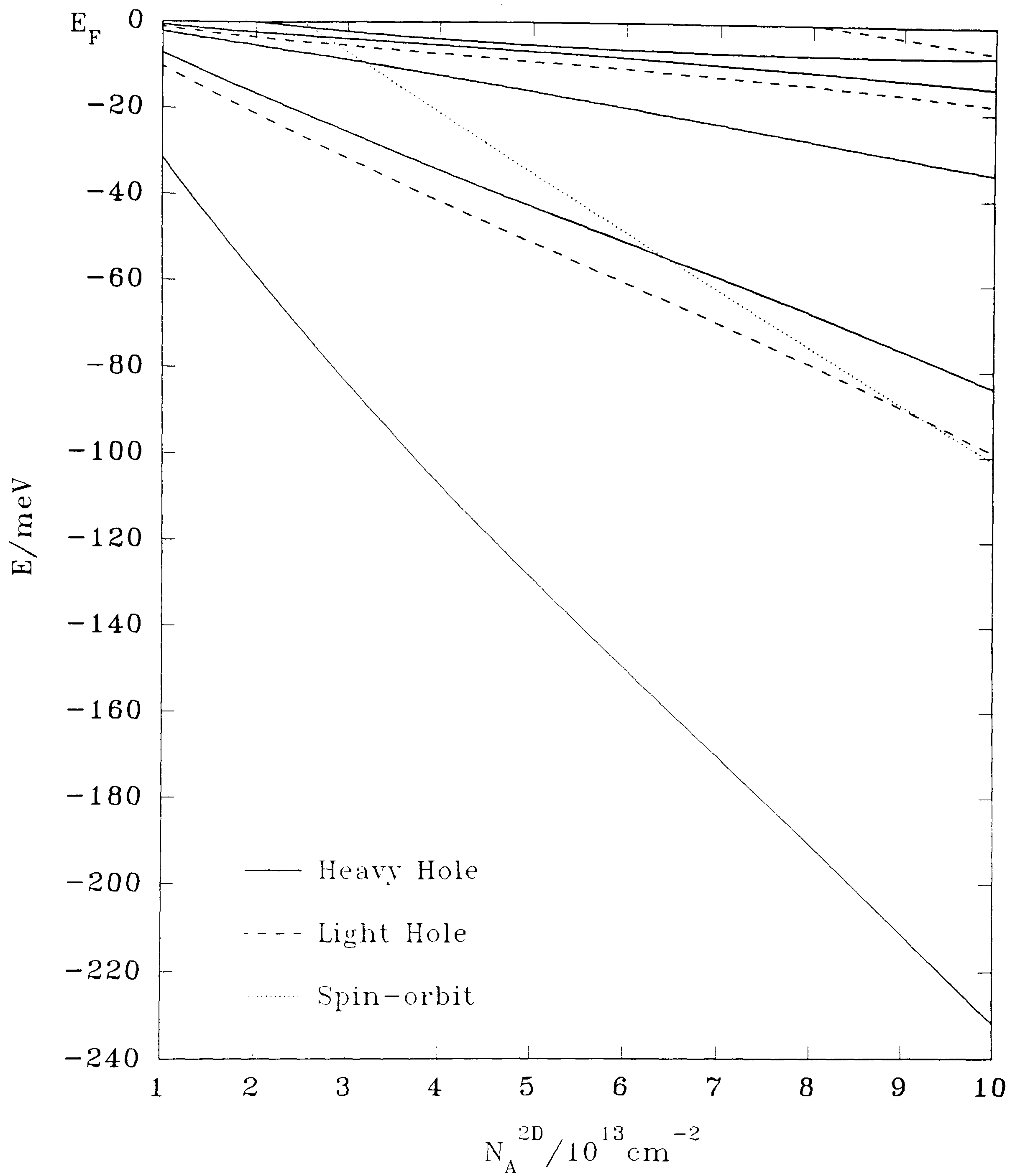

Figure 6.17.

Calculated subband energies for B δ layers as a function of sheet density.

Figures 6.18, 6.19 and 6.20 show the magnetoresistance of the three samples above at temperatures of 1.3K, 2K and 4K with the magnetic field perpendicular and parallel to the δ layer. It seems reasonble to use 2D transport formulae provided the cyclotron radius $L_c=(h/2\pi eB)^{1/2}$ is greater than the confinement width, w of the δ layer. From table I w ~ 3nm and thus 2D behaviour should occur for B < 70T. According to theory, the parallel magnetoresistance is soley due to a Zeeman spin-splitting effect in the interaction correction given by (Lee and Ramakrishnan, 1985),

$$\Delta\sigma = \frac{-e^2}{4\pi^2\hbar} F^* G\left(\frac{g\mu_B B}{kT}\right) \tag{6.5}$$

$$\text{with } \frac{\Delta R(B)}{R_\square(0)} = -R_\square(B)\,\Delta\sigma \tag{6.6}$$

This term should be proportional to B^2 at low magnetic fields and lnB at high fields, crossing over at $B_c \sim kT/g\mu_B$ (see equations 6.3 and 6.4). For g=2 and $m^*=0.33m_0$ B_c amounts to 0.35T. Calculated values are compared to the experimental values in table II with B=12 T and assuming $F^*=0.9$. The theoretical values are too small by factors of between 1.6 and 2.1. Similar discrepancies were observed by Bishop et al (1982) for the 2DEG in the Si inversion layer. Putting g=3, as reported by Englert et al (1980) and using a smaller value of $m^*=0.16m_0$ gives satisfactory agreement, but this is stretching the analysis. More significantly, $\Delta R_{\parallel}$ is not a universal function of B/T as shown in figure 6.21.

The theory also predicts that the magnetoresistance will be anisotropic by virtue of orbital terms in the localisation and interaction contributions. An

estimate of the phase relaxation time τ_ϕ is required , taking the result of Fukuyama (1984),

$$\tau_\phi = \frac{\left(\frac{2E_F\tau}{FkT}\right)}{\ln\left(\frac{4E_F}{\hbar}\right)} \tag{6.7}$$

The values shown in Table II are obtained and are in reasonable agreement with experimental values of τ_ϕ quoted in the literature (Uren et al, 1981) despite the low values of $E_F\tau/h$. The orbital terms are given by (Fukuyama, 1981, Isawa and Fukuyama, 1984, Altshuler et al, 1980),

$$\Delta\sigma(B) = \frac{e^2\alpha}{2\pi^2\hbar}[1-\overline{g_4}]\psi\left(\frac{1}{2}+\frac{\hbar}{4eDB\tau_\phi}+\ln\frac{4eDB\tau_\phi}{\hbar}\right) \tag{6.8}$$

where the orbital interaction factor $g_4 \sim 0.1$, and ψ is the digamma function. D and α are obtained from Table I assuming p=1. Equation 6.8 should be valid for $B \leq (h/8\pi eD\tau)$ ie ≤ 80T in the present case. Finally, $\Delta R_\perp(B)/R_\square(0)$ is taken as the sum of the three terms. The calculated values predict considerable anisotropy, as shown in Table II, which is not supported by experiment. However an error in the calculated value of τ_ϕ, which is certainly plausible, is sufficient to explain the difference between theory and experiment.

In summary, the above analysis gives order of magnitude agreement with the experimental magnetoresistance data. However it fails in important respects to account for the details of the parallel magnetoresistance, particularly its temperature dependence.

Table II.

Fractional change in resistance for an increase in field of 12T at a temperature of 1.3K.

	Theory	Experimental
Sample 1		
$R_{\square}$ (1.3K)		3.72 k Ω
Interaction (Zeeman)	0.078 ($\perp$, $\parallel$)	
Interaction (Orbital)	-2.5×10^{-3}	
Localization (Orbital)	0.025	
$\Delta R_{\perp}/R_{\square}(0)$	0.10	0.12
$\Delta R_{\parallel}/R_{\square}(0)$	0.078	0.12
τ_{ϕ} s	9×10^{-12}	
Sample 2		
$R_{\square}$ (1.3K)		7.4 kΩ
Interaction (Zeeman)	0.193 ($\perp$) 0.194 ($\parallel$)	
Interaction (Orbital)	4×10^{-4}	
Localization (Orbital)	-3.6×10^{-3}	
$\Delta R_{\perp}/R_{\square}$	+ 0.19	0.39
$\Delta R_{\parallel}/R_{\square}$	0.194	0.40
τ_{ϕ} s	8×10^{-12}	
Sample 3		
$R_{\square}$ (1.3K)		11.7 k Ω
Interaction (Zeeman)	0.33 ($\perp$) 0.36 ($\parallel$)	
Interaction (Orbital)	0.025	
Localization (Orbital)	- 0.21	
$\Delta R_{\perp}/R_{\square}$ (0)	0.145	0.51
$\Delta R_{\parallel}/R_{\square}$ (0)	0.36	0.60
τ_{o} s	8×10^{-12}	

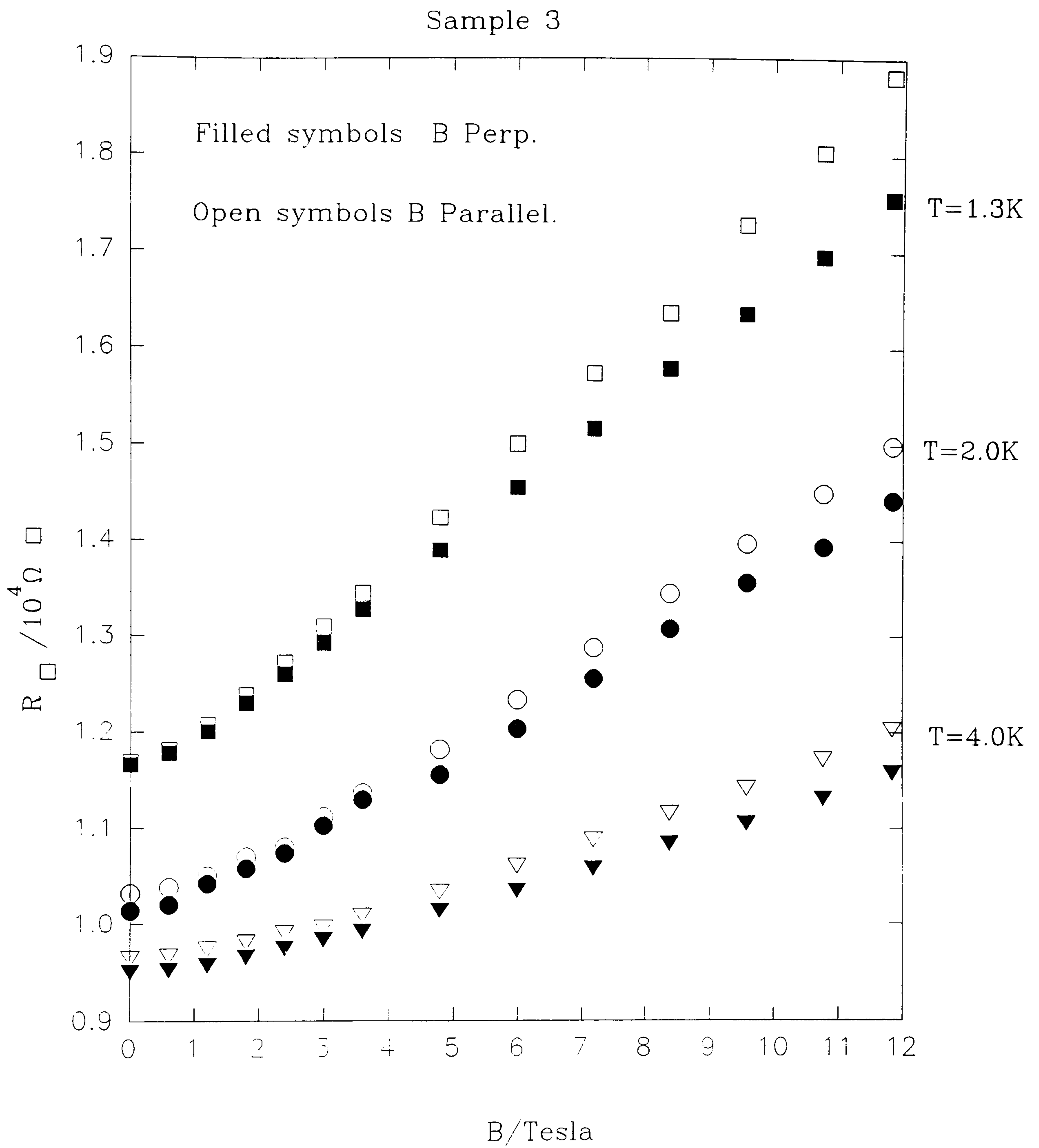

Figure 6..18

Magnetoresistance of the sample of Figure 6.14

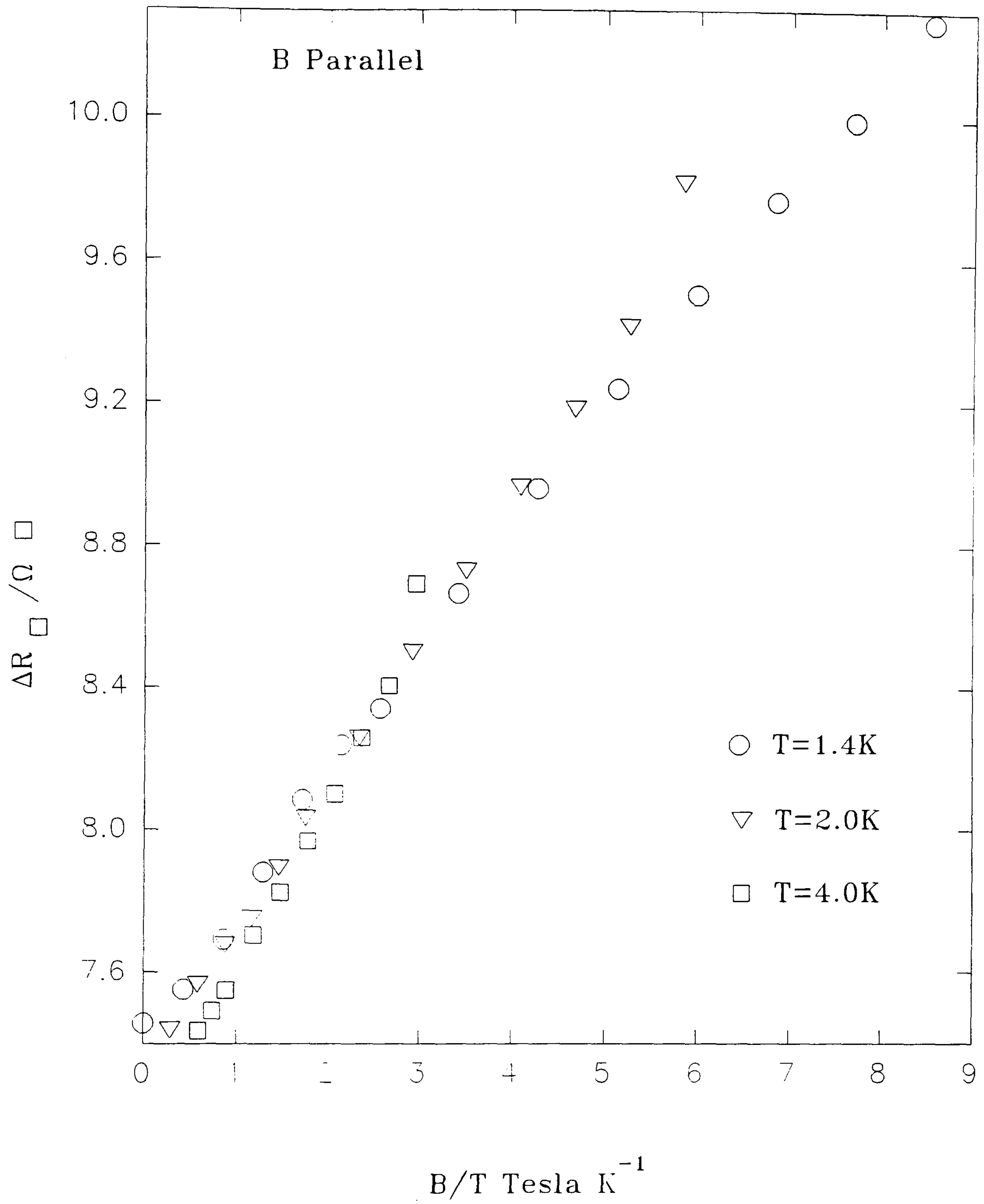

Figure 6.19.

Parallel magnetoresistance for sample 2. plotted versus B/T.

A more promising explanation of the magnetoresistance results would appear to be found in the concept of wavefunction shrinkage (Shklovskii and Efros, 1984). It is believed that a magnetic field induced metal-insulator transition to a strongly (ie. exponentially) localised state has occurred. Transport at the highest fields is then by 2D variable range hopping, for which Usov, Ulinich and Grebenschikov (1982) write,

$$\sigma = \sigma o \exp -\left(\frac{To}{T}\right)^{1/2} \qquad \textbf{(6.9)}$$

with

$$To = \frac{eB}{N(E_F)k\hbar} \qquad \textbf{(6.10)}$$

where $N(E_F)$ is the density of states at the Fermi level. The resistance in a field parallel to the 2DHG is plotted versus $B^{1/2}$ in figure 6.20. Linear behaviour is observed for high fields, the gradient increasing as the temperature is lowered. This is explained by noting that the condition for applicability of equations (6.9) and (6.10) is

$$R > \frac{L_c^2}{a} \qquad \textbf{(6.11)}$$

where R is the hopping distance Lc is the cyclotron radius and a is the radius of the wavefunction in zero field. Following Mott's original analysis (1968) for variable range hopping gives,

$$B > \left(\frac{\hbar}{e}\right)\left[\frac{\pi N(E_f)kT}{2a^4}\right]^{\frac{1}{3}} \tag{6.12}$$

From the slope of the plot at 1.3K - figure 6.20 - $N(E_F) \approx 4 \times 10^{20}\ e^{-}\ V^{-1}\ m^{-2}$. Figure 6.21 shows ln R plotted versus $T^{-1/2}$ between 0.5K and 4K from which $N(E_F) \sim 4.5 \times 10^{20}\ eV^{-1}\ m^{-2}$ is obtained, in satisfactory agreement with the analysis of the magnetoresistance isotherm.

A possible explanation of this result is as follows:

Presuming impurity band conduction is occuring, with overlapping Hubbard bands at B = 0. Application of a magnetic field leads to wavefunction shrinkage which splits the bands and gives rise to hopping. In other words there is both Mott and Anderson localisation. For a relatively small splitting of the the Hubbard bands, $N(E_F) \sim 4\pi\epsilon N_s^{1/2}/e^2$, where ϵ is the absolute permittivity and N_s is the acceptor sheet density (Schklovskii, 1983). With $\epsilon_r = 12$ for Si $N(E_F) \sim 4 \times 10^{18}\ eV^{-1}\ cm^{-2}$ is obtained. A possible explaination for the large discrepancy between this value and the experimental one is the fact that the dielectric constant is expected to be very large near a metal-insulator transition --the dielectric catastrophe (Mott, 1991). Obtaining a from the expression $a = \hbar/\sqrt{2mE_0}$ with $E_0 = 45$ meV, the ionization energy of boron in the low concentration limit and using the experimental valve of $N(E_F)$ it is found that equation (6.10) should be applicable for B > 93T! ie. much larger values of a are needed to obtain a sensible result. This is quite consistent with what has

been stated above. In the present picture a should be replaced by a localisation length ξ which tends to infinity as the transition from an insulator to a metal approaches (Mott and Kaveh, 1985, write $a/\xi = \text{const}\ (Ec-E)^s$ as $E \rightarrow Ec$ from below with $s \sim 1$).

Similar analyses may be carried out for samples 1 and 2 as shown in figures 6.22 and 6.23, but the critical field Bc for onset of this behaviour seems to be higher in sample 1 (table III) as expected from equation (6.10). The gradients at 1.3K decrease as $R_\square$ decreases, this may be attributed to the greater overlap of Hubbard bands as Ns increases.

Table III

Slopes and Critical Fields of $LnR_{\square}$ versus $B^{1/2}$ plots

Sample No	Slope/$T^{-1/2}$	Bc/T	Temp/K
1	0.056	7.8	1.34
2	0.16	4.8	1.4
3	0.24	4.8	1.3

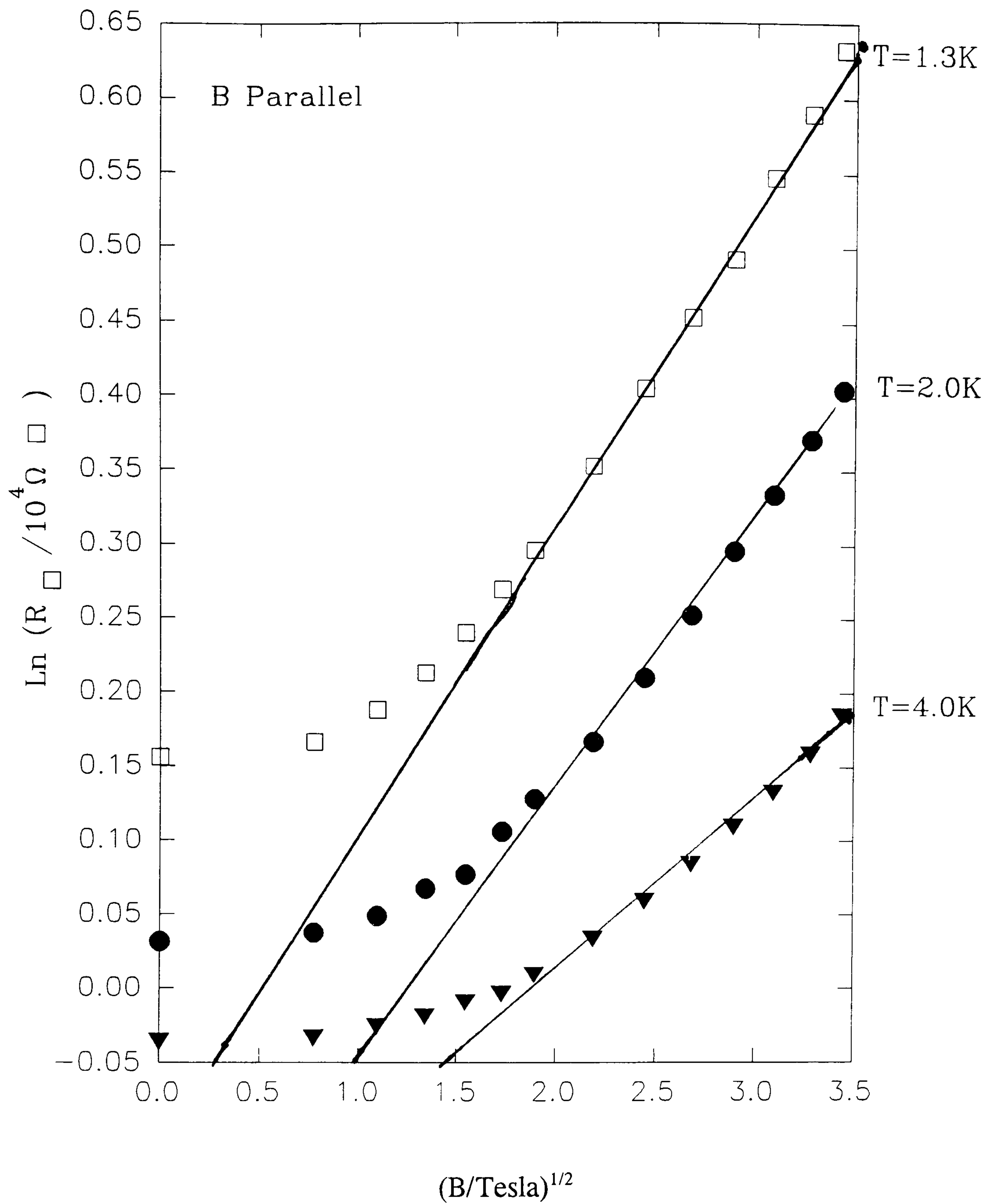

Figure 6.20.

Ln $R_{\square}$ plotted versus $B^{1/2}$ for the sample of sheet density $1.8 \times 10^{13} cm^{-2}$. $R_{\square}$ is the resistance and B is the magnetic field.

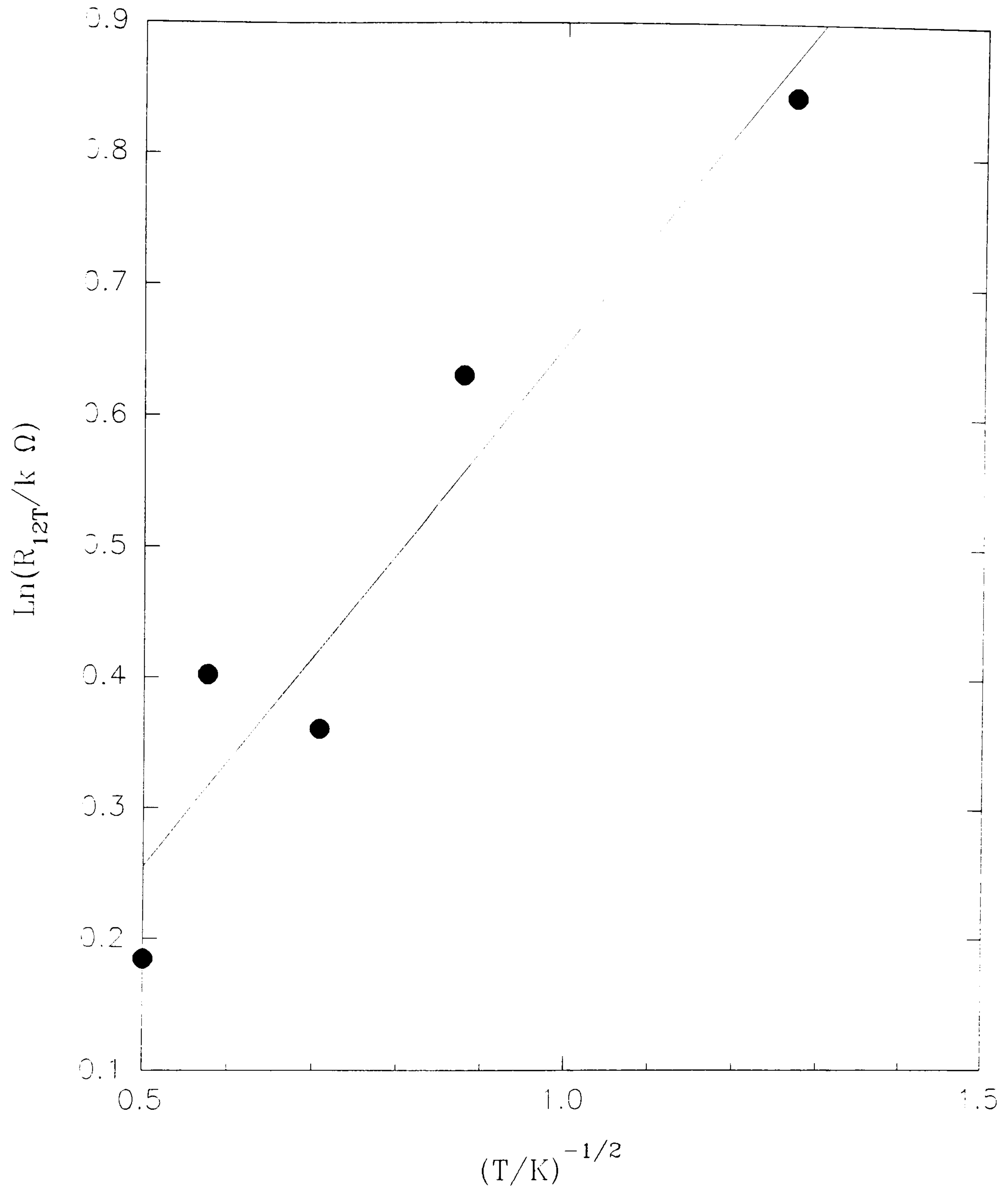

Figure 6.21.

Ln R versus $T^{-1/2}$ at B= 12T for the sample of sheet density $1.8 \times 10^{13} cm^{-2}$.

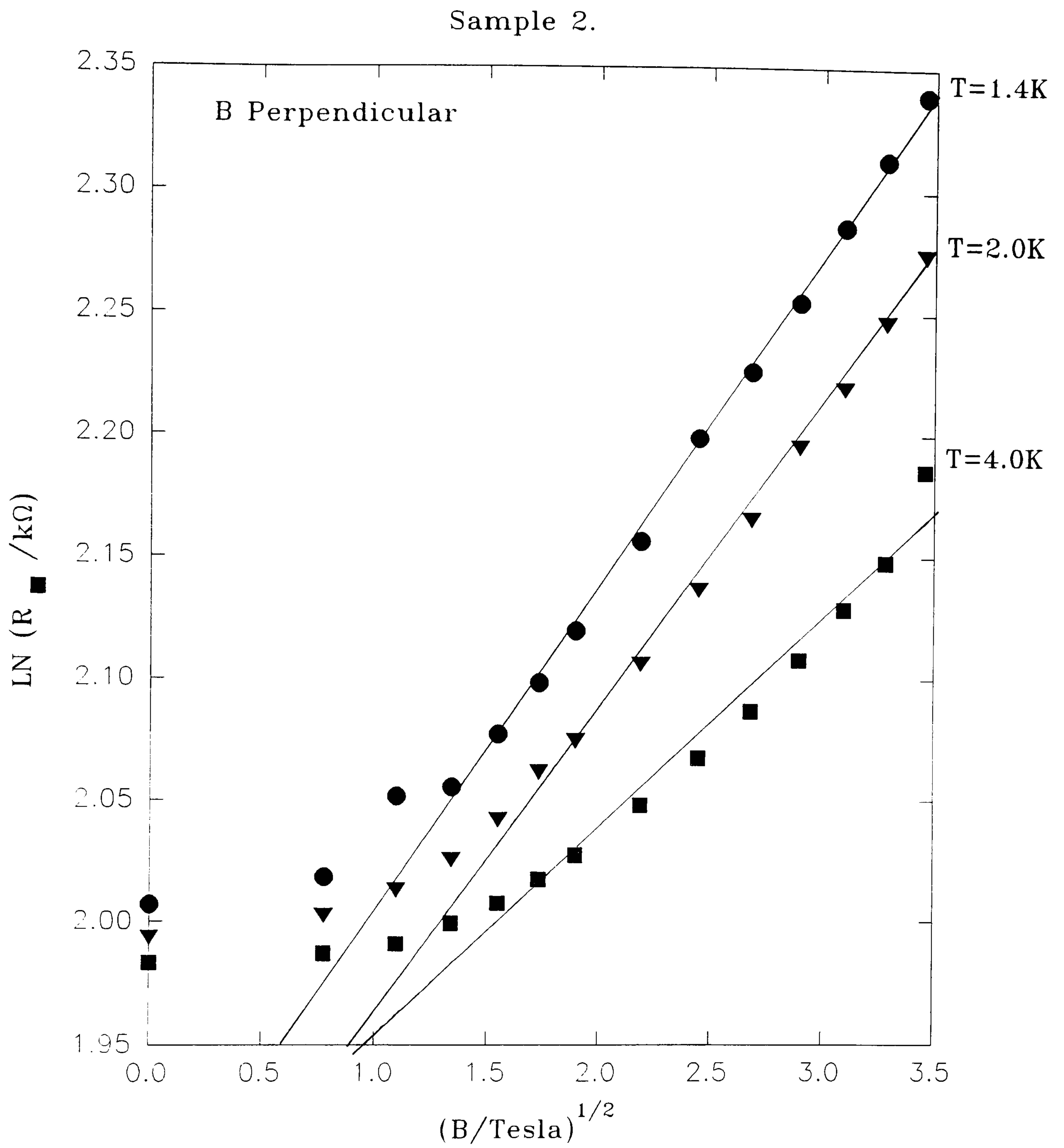

Figure 6.22

Ln R versus $T^{1/2}$ for the sample of sheet density $2.3 \times 10^{13} cm^{-2}$.

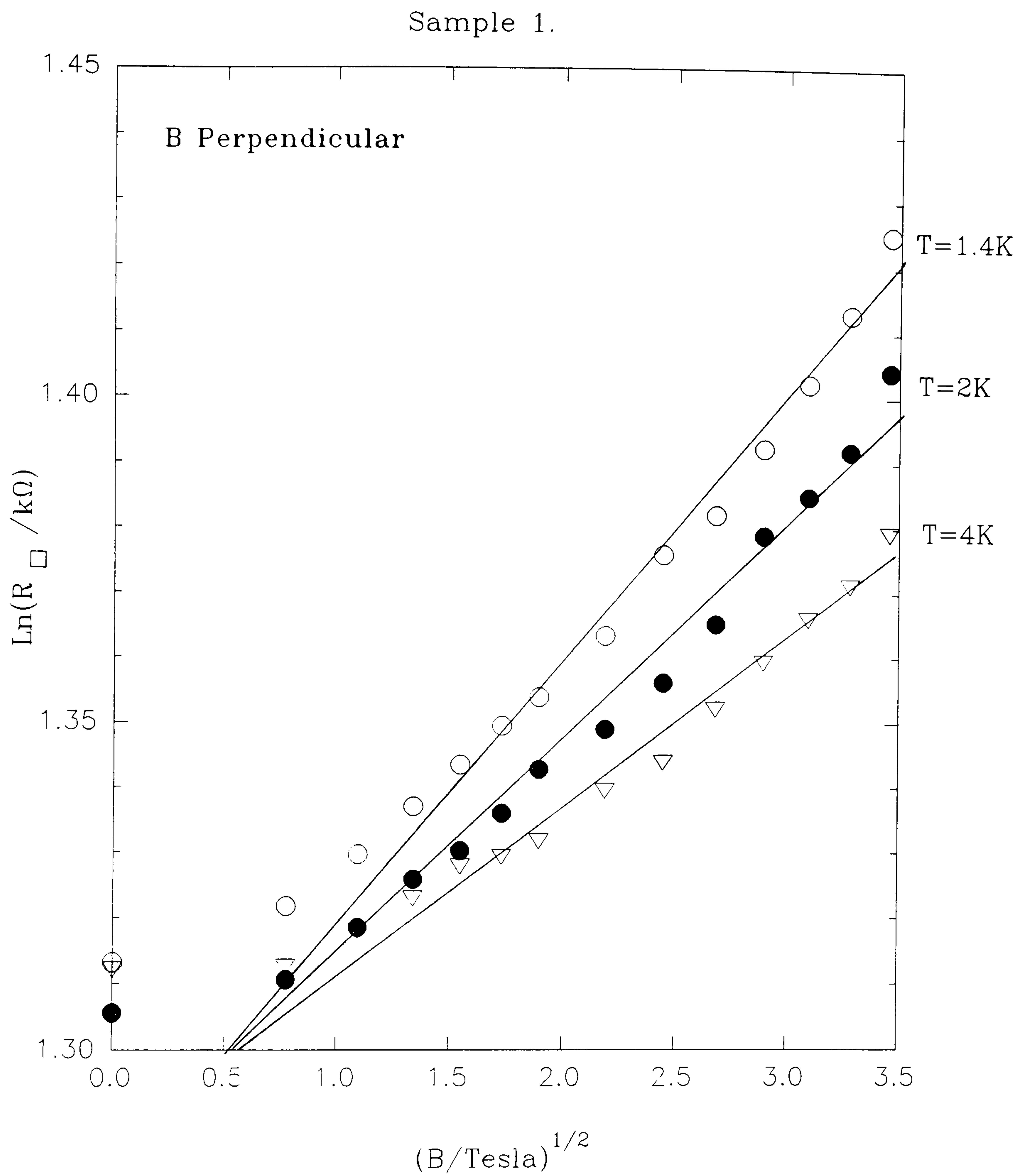

Figure 6.23.

Ln R versus $B^{1/2}$ for the sample of sheet density $8 \times 10^{13} cm^{-2}$

Figure 6.24 shows a log-log plot of the sheet resistance $R_{\square}$ of δ layers having sheet carrier densities in the range $4x10^{12}$ to $3.5x10^{13}$ cm^{-2}. The rapid rise in $R_{\blacksquare}$ for sheet densities below 10^{13} cm^{-2} provides evidence for a metal-insulator transition with $N_C \sim 1x10^{13} cm^{-2}$. The electrical properties of a δ layer of sheet density $9x10^{12}$ cm^{-2} are thus of particular interest. In this case the background doping is n^- ($\sim 10^{15} cm^{-3}$). The measured Hall mobility in the layer at a temperature of 300K is 30 $\pm$ 5 cm^2 $V^{-1}s^{-1}$, which is somewhat lower than the figure of $53cm^2$ $V^{-1}s^{-1}$ (Kubiak et al, 1987) obtained in uniformly doped MBE Si:B of the equivalent doping concentration (ie. $2x10^{19}$ cm^{-3}). The calculated subband structure (Figure 6.17) suggests that the confinement splits the valence band degeneracy and lowers the energy of the ground state heavy hole subband with respect to that of the light holes. A similar result was reported by Bangert, et al (1974) for a p-type Si inversion layer. It is therefore possible that transport in heavy-hole states dominates, with a consequent increase in effective mass and in scattering as compared to bulk.

Figure 6.25 shows the variation of the conductivity of this layer with temperature. Assuming the conductivity is due to a series of exponential terms with activation energies ϵ_i and pre-exponential factors σ_i, the data were fitted to,

$$\sigma(T) = \sum_{i=1}^{3} \sigma_i e^{\frac{-e_i}{kT}} \quad (6.13)$$

The resulting values are given in table IV:

Table IV

Pre-exponential factors and activation energies obtained from fitting the data of Figure 6.25 to equation 6.13

i	$\sigma_i/10^{-5}\ \Omega^{-1}$	ϵ_i/meV
1	23.1±0.40	20±0.3
2	1.80±0.10	0.76±0.02
3	1.79±0.09	0.58±0.03

At the highest temperatures ϵ_1 is indicative of the excitation of holes into the valence band, from which it is concluded that E_F lies in impurity states. For temperatures below $\sim$70K impurity conduction is dominant. The activation energy ϵ_2 is taken as evidence for transport in an upper Hubbard (A^+) band whilst ϵ_3 is thought to be associated with nearest neighbour hopping in the lower Hubbard (A) band. The observation of conduction in the A^+ band together with the low values of activation energy suggests that the impurity separation in this sample is close to, but above, the critical value for the metal-insulator transition (Mott and Davies, 1979).

In uniformly doped Si:B the onset of metallic behaviour occurs at an average impurity separation of 3.5nm (Chroboczek et al, 1984), whereas the average impurity separation in the δ layer is 2.2 $\pm$ 0.1nm, as deduced from the peak concentration of the SIMS profile (2.2 x 10^{19} cm^{-3}), itself an underestimate. This discrepancy cannot be explained by broadening of the δ layer during Hall bar fabrication. Resolution-limited SIMS measurements (using 2.2keV/0^+ primary ions) showed, to within experimental error, no change in the profile after annealing. Thus, it is deduced that the layer is broadened to a maximum FWHM of $\simeq$5nm implying an increase in the average impurity separation, assuming a Gaussian impurity profile, to $\simeq$2.9nm which is still significantly below the predicted critical value.

Similar behaviour has been observed in Sb (Van Gorkum et al, 1989) and As δ layers in Si (Denhoff et al, 1989). In contrast the transition does occur at the predicted impurity separation for Si δ-layers in GaAs (Qui-Yi et al, 1989).

Theoretical work on the Mott transition (Krieger and Nightinggale, 1971,

Martino et al, 1973) has shown that the critical separation R_c depends on carrier effective mass and on the number of valleys populated by the charge carriers. It is therefore possible that the observed decrease in R_c in δ doped Si:B is due to splitting of the valence-band degeneracy due to the carrier confinement, which is also suggested by the low value of the room temperature Hall mobility.

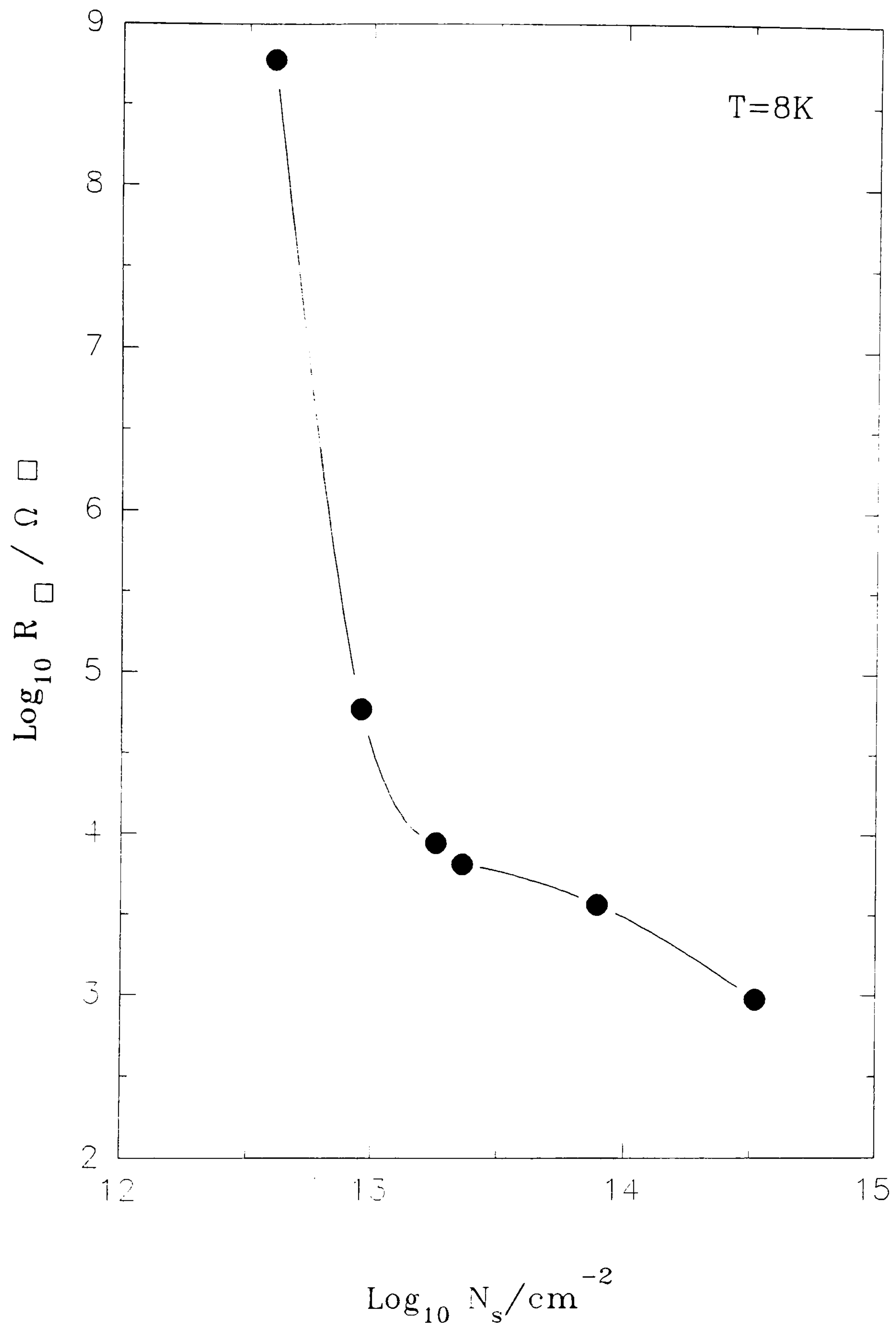

Figure 6.24

Log–Log plot of resistance at 8K versus sheet carrier density for Si:B δ layers.

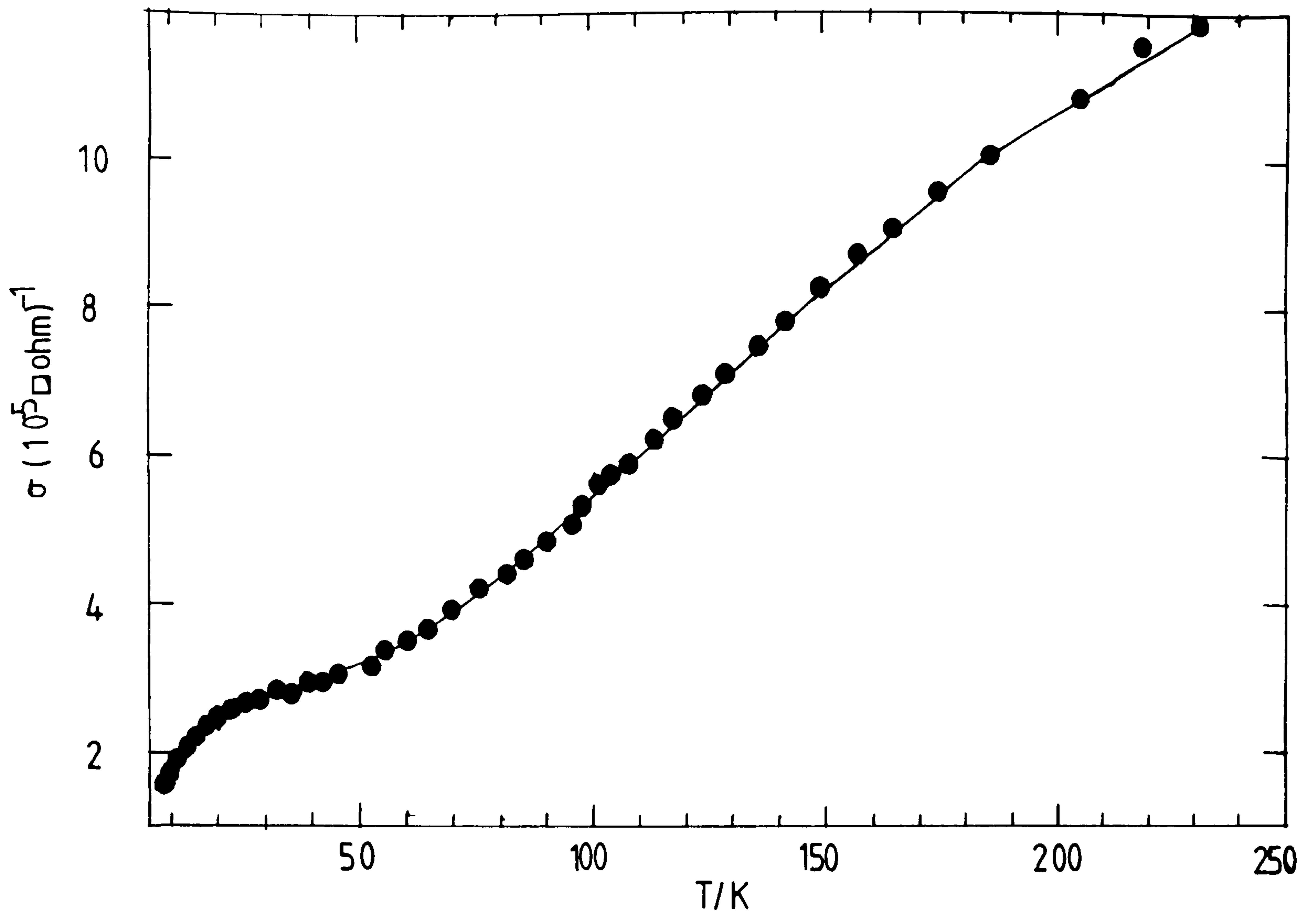

Figure 6.25.

Temperature dependence of the conductivity of an Si:B δ layer of sheet density $9x10^{12}cm^{-2}$.

Chapter 7.

CONCLUSIONS AND FURTHER WORK

MBE has been used to produce the first reported B δ layers in Si. From the analysis of SIMS data taken over a range of primary ion energies it is concluded that the FWHM of as grown Si:B δ layers is <2nm, as is confirmed by TEM. Modelling the rocking curved obtained from XRD implies an maximum width of 1nm suggesting that these are the narrowest δ layers produced to date. Hall measurements have been used, along with XRD data, to demonstrate complete activation for δ layers of sheet density up to ½ monolayer ($\sim 3.5 \times 10^{14} cm^{-2}$). CV measurements indicate that the width of the carrier distribution is ~3nm, which is consistent with monolayer doping.

Hall bars have been fabricated using a specially designed mask set and low thermal budget processing (in collaboration with the University of Edinburgh microfabrication facility). Designs have also been produced to fabricate MESFET and MOSFET structures along with gated Hall bars for device applications and future transport studies.

Following the development of suitable techniques, measurements of resistivity, magnetoresistance and the Hall effect have been carried out at temperatures down to 0.3K and at magnetic fields of up 12T. 2D weak localisation phenomena along with associated electron-electron interaction and spin-orbit scattering effects have been observed for the first time in such structures.

More detailed measurements at low magnetic fields will be required to evaluate further the relative contributions of the localisation and interaction terms. More theoretical work is needed to investigate the effects of the multisubband conduction and relatively high degree of disorder.

A magnetic field induced metal-insulator transition has been inferred from magnetoresistance measurements. From the temperature dependence of the resistance at a magnetic field of 12T, conduction is believed to be due to hopping (LnR varies as $1/T^{1/2}$).

The critical sheet density ($\sim 1 \times 10^{13}$ cm^{-2}) for the metal-insulator transition seems to be larger than the equivalent bulk value in the present samples and should be the subject of further experimental and theoretical investigation. In particular, knowledge of the critical sheet density for p-type δ layers in GaAs would be useful, an enhanced value would support the conjecture that the enhancement is due to the splitting of the electron or hole degeneracy due to the confinement (no such enhancement is observed in n-type GaAs with a singly degenerate conduction band minima).

Delta layers offer an attractive system for studies of localisation phenomena, a major advantage being that the disorder can be relatively accurately modelled. Although the presence of multisubband conduction is a complication. However, it may be possible to design structures of appropriate profile (i.e. width and doping concentration) which would minimize this and hence lead to information on its role in electrical transport. The fabrication of gated structures, for which suitable masks have been designed, would enable the metal-insulator transition to be studied in more detail. Also of interest is the

temperature dependence of the resistivity on the insulating side of the transition to determine the role of the Coulomb gap in variable range hopping.

REFERENCES

Abrahams E, Anderson P W, Licciardello D C, Ramakrishnan T V, 1979, Phys. Rev. Lett. 42, 673.

Altshuler B.L., Aronov A.G., Larkin P.I. and Khemlnitskii D.E., 1981, Sov. Phys. JETP, 54, 411.

Altshuler B L, Aronov A G, 1985, "Electron-electron Interactions in Disordered systems", Efros A L, Pollak M eds, North-Holland, Amsterdam.

Altshuler B.L., Khmelnitskii D., Larkin A.I. and Lee P.A., 1980, Phys. Rev. B., 22, 5142.

Anderson P W, 1958, Phys Rev. 102, 1008.

ASTM F76-78., 1978, American National standards institution.

Bangert E, Von Klitzing K and Landwehr G; 1974, Proc 12th Int. Conf. Phys. Semicond (M.H.Pilkuhn, Ed.), p.714, Teubner, Stuttgart.

Bass S J, 1979, J. Cryst. Growth, 47, 613.

Baxter C S, 1988, Presented at LDS summer school, Fitzwilliam College, Cambridge.

Bergmanm G, 1987, Phys. Rev. B35, 4205.

Bishop D J, Tsui D C, Dynes R C, 1980, Phys. Rev. Lett. 44, 1153.

Biswas R G, Braithwaite G, Phillips P J, Kubiak R A A, Parker E H C and Whall T E; Wood A, and O'Neill A, 1991, MRS Proc 220, in press.

Biswas R G, 1991, Electrical Characterisation of High Resolution Doping Structures Grown By Silicon Molecular Beam Epitaxy, PhD Thesis, University of Warwick, to be submitted.

Blood P, 1986, Semicond. Sci. Technol. 1, 7.

Booker G R and Whitehurst J R, 1990, Thin Solid Films, 184, 15.

Burdis M S, Dean C C, 1988 Phys. Rev. B38(15), 3219.

Chroboczek J A, Pollack F H, Staunton H F, 1984, Phil. Mag. B50 (1), 113.

Clegg J B, 1990, in "Growth and Characterisation of Semiconductors", Stradling R A and Klipstein P J eds. Adam Hilger.

Collins R, Jimenez Rodriquez J J, Wadsworth M, Buchheka R, Presented at 3rd Conf. on Rad. Effects in Insulators, Guildford, England, July 1985.

Denhoff M W, Jackman T E, McCaffrey J P, Jackman J A, Lennard W N, Massoumi G, 1989, Appl. Phys. Lett. 58 (14), 1332.

Deutscher G, and Fukayama H, 1982, Phys. Rev. B25, 4298.

Dineen C, Isherwood B J, 1989, Presented at the school on the growth and characterisation of semiconductors, Imperial College, University of London.

Döhler G H, 1978, Surf. Sci. 73, 97.

Dolan D J, Osheroff D D, 1979, Phys. Rev. Lett. 43, 721.

Dowsett M G, Clark E A, Spiller G D T, Augustus P D, Thomas G R, Webb R, 1988, UK IT 88, IEE/BCS, 512.

Dowsett M G, Barlow R D, Fox H S, 1991, J. Vac. Sci., in press.

Dugdale J S, 1987, Contemp. Phys. 28 (6), 547.

Edwards P P, Sienko M J, 1978, Phys. Rev. B17(6), 2575.

Eisele I, 1989, Appl. Surf. Sci., 36, 39.

Englert Th., von Klitzing K., Nicholas R.J., Landwehr G., Dorda G. and Pepper M, 1980, Phys. Stat. Sol., 99, 237.

Fukuyama H., 1980, J.Phys. Soc. Jpn, 49, 649.

Fukuyama H, 1982, Surf. Sci. 113, 489.

Gillmann G, Bois P, Barbier E, Vinter B, Lavielle D, Stohr M, Najda S, Briggs A, Portal J C, 1988, Semicond. Sci Technol. 3, 620.

Greene R L, Aldrich C, Bajaj K K, 1977, Phys. Rev. B15(4), 2217.

Gusev G.M., Kvon Z.D., Neizvestnyi L.G., Ovsyuk, V.N. and Palkin A.M., 1982, JETP Lett, 35, 256.

Harris J J, Pals J A, Woltjer R, 1989, Rep. Prog. Phys. 52, 1217.

Headrick R L, Weir B E, Levi A F J, Eaglesham D J, Feldman L C, 1990, Appl. Phys. Lett. 57(26), 2779.

Headrick R L, Levi F J, Luftman H S, Kovalchick J, Feldman L C, 1991, Phys. Rev. B43(18), 14711.

Houghton R F, 1991, The Growth and Evaluation of Epilayers by Silicon Molecular Beam Epitaxy, PhD Thesis, University of Warwick, Unpublished.

Humer-Hager T, 1988, Semicond. Sci. Technol. 3, 553.

Isawa Y. and Fukuyama H., 1984, J.Phys. Soc. Jpn, 53, 1415.

Iwabuchi S. and Nagoaka Y., 1989, J.Phys. Soc. Jpn, 58, 1325.

Kearney M.J. and Butcher P.N., 1988, J.Phys. C. Solid State Phys., 21, 2539.

Kennedy D P, Murley P C, Kleinfelder W, 1968, IBM J. Res. Develop. 12, 399.

Kichigin D.A., Igumenov V.T., Mironov O.A. and Chrisyakov S.V., 1984, JETP Lett, 36, 151.

Koch F, Zrenner A, 1989, Mat. Sci. and Eng. B1, 221.

Koch F, Private communication.

Krieger J B and Nightinggale M, 1971, Phys. Rev. B4, 1266.

Kubiak R A A, Newstead S M, Leong W R, Houghton R F, Parker wH C and Whall T E, 1987, App. Phys. A42, 197.

Kubiak and Parry, 1991, MRS Symposium Proc. 220, in press

Landwehr G. and Uchida S., 1986, Surf. Sci., 170, 719.

Lee P.A. and Ramakrishnan T.V., 1985, Rev. Mod. Phys., 57, 287.

Li H M, Willander M, Ni W, Berggren K F, Sernelius B, Hansson G V, 1989, Thin Solidwilms 183, 331.

Maliepaard M.C., 1988, The Metal-Insulator Transition in GaAs and $In_{0.53}Ga_{0.47}As$', PhD Thesis, University of Cambridge, (unpublished).

Martino F, Lindell G and Berggren K F, 1973, Phys. Rev, B8, 6030.

Mattey N L, Hopkinson M, Houghton R F, Dowsett M G, McPhail D S, Whall T E, Parker E H C, Booker G R, Whitehurst J, 1990b, Thin Solid Films, 184, 15.

Mattey N L, Hopkinson M, Houghton R F, Whall T E, Parker E H C, 1989, 5th European Workshop on MBE, Grainau, Germany.

Mattey N L, Dowsett Mw, Parker E H C, Whall T E, Taylor S, Zhang J F, 1990a, Appl. Phys. Lett. 57 (16), 1648.

Mott N F, 1968, J. Non. Crys. Solids. 1,1.

Mott N F, 1991, "Metal Insulator Transitions", Twlor and Francis, London.

Mott N.F. and Kaveh, 1985, Adv Phys. 34, 329.

Mott N F, Davies E A, "Electronic Processes in non-crystalline materials" 1979, 2nd ed. Clarendon, Oxford.

O'Neill A G, Private communication.

Park J S, Karunasiri P G, Mii Y J, Wang K L, 1990, Appl. Phys. Lett., 58(10), 1083.

Parker E H C, Ed, 1985, "The Technology and Physics of MBE", Plenum press, New York.

Parry C P, Kubiak R A A, Newstew S M, Whall T E, Parker E H C, 1991a, MRS Symposium Proc. 220, in press.

Parry C P, Newstead S M, Barlow R D, Augustus P, Kubiak R A A, Dowsett M G, Whall T E, Parker E H C, 1991b, Appl. Phys. Lett., 57(17), 1763.

Pepper M, 1985, Contemp. Phys. 26 (3), 257.

Phillips P J, Whall T E, Parker E H C, 1989, J. Phys. E: Sci. Instrum. 22, 986.

Ploog K, Hauser M, Fischer A, 1988, Appl. Phys. A 45, 233.

Ploog K, Hauser M, Fischer A, 1988, Appl. Phys. A45, 233.

Ploog K, 1978, J. Cryst. Growth, 81, 304.

Poole D A. Pepper M, Hughes A, 1982, J. Phys. C. Solid State Phys. 15, L1137.

Powell A R, Mattey N L, Kubiak R A A, Parker E H C, Whall T E, Bowen D K, 1991a, Semicond. Sci. Technol. 6, 227.

Powell A R, Kubiak R A A, Newstead S M, Parry C, Mattey N L, Smith D W, Brighten J C, Emeleus C J, Naylor T, Basaran E, Whall T E, Dowsett M G, Barlow R D, Parker E H C, Bowen D K, 1991c, J. Cryst. Growth, 111, 907.

Powell A R, Kubiak R A A, Whall T E, Parker E H C, Bowen D K, 1991b, Proc. Mat. Res. Soc. in press.

Qui-Yi Ye, Shklovskii B I, Zrenner A, Koch F, 1990, Phys. Rev. B, 41 (12), 8477.

Qui-Yi Ye, Zrenner A, Koch F, Ploog K, 1989, Semiconductor Sci. Technol. 4, 500.

Rhoderick E H, 1978, "Metal-Semiconductor Contacts", Oxford University Press.

Schklovskii B I, and Efros, 1984, "Electronic Properties of Doped Semiconductors" Springer-Verlag, Berlin.

Schubert E F, Fischer A, Ploog K, 1986, IEEE Trans. ED-33 (5), 625.

Schubert E F, Kopf R F, Kuo J M, Luftman H S, Garbinski P A, 1990 Appl. Phys. Lett. 57 (5), 497.

Schubert E F, Kopf R F, Kuo J M, Luftman H S, Garbinski P A, 1990b, Appl. Phys. Lett. 57(5), 497.

Schubert E F, 1990a, Surf. Sci. 228, 240.

Schubert E F, Ploog K, 1985, Jpn. J. Appl. Phys., 24(8), L608.

Smith D W, Houghton R F, Hopkinson M, Parker E H C, Whall, T E, 1988, Proc 2nd Int. Symp. Si-MBE, Electrochem. Soc.

Smith D W, Houghton R F, Parker E H C, Whall T E, 1990, Thin solid films, 184, 177.

Sze S M, 1981, "The Physics of Semiconductor Devices", 2nd ed., Wiley-interscience.

Taboryski R, Lindelof P E, 1990, Semicond. Sci. Technol. 5, 933.

Taylor S, Eccleston W, Watkinson P, 1987, Electron. Lett, 23(14), 732.

Tempel G, Müller F, Schwarz N, Koch F, Weimann G, Zeindl H P, Eisele I, 1990, Surf. Sci. 228, 247.

Tsui D C, Stormer H L, 1986, IEEE J. Quantum Elect. QE-22 (9), 1711.

Uren M J, Davies R A, Kaveh M, Pepper M, 1981, J. Phys C14, 5737.

Usov N A, Ulinich F R, Grebenschikov Yu B, Solid State Commun. 43(6), 475.

Van Gorkum A A, Yamaguchi K, 1989, IEEE Trans. ED-36 (2), 410.

Van Gorkum A A, Nakagawa K, Shiraki Y, 1989, J. Appl. Phys. 65 (16), 2485.

Van Gorkum A A, Nakagawa K, Shiraki Y, 1989, J. Cryst. Growth, 95, 480.

Van der Pauw L J, 1959, Philips Techn. Rev., 20, 220.

Weider H H, 1979, "Laboratory Notes on Electrical and Galvanomagnetic Measurements", Elsevier, Oxford.

Wharam D A, Pepper M, Ahmed H, Frost J E F, Hasko D G, Peacock D C, Ritchie D A, Jones G A C, 1988, J. Phys. C, 21, L887.

Whitehurst J, Private communication.

Wittmaack K, Wach W, 1981, Nuclear Inst. Methods, 191, 327.

Wood G E C, Metze G, Berry J, Eastman L F, 1980, J. Appl. Phys. 51, 383.

Wood A, 1991, Private communication

Wood A, O'Neill A G, 1991, MRS Proc. Spring 1991.

Zeindl H P, Wegehaupt T, Eisele I, Oppolzer H, Reisinger H, Tempel G, Koch F, 1987, Appl. Phys. Lett. 50(17), 1164.

Zeindl H P, Bullemer B, Eisele I, Templ G, 1989, J. Electochem. Soc. 136(4), 1129.

Zrenner A, Koch F, Leotin J, Goiran M, Ploog K, 1988, Semicond. Sci. Technol. 3, 1132.